

Spring 2003

The consolidation analysis of a clay layer in the city of Belem do Para, Brazil

John Bezerra Jr.

New Jersey Institute of Technology

Follow this and additional works at: <https://digitalcommons.njit.edu/theses>



Part of the [Civil Engineering Commons](#)

Recommended Citation

Bezerra, John Jr., "The consolidation analysis of a clay layer in the city of Belem do Para, Brazil" (2003). *Theses*. 610.
<https://digitalcommons.njit.edu/theses/610>

This Thesis is brought to you for free and open access by the Theses and Dissertations at Digital Commons @ NJIT. It has been accepted for inclusion in Theses by an authorized administrator of Digital Commons @ NJIT. For more information, please contact digitalcommons@njit.edu.

Copyright Warning & Restrictions

The copyright law of the United States (Title 17, United States Code) governs the making of photocopies or other reproductions of copyrighted material.

Under certain conditions specified in the law, libraries and archives are authorized to furnish a photocopy or other reproduction. One of these specified conditions is that the photocopy or reproduction is not to be “used for any purpose other than private study, scholarship, or research.” If a user makes a request for, or later uses, a photocopy or reproduction for purposes in excess of “fair use” that user may be liable for copyright infringement,

This institution reserves the right to refuse to accept a copying order if, in its judgment, fulfillment of the order would involve violation of copyright law.

Please Note: The author retains the copyright while the New Jersey Institute of Technology reserves the right to distribute this thesis or dissertation

Printing note: If you do not wish to print this page, then select “Pages from: first page # to: last page #” on the print dialog screen

The Van Houten library has removed some of the personal information and all signatures from the approval page and biographical sketches of theses and dissertations in order to protect the identity of NJIT graduates and faculty.

ABSTRACT

THE CONSOLIDATION ANALYSIS OF A CLAY LAYER IN THE CITY OF BELEM DO PARA, BRAZIL

**by
John Bezerra Jr.**

In this study, an analysis was done on a particular clay layer found in the city of Belem do Para, Brazil. Various soil tests were conducted including a consolidation analysis. Data were gathered and analyzed in order to obtain a better understanding of how the soil responds under certain loading conditions. There have been no previous studies done on this material and so when it has been encountered in the field geotechnical engineers provide the safest, but not necessarily best design method possible. In the case of large buildings, piles are driven past this material to competent sand. There have been many instances where small buildings or homes were built on a highly compacted sand layer that overlies this clay. Eventually these structures failed due to differential settlement (Alencar, 1999). The data obtained from this analysis will be used as a guide to the construction of certain structures in this area.

The area of study was chosen because there have been no previous studies done on this material and since the city is fairly young, the problem of long-term settlement could cause a threat to existing structures in which certain design criteria may have been overlooked.

**THE CONSOLIDATION ANALYSIS OF A CLAY LAYER
IN THE CITY OF BELEM DO PARA, BRAZIL**

**by
John Bezerra Jr.**

**A Thesis
Submitted to the Faculty of
New Jersey Institute of Technology
In Partial Fulfillment of the Requirements for the Degree of
Master of Science in Civil Engineering**

Department of Civil and Environmental Engineering

May 2003

APPROVAL PAGE

THE CONSOLIDATION ANALYSIS OF A CLAY LAYER IN THE CITY OF BELEM DO PARA, BRAZIL

John Bezerra Jr.

Dr. Raj Khera, Thesis Advisor
Professor of Civil and Environmental Engineering, NJIT

Date

Dr. Dorairaja Raghu
Professor of Civil and Environmental Engineering, NJIT

Date

Dr. John Schuring
Professor and Chair of Civil and Environmental Engineering, NJIT

Date

BIOGRAPHICAL SKETCH

Author: John R. Bezerra Jr.

Degree: Master of Science

Date: May 2003

Undergraduate and Graduate Education:

- Master of Science in Civil Engineering
New Jersey Institute of Technology, Newark, NJ, 2003
- Bachelor of Science in Civil Engineering,
Lafayette College, Easton, PA, 1997

Major: Civil Engineering

To my family and
loved ones

ACKNOWLEDGEMENT

I would like to first thank my Advisor Dr. Raj Khera, who guided and helped me tremendously through this long journey. I would like to thank Dr. Dilce Fatima Rossetti and Dr. Werner Truckenbrodt for providing valuable information on the geologic history of Belem. I would like to express my deepest appreciation to Dr. Julio Alencar Jr., who guided the initial stages of my thesis and provided me with many resources in Belem. One of these resources was the work of Joao Luiz Castro Sampaio Jr., which I based the format of my thesis on. I hope this thesis can compliment Mr. Sampaio's work and help future foundation designs in Belem.

TABLE OF CONTENTS

Chapter	Page
1 INTRODUCTION	1
1.1 Scope and Objective	1
1.2 General Information	1
2 GEOLOGIC STUDY AND SITE DESCRIPTION	6
2.1 General Geology	6
2.2 Barreiras Group and Post Barreiras Formation	11
2.3 Subsurface Exploration	16
2.4 Strata Classification	19
3 TESTING PROCEDURES AND RESULTS	22
3.1 General	22
3.2 Moisture Content & Specific Gravity	23
3.3 Particle Size Analysis – Hydrometer Method	24
3.4 Atterberg Limits & Organic Content	26
3.5 Consolidation Analysis	27
3.6 Triaxial Test	42
4 CONCLUSIONS AND RECOMMENDATIONS	45
4.1 Conclusions.....	45
4.2 Recommendations	47
APPENDIX A TIME RATE OF CONSOLIDATION GRAPHS	49
APPENDIX B TRIAXIAL TEST GRAPHS	81
REFERENCES	90

LIST OF TABLES

Table	Page
2.0 Translated Soil Borings	17
3.1 Lab Test Summary Data #1	23
3.2 Hydrometer Test Data (S-1)	24
3.3 Hydrometer Test Data (S-2)	25
3.4 Lab Test Summary Data #2	31
3.5 Summary of C_v , Graphical Procedure	32
3.6 Consolidation Raw Data (S-1 & S-2)	37
3.7 Consolidation Raw Data (S-3)	38
3.8 Typical Values of the Coefficient of Consolidation, C_v	39
3.9 Typical Values of the Compression Index, C_c	39
3.10 Values of C_α/C_a for Natural Soils.....	41
3.11 Consolidation Test Results for Sampaio Jr. Clay Analysis	46

LIST OF FIGURES

Figure	Page
1.1 Map of Para State and a Close up of Belem's Districts and Elevations	2
1.2 General soil profile representing the lower elevations of Belem do Para	4
1.3 General foundation system for the given soil profile	5
2.1 General Geology of South America	7
2.2 Lithological Stratification of the Braganca Region	9
2.3 Geologic Classification of Belem and Adjacent Areas	10
2.4 Lithological Associations of the Barreiras & Post Barreiras Sediments in NE Para	12
2.5 Lithological Depositional Sequence in NE Para	14
2.6 Depositional Model of the Barreiras Group in NE Para	15
2.7 Boring Location Plan	19
2.8 Shelby Tube Log	21
3.1 Hydrometer Analysis Plot (S-1)	25
3.2 Hydrometer Analysis Plot (S-2)	26
3.3 Strain vs. Log Pressure (S-1)	28
3.4 Strain vs. Log Pressure (S-2)	29
3.5 Strain vs. Log Pressure (S-3)	30
3.6 Strain vs. Log Pressure (S-3)	33
3.7 Void Ratio vs. Log Pressure (S-3), Schmertman	34
3.8 Void Ratio vs. Log Pressure (S-1,2,3)	35

LIST OF FIGURES (Continued)

Figure	Page
3.12 Modified Secondary Compression Index Versus Natural Water Content	40
3.13 Undrained Strength Ratio Versus Overconsolidation Ratio form Direct Simple Shear Tests on Six Clays	44
A.1 Logarithm of time method (a) and square root of time method (b) for S-1/L-1..	50
A.2 Logarithm of time method (a) and square root of time method (b) for S-1/L-2..	51
A.3 Logarithm of time method (a) and square root of time method (b) for S-1/L-3..	52
A.4 Logarithm of time method (a) and square root of time method (b) for S-1/L-4..	53
A.5 Logarithm of time method (a) and square root of time method (b) for S-1/L-5..	54
A.6 Logarithm of time method (a) and square root of time method (b) for S-1/L-6..	55
A.7 Logarithm of time method (a) and square root of time method (b) for S-1/L-7..	56
A.8 Logarithm of time method (a) and square root of time method (b) for S-1/L-8..	57
A.9 Logarithm of time method (a) and square root of time method (b) for S-2/L-1..	58
A.10 Logarithm of time method (a) and square root of time method (b) for S-2/L-2 ..	59
A.11 Logarithm of time method (a) and square root of time method (b) for S-2/L-3 ..	60
A.12 Logarithm of time method (a) and square root of time method (b) for S-2/L-4 ..	61
A.13 Logarithm of time method (a) and square root of time method (b) for S-2/L-5 ..	62
A.14 Logarithm of time method (a) and square root of time method (b) for S-2/L-6 ..	63
A.15 Logarithm of time method (a) and square root of time method (b) for S-2/L-7 ..	64
A.16 Logarithm of time method (a) and square root of time method (b) for S-2/L-8 ..	65
A.17 Logarithm of time method (a) and square root of time method (b) for S-3/L-1 ..	66
A.18 Logarithm of time method (a) and square root of time method (b) for S-3/L-2 ..	67

LIST OF FIGURES (Continued)

Figure	Page
A.19 Logarithm of time method (a) and square root of time method (b) for S-3/L-3 ..	68
A.20 Logarithm of time method (a) and square root of time method (b) for S-3/L-4 ..	69
A.21 Logarithm of time method (a) and square root of time method (b) for S-3/L-5 ..	70
A.22 Logarithm of time method (a) and square root of time method (b) for S-3/L-6 ..	71
A.23 Logarithm of time method (a) and square root of time method (b) for S-3/L-7 ..	72
A.24 Logarithm of time method (a) and square root of time method (b) for S-3/L-8 ..	73
A.25 Logarithm of time method (a) and square root of time method (b) for S-3/L-9 ..	74
A.26 Logarithm of time method (a) and square root of time method (b) for S-3/L-10	75
A.27 Logarithm of time method (a) and square root of time method (b) for S-3/L-11	76
A.28 Logarithm of time method (a) and square root of time method (b) for S-3/L-12	77
A.29 Logarithm of time method (a) and square root of time method (b) for S-3/L-13	78
A.30 Cv vs. Pressure (S-1)	79
A.31 Cv vs. Pressure (S-2)	79
A.32 Cv vs. Pressure (S-3)	80
B.1 Effective principal stress vs. strain (S-1)	82
B.2 Effective principal stress vs. strain (S-2)	82
B.3 Effective principal stress vs. strain (S-3)	83
B.4 Effective shear stress vs. strain (S-1)	83
B.5 Effective shear stress vs. strain (S-2)	84
B.6 Effective shear stress vs. strain (S-3)	84

LIST OF FIGURES (Continued)

Figure	Page
B.7 Obliquity vs. strain (S-1)	85
B.8 Obliquity vs. strain (S-2)	85
B.9 Obliquity vs. strain (S-3)	86
B.10 Excess pore pressure vs. strain (S-1)	86
B.11 Excess pore pressure vs. strain (S-2)	87
B.12 Excess pore pressure vs. strain (S-3)	87
B.13 Total corrected stress paths (S-1, S-2, S-3)	88
B.14 Effective non-corrected stress paths (S-1, S-2, S-3)	88
B.15 Mohr's circle (S-1, S-2, S-3)	89

LIST OF SYMBOLS

Ash (%)	-	Ash content.
C_{α}	-	Secondary compression index
C'_{α}	-	Modified secondary compression index
C_c	-	Compression index
C_v	-	Coefficient of consolidation
E	-	Strain
e_0	-	Initial void ratio
e_f	-	Final void ratio
ε	-	Strain
γ	-	Unit weight
G_s	-	Specific gravity
LL	-	Liquid limit
OC (%)	-	Organic content
OCR	-	Overconsolidation ratio
P	-	Vertical load
p	-	Shear stress path
PL	-	Plastic limit
PI	-	Plasticity index
P_c	-	Preconsolidation pressure
P_o'	-	Effective overburden pressure
q	-	Normal stress path
SPT	-	Standard penetration test
σ_1'	-	Effective major principal stress
σ_3'	-	Effective minor principal stress
σ_1	-	Total major principal stress
σ_3	-	Total minor principal stress
σ_0'	-	Effective overburden pressure
t	-	Time
τ_f	-	Shear stress
U	-	Pore water pressure
w (%)	-	Water content
WT	-	Water table

CHAPTER 1

INTRODUCTION

1.1 Scope and Objective

The objective of this thesis is to test and analyze samples taken from a soft clay layer that underlies most of the low terrain in the city of Belem do Para, Brazil. Various soil properties are analyzed to see how the soil would react under certain loading conditions. This information will be of value to geotechnical engineers working with this material, due to the lack of information or previous research that has been performed on this particular clay layer. Recommendations will be given on the capacity and compressibility of the soil along with a safe and economic manner in which to construct and monitor structures that overlie this material.

1.2 General Information

The city of Belem lies on the northern region of the state of Para. It is located on the mouth of the Amazon River and is situated on the margins of the Guama River and Guajara Bay (Figure 1.1). The city's recent geology consists of soils formed from alluvial deposits with some marine influence. According to Aziz Ab'Saber's classification, this area is categorized as plains and Amazon low lands. Three different altimetric levels can be located in the northern region of the country (i.e. Belem do Para). First; the valleys, which comprise of lands of recent formation near the margins of the rivers. Second; the fluvial terraces with maximum altitudes of 30m that are periodically flooded. And, third;

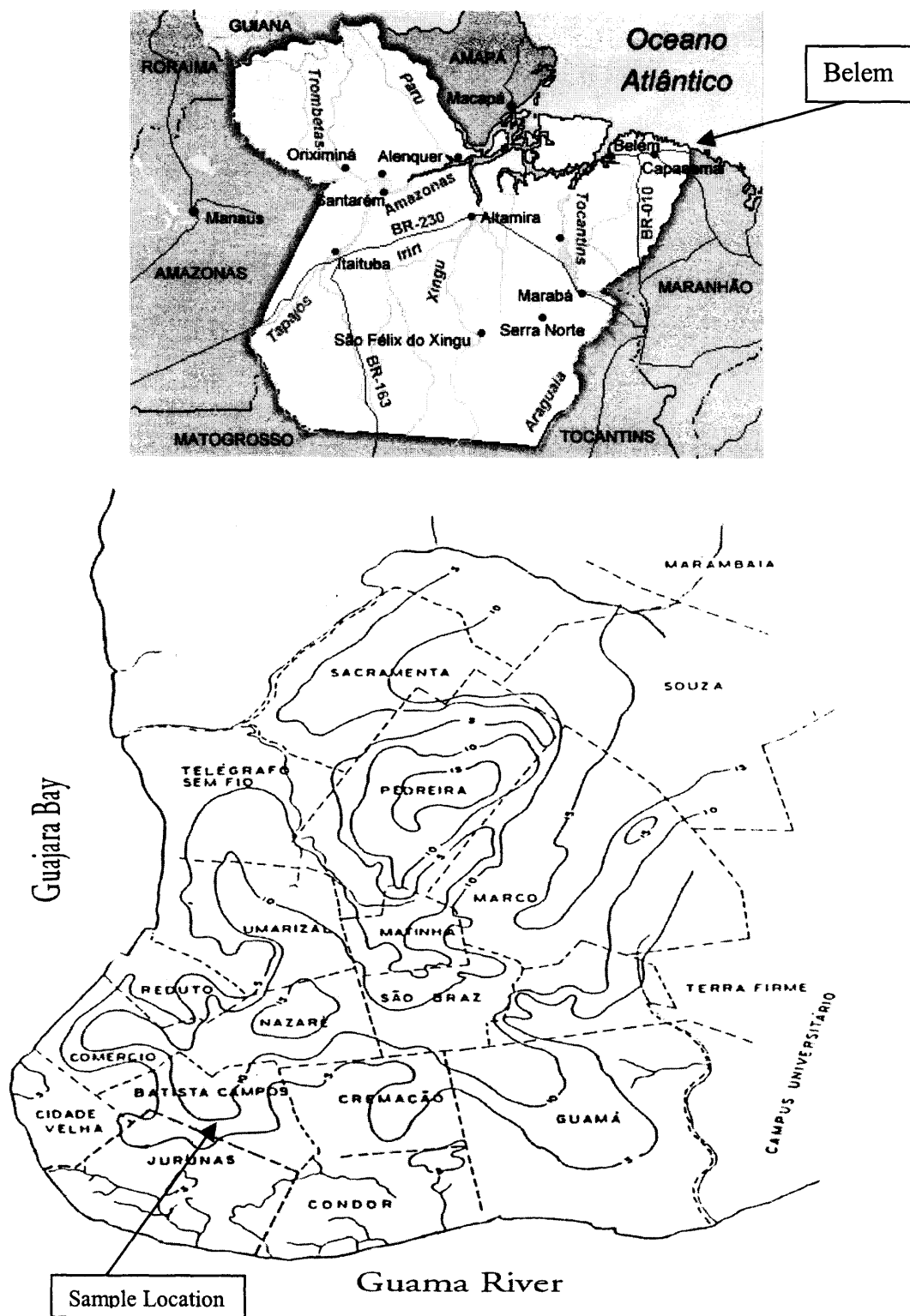


Figure 1.1 Map of Para State and a close up of Belem's districts and elevations. (Sampaio Jr., 1995)

low plateaus that were formed by lands of the Tertiary period (Machado, 1996). The clay layer being analyzed generally encompasses the low plateau region of Belem. Both high and low areas have similar soil profiles; the main difference is the clay layer that lies at a depth of about 8-10 meters. This layer can be categorized into two types of soil, which will later be discussed.

The general profile consists of three main layers, which are depicted in Figure 1.2. The first layer consists of a light gray organic silt and clay with little sand. Silt and sand percentages seem to diminish with depth. This layer has an average depth of 4 meters. The water table lies in this layer at approximately 1.5 meters.

The second layer consists of orange to red coarse to fine sand with gravel and clayey silt percentages varying from 5-15%. This layer has an average depth of 4 meters and is generally where most small buildings are founded on with predrilled reinforced concrete piles (Figure 1.3).

The third layer is broken down into two types of clay. The first is a light gray to yellowish red soft clay, which is being subjected to a laterization process due to quantities of iron oxide. This layer has been previously researched by Joao Luiz Castro Sampaio Jr. from the Pontificia Universidade Catolica do Rio de Janeiro. The second type, which is analyzed in this thesis, consists of a dark gray very soft silt and clay, trace fine sand (varved). This layer averages 6 meters in depth. The following soils consist of alternating layers of stiff clay and compacted sand. Generally higher buildings are founded on this compacted sand or stiff clay layer. Figure 1.2 also shows estimates of unit weights used for calculating the present overburden pressure. These estimates were made using values found in Sampaio Jr. (1995) thesis and tables from Das (1994) and

Holtz & Kovacs (1981). The effective overburden pressure (σ_o') using Sampaio's values was approximately 82.5 kPa. The effective overburden pressure (σ_o') using values from Das (1995) and Holtz & Kovacs ranged from 63 kPa-105 kPa with an average of 84 kPa. When Sampaio's values for the overlying soils and the calculated unit weight for this soil were used, a value of 91 kPa was found. This is probably the most accurate estimate and so 91 kPa was used for σ_o' in subsequent calculations.

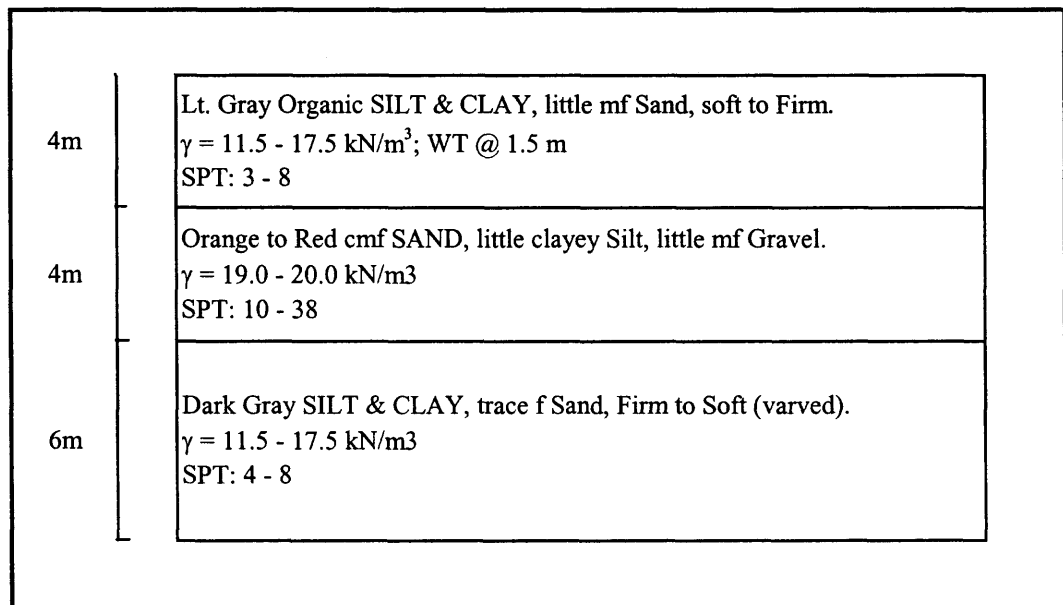


Figure 1.2 General soil profile representing the lower elevations of Belem do Para.

Little is known about the soft dark gray clay layer mentioned above. There has been no research previously done on this soil. Engineers currently make a judgment call as to whether they should build, go through this clay layer or if the above sand layer can withstand the pressure while maintaining minimal settlement to the underlying clay.

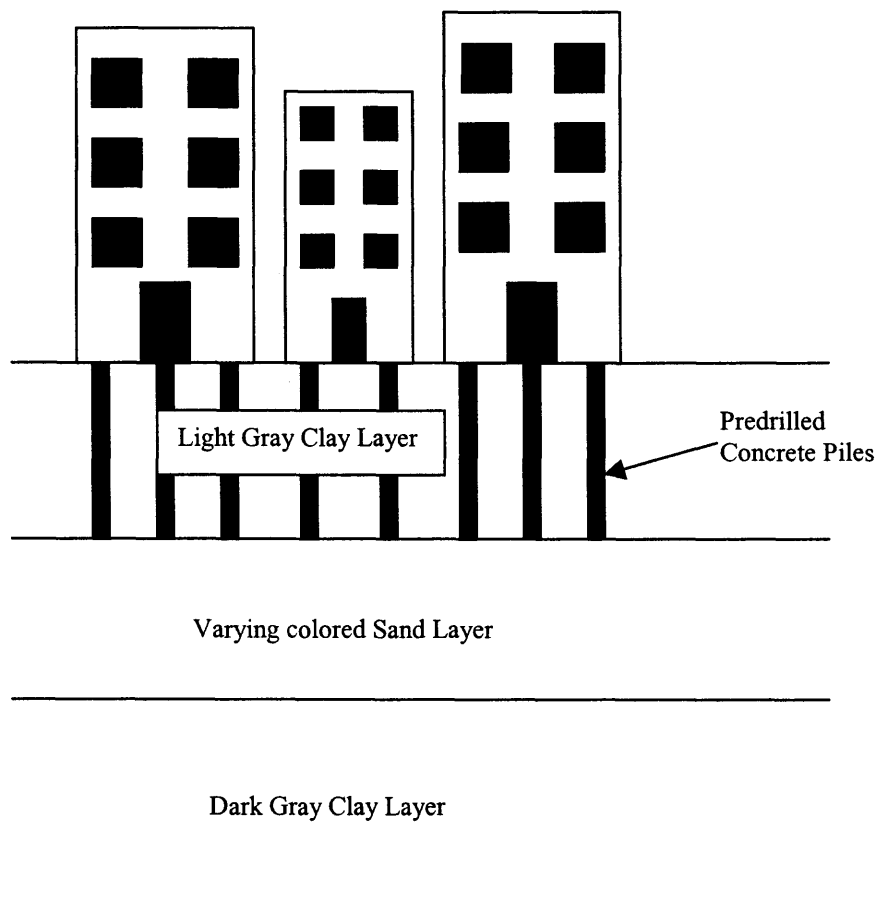


Figure 1.3 General Foundation system for the given soil profile.
(Sampaio Jr., 1995)

The only information currently used in this analysis is correlations from the standard penetration test (SPT). There were a number of cases with houses and buildings where engineers were called to design new or supplementary foundations because differential settlement was occurring due to this clay layer (Alencar, 1999).

CHAPTER 2

GEOLOGIC STUDY AND SITE DESCRIPTION

2.1 General Geology

In order to completely understand the properties of this soil it is necessary to study and analyze the geologic history and depositional setting that occurred in the northeastern state of Para. This chapter will discuss the general geology of Belem and will analyze the geologic formation in which this clay is believed to have occurred. Once this is done it is then possible to correlate data retrieved during the subsurface exploration stage and identify its depositional setting.

The general geology of this region consists of Precambrian granitic intrusions and gneisses that have been concentrated in the Guyana and Guapore Craton (See Figure 2.1). A thin belt of Early Paleozoic rock is found along these two cratons parallel to the Amazon River. Younger formations of Tertiary and Quaternary periods have been deposited between these two cratons. During this era, from approximately 65 million years to the present, sediments, partly marine and freshwater continued to be deposited along the Amazon valley (Derry, 1980).

Farias et al. (1992) categorizes rocks of Precambrian or Achaean time into different formations within the Northeastern state of Para. These rocks are grouped into the Maracacume Complex, Santa Luzia Formation, Tromai Formation, Gurupi formation, Viseu Formation, Igarape de Areia and Granito Cantao Formation, which follow the Piria Formation of the Paleozoic era.

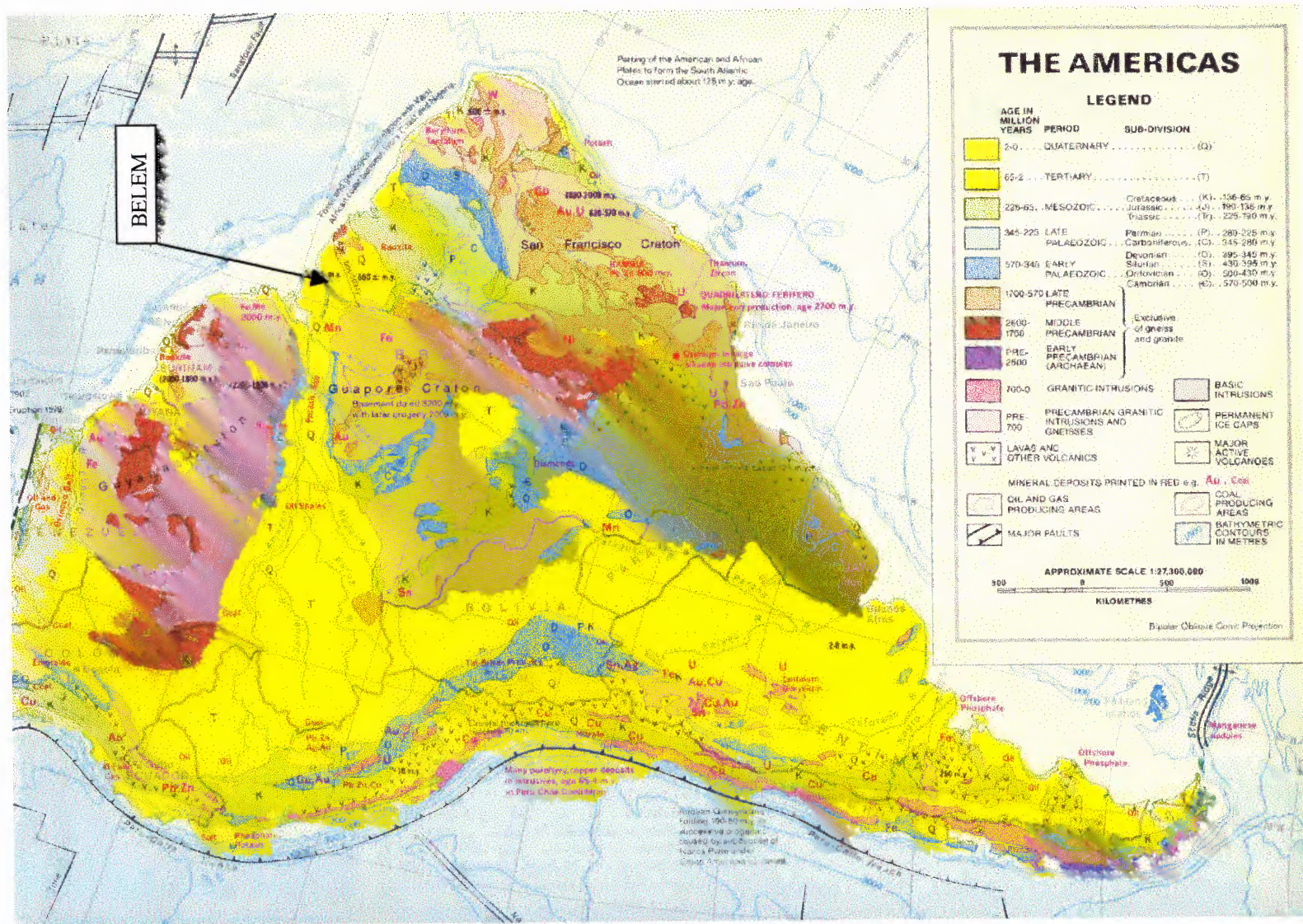


Figure 2.1 General Geology of South America. (Derry, 1980)

The geologic history or era of this clay can be found during the Cenozoic era on the geologic scale. There are three major formations that can be identified during this era. The Pirabas Formation, belonging to the early to mid Tertiary period. The Barreiras Formation, belonging to mid Tertiary to early Quaternary. This Group will later be analyzed in order to understand its historical sedimentation processes. The third formation is referred to as the Post Barreiras Group, belonging to early to mid Quaternary period. According to Farias's et al. (1992) interpretation, the soils formed during the Tertiary and Quaternary periods are found throughout the Braganca region, northeastern state of Para. "The sediments of the Barreiras group cover around 65% of area in this region, which are then covered by Quaternary Post Barreiras and alluvial Holocene sediments" (Farias et al. 1992). Figure 2.2 represents a general stratigraphic column of the Braganca region proposed by Farias et al., 1992.

A closer look is taken at the metropolitan area of Belem and its adjacent regions. Braz, 1985 (as cited in Sampaio Jr., 1995) classifies this region into four principal units; 1) sedimentary deposits of the Tertiary period (Barreiras Group); 2) sedimentary deposits of the Quaternary period (Pleistocene); 3) recent non-consolidated sediments along flood areas; 4) non-consolidated sediments of fluvial-marine planes with rivers and streams (Figure 2.3).

According to Pinheiro, (1987) the company Docas do Para (as cited in Sampaio, 1995) advanced 24 borings to a depth of 45 meters in the Port of Belem and defined the subsoil as Pleistocene/Holocene sediments. Pinheiro confirmed that the sediments correlate to the Post Barreiras sequence between the Pleistocene and Holocene epochs.

Pinheiro, 1987 (as cited in Sampaio, 1995) & Goes (1982) classifies the Post Barreiras formation as argilous materials that are found with significant erosive discordance above sediments belonging to the Barreiras group.

CENOZOIC	Quaternary	Holocene	Unconsolidated Sediments	Medium to fine Sands with quartzite distributed along the coastline, the bottom of river and creek beds; fluvial stone laminations; Silts and Clays tied to swamps.
		Pleistocene	Post Barreiras	Unconsolidated sediments; Sandy Clays & Clayey Sands ranging in color from yellow to red w/ quartzite and ironstone fragments.
	Tertiary	Miocene-Pleistocene	Barreiras Formation	Siliclastic sediments consisting of Claystones, Siltstones, Sandstones and occasionally Conglomerates of varying colors commonly rusted from iron oxide quantities. Plant fossils and primary sedimentary structures.
		Oligo-Miocene	Pirabas Formation	Calcites, Micrites, Bioclastics, Biohermites, Dolomicrite, occasionally varved with greenish gray laminations of above and calcium rich clays with abundant fossil content.
EO-PALEOZOIC			Piria Formation	Arkosic and Sub-Arkosic Sandstones, fine to coarse grains with conglomerates.
PRE-CAMBRIAN				<p>Maracume Complex: metamorphic w/ diverse migmatites</p> <p>Sta. Luzia Formation: Biotite Schists, muscovite schists to estaurolite and graphites</p> <p>Tromai Formation: Tonalites, quartzo-andesites, granites, trondjemites, grandodiorites and rhyolites</p> <p>Gurupi Formation: Cerrussite filonites, carbonitic filonites and schists.</p> <p>Igarape de Area Formation: Arkosiccosios and fine sandstones to conglomerates</p> <p>Viseu Formation: Fine metasandstones to conglomerates arkosic, with metargilites</p> <p>Cantao Granito: Gray biotite monzogranite</p>

Figure 2.2 Lithological Stratification of the Braganca Region. (Farias et al., 1992)

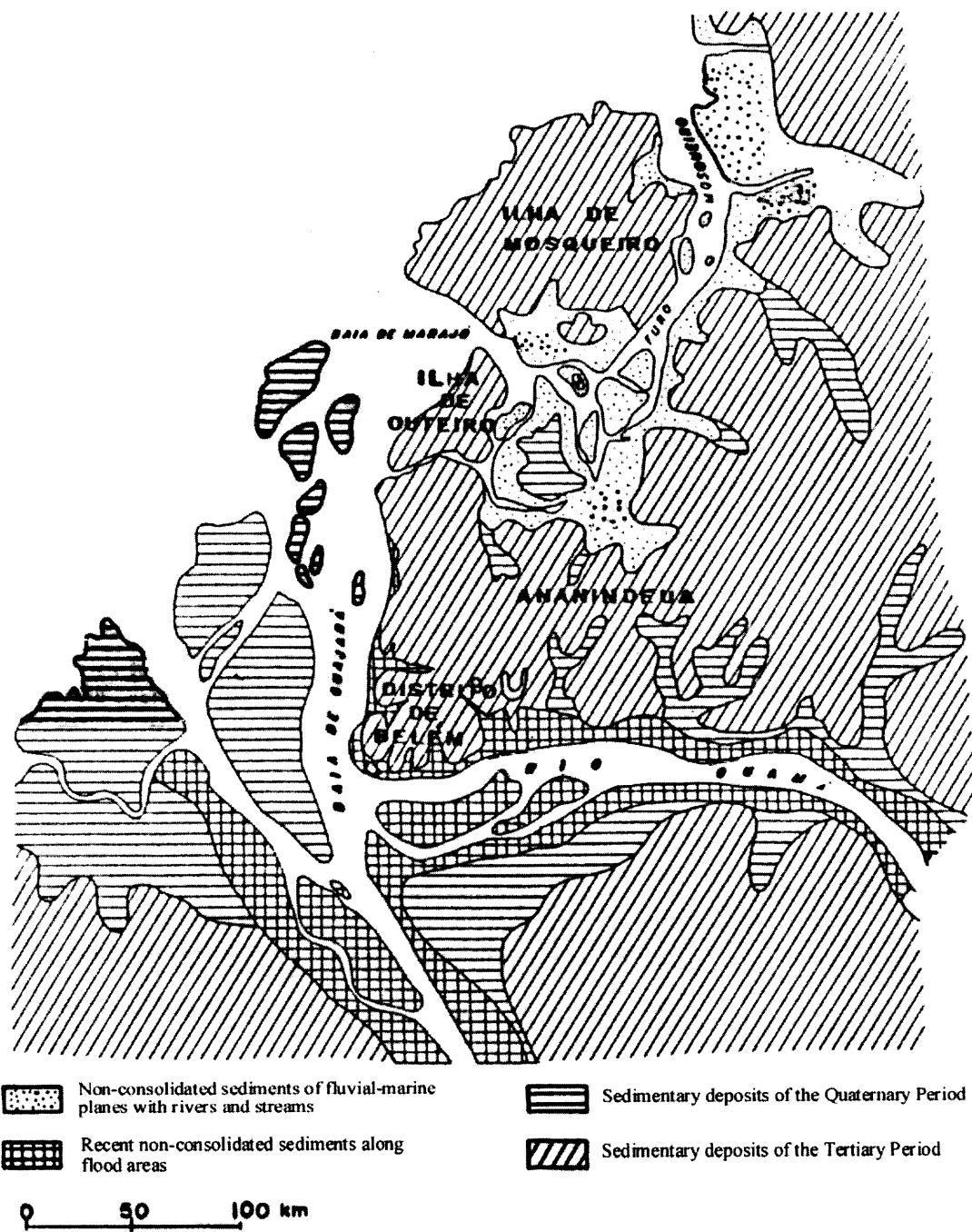


Figure 2.3 Geologic classification of Belem and adjacent areas Braz, 1985 (as cited in Sampaio, 1995).

Ferreira (1982) states that sediments of continental origin that lie above the clastic marine formation Pirabas are recognized as belonging to the Barreiras formation.

2.2 Barreiras Group & Post Barreiras Formation

This section analyzes the findings of various authors with respect to the Barreiras and Post Barreiras Formations. There is some discordance among geologists over the sediments that occur in and around the Barreiras Formation. It is therefore necessary to achieve a general accordance by analyzing various research works. This will help to properly classify the geologic depositional setting of this clay.

“The sediments that generically are designated the term Barreiras correspond to an extensive siliciclastic sequence of poorly sorted conglomerates and clays that occur in an extended belt along the Brazilian coastline from the mouth of the Amazon River to Rio de Janeiro” (Rossetti et al., 1990).

Rossetti, Goes & Truckenbrodt characterize the Barreiras sediments of the Braganca region, northeastern State of Para, into three distinct categories or associations as the authors describe it. The first (A), located in the southern region primarily consists of massive polymictic conglomerates. These deposits are attributed to a fluvial lacustrine environment referred to as the Pirabas and lower Barreiras Formation (Rossetti et al., 1989). Association B, lies between A and C and is primarily composed of sand when situated close to A. It is also composed of equal proportions of sand and clay in the proximity of C. “Association C, occurring in the northern part, consists mainly of laminated and massive claystone” (Rossetti et al., 1990). Rossetti attributes the latter two deposits to tidal processes within estuaries and stratigraphically denotes them as mid to

upper portions of the Barreiras Formation. Category D is mentioned as an erosive phase succeeding the Barreiras sediments. These sediments have been deposited by debris and eolian flows. This sequence or phase is referred to as Post Barreiras (See Figure 2.4).

Association	Barreiras			Post-Barreiras
	A	B	C	D
Lithology	Conglomerate an polymictic sediments, generally massive. Local stratification; increasing grain size with decreasing depth.	Sandy sediments close to Association A, with varying layers of sands and clays in proximity of Association C. Presents diverse structures & locally; plant fossil remains.	Predominantly varved and massive clays. Commonly covered by eroded fragments of clayey rocks. Presence of plant fossil remains.	Sandy Clay or Clayey Sand sediments with out structure or with dissipating structures of eolian dunes.
Facies	Cm.	Sm, Sw, Sc, Sa, St, SG, Ss, Al.	Al, Am, Ma	AA, BS
Ambient	Alluvial fan system	Sand flat w/ canals	Mud flat with marine intrusions	Subareal with an erosive phase and dissipation structures of aeolin dunes.

Cm =	Polymictic Conglomerates with out structure
Sm =	Sands with out structure
Sw =	Clayey Sands with wavy structure
Sc =	Sands with superior (on top) laminated structures
Sa =	Sands with canalized cross stratification
St =	Sands with tubular cross stratification
SG =	Coarse Sands to Conglomerates
Ss =	Sands with simoidal stratification or lamination
Al =	Laminated or varved clays (argillites)
Am =	Massive homogeneous clays (argillites)
AA =	Massive Sandy Clays
BS =	Sand & Ironstone blocks or fragments

Figure 2.4 Lithological Associations of the Barreiras & Post Barreiras Sediments in NE Para. (Rossetti et al., 1989)

Despite some discordance among geologists as to the age, beginning and contents of the Pirabas and Barreiras Formation, there is a general agreement where the Post Barreiras Formation begins. All of the literatures cited in this thesis have described a distinct break or separation between Barreiras and Post Barreiras of extreme weathering and erosive conditions that correlate to a major marine regression and arid conditions.

According to Farias et al., 1992 (as cited in Sampaio, 1995) the outcrops found in the Bragantina region of the sate of Pará can distinctively be subdivided into Barreiras & Post Barreiras by the presence of erosion. Goes (1981) classifies the Barreiras formation

as sediments that contain fine grain, are more compact, with varying colors and contain ironstone concretions formed in-situ. The Post Barreiras formation is classified as sediments containing fine to coarse grained sands with quartzite fragments and reworked ironstone concretions.

Goes (1981) divides the Barreiras formation into three categories; conglomeritic, sandy clay and sand lithofacies. “Textural immaturity and abundant mud supported clastics in particular, suggest depositions mainly by debris flows under semiarid conditions” (Goes, 1981 pg.3). The clay facies presents varying colors with low plasticity and a massive structure. Gradually with depth these sediments become more plastic and less massive in structure. They take on a dark greenish gray color with frequent sand seams that are closely spaced or varved.

Rossetti (1999) also recognizes three depositional sequences with in the Cenozoic. As mentioned before, she characterizes the lower part of this sequence as Pirabas and Lower Barreiras Formation. Figure 2.5 represents Rossetti’s stratigraphic interpretation.

AGE		DEPOSITIONAL SEQUENCE	LITHOSTRATIGRAPHIC UNIT	DESCRIPTION
PLIO- PLEISTOCENE		C	post-Barreiras	yellowish, well-sorted, fine-grained massive sandstone.
MIOCENE	LATE	sequence boundary 3 (lateritic soil)		
	MIDDLE	B	middle/upper Barreiras Fm.	mudstone with plane-parallel, lenticular, wavy and flaser beddings; massive and cross-stratified sandstone with reactivation surfaces and mud drapes forming thick/thin couplets attributed to tidal cycles. Variegated colors.
	EARLY	A	sequence boundary 2	terrigenous limestone, carbonaceous black mudstone and calcareous yellowish sandstone interfingering with mudstone and sandstone with variegated colors and showing plane-parallel, lenticular, wavy and flaser beddings, as well as cross stratification, reactivation surfaces and mud drapes forming thick/thin couplets attributed to tidal cycles.
LATE OLIGOCENE			lower Barreiras Fm. Pirabas Fm.	
		sequence boundary 1 (lateritic/bauxitic soil)		
CRETACEOUS			Itapecuru Group	

Figure 2.5 Lithological Depositional Sequence in NE Para (Rossetti, 1999).

Rossetti, Goes & Truckenbrodt have postulated an alluvial fan-sand flat-mud flat depositional model for the Barreiras sediments for the Braganca region and that part of the sediments of association C was deposited under tidal influences. Streams that emerge out of steep mountains form an alluvial fan or piedmont type alluvial deposit see Figure 2.6 (Schuring, 1998). The melting of the last glacial maximum along with drastic climatic changes may have caused periods of high flows along the Amazon basin, giving rise to these alluvial fans.

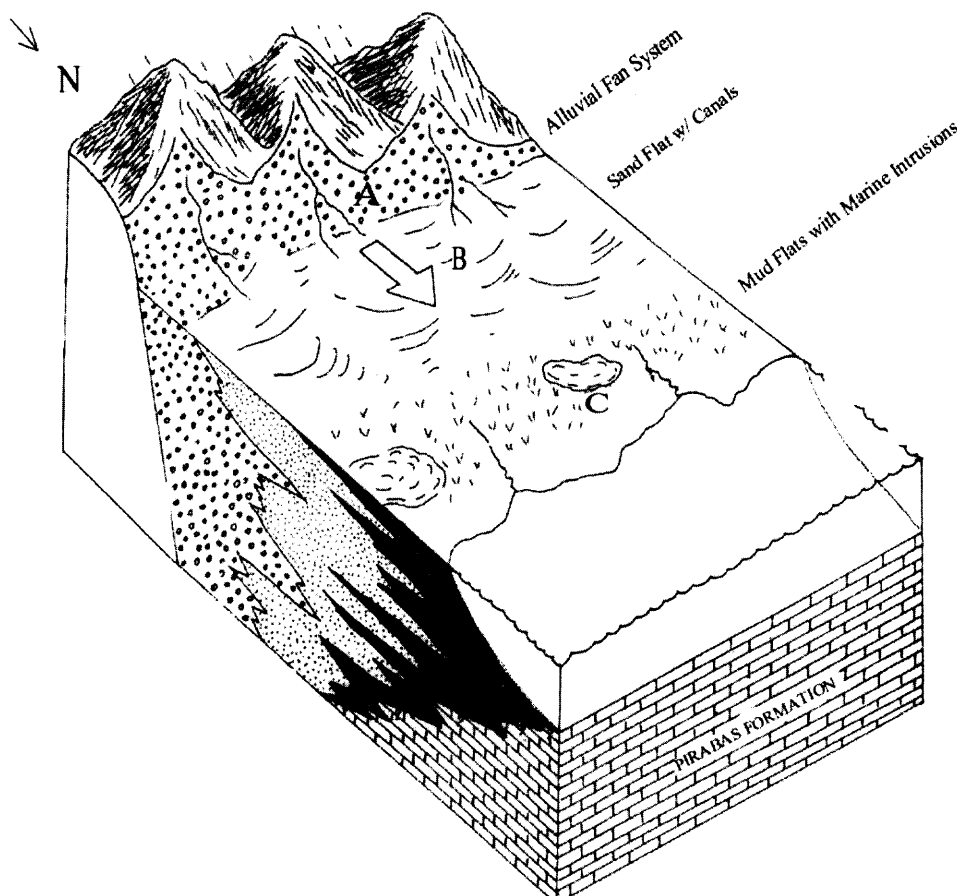


Figure 2.6 Depositional Model of the Barreiras Group in NE Para.

There is recorded evidence of marine transgressions in various parts of the world. “Relative sea level rose during the middle to early late Miocene, covering the Bragantine and Para platforms and resulting in deposition of estuarine cross-stratified sandstones and mudstones of the mid to upper Barreiras Formation” (Rossetti, 1999 pg 11). Evidence of marine transgressions throughout the world have been recorded and coincide with the transgression reported in the Northeast state of Para. Further evidence of marine influence on the Barreiras Formation can be proved by data collected from a palynological analysis conducted by Arai et al. (1988). A piece of varved organic clay

was sampled and tested. Results showed various marine and fresh water organisms as well as land (terrestrial) plant fragments.



The rising and lowering of the sea level may also have caused marine intrusions or sediments to overlay existing alluvial sediments. This occurrence may have only extended a short distance west of the Amazon delta. These marine sediments may also have been deposited in a lacustrine setting due to deep estuarine valleys and possible sediment barriers trapping water during the lowering of sea level.

2.3 Subsurface Exploration

The sample was taken from a construction site in Belem on Rua Padre Eutiquio between Rua Timbiras and Rua Eng. Fernando Guilhon in the district of Batista Campos (Figure 1.1). Soil borings were advanced 15.24 meters North of where the sample was extracted and the procedure was followed in accordance to the ASTM 1586 method for sampling soil. Samples and blow counts were collected using a 45 cm standard split spoon sampler. Blow counts were taken every 15 cm and data was used from the 15-45 cm interval, the first interval is considered to be exploratory and is not taken into account for design aspects. These borings were supervised and classified by Dr. Julio Alencar. Table 2.0 represents the English translation of the soil borings using the Burmeister classification system.

The sample was extracted from a pre-drilled pile location (refer to boring location Plan, Figure 2.7). Drilling was accomplished using a small track rig with pressurized water (jetting) connected to 5m incremented hollow stem sleeves.

Table 2.0 Translated Soil Boring Log

 <p>SOLOS & ROCHAS Engenharia de Obras Geotécnicas Ltda.</p>					PROJECT <u>MASTERS THESIS</u> <u>BELEM DO PARA BRAZIL</u>		SHEET <u>1</u> OF <u>2</u> BORING NO. <u>SP-06</u> LOCATION <u>SEE PLAN</u> OFFSET _____	
DEPTH OF WATER _____ FT. W/ _____ FT. CASING OUT ON _____ DEPTH OF WATER _____ FT. W/ ALL CASING OUT ON _____					DATE STARTED <u>01/03/00</u> DATE FINISHED <u>01/04/00</u>		GROUND ELEV. _____ GROUND WATER ELEV. _____	
WEIGHT OF HAMMER: _____ CASING _____ KG SAMPLER _____ KG INSIDE LENGTH OF SAMPLER: _____ (cm).					CASING: O.D. _____ I.D. _____ SAMPLER: O.D. _____ I.D. _____ COUPLING: O.D. _____ I.D. _____		HAMMER FALL ON: _____ CASING _____ SAMPLER _____	
DEPTH BELOW SURFACE	CASING BOWS PER FOOT	SAMPLE NUMBER DEPTHS BELOW SURFACE (m)	BLOWS PER 15 (cm) ON SAMPLER				PROFILE CHANGE DEPTH ELEV.	IDENTIFICATION OF SOILS / REMARKS
			0-15	15-30	30-45	Final 30		
0		0.00-1.00						
		H S-1	1	1	2	3/30	 at 1.5 m	S-1: Light Gray SILT & CLAY, little c(-)mf Sand (Sticky).
		S 1.00-1.45						S-2: Same as S-1.
		A S-2	1	2	2	4/30		S-3: Light Gray & Tan Silty CLAY, trace(+) mf Sand (Soft & Sticky).
		2.00-2.45						S-4: Light Gray cmf SAND, little(+) Clayey Silt, little f Gravel (Moist).
		S-3	3	3	5	8/30		S-5: Light Orange-Tan mf SAND, trace(+) f Gravel, trace Silt (Moist)
		3.00-3.45						S-6: Light Gray cmf SAND, little Clayey Silt, trace(+) f Gravel (Moist).
		S-4	4	4	6	10/30		S-7: Red mf SAND, some(-) Silt, trace f Gravel (Moist).
		4.00-4.45						S-8: Dark Gray SILT & CLAY, trace f Sand (V. Soft).
		S-5	10	15	18	33/30		S-9: Dark Gray SILT & CLAY, trace f Sand.
		5.00-5.45						S-10: Same as S-9.
		S-6	8	10	11	21/30		S-11: Same as S-9.
		6.00-6.45						S-12: Same as S-9.
		S-7	25	13	-	38/30		S-13: Same as S-9.
		7.00-7.45						S-14: TAN m(-)f(+) SAND, trace Silt (Wet).
		S-8	4	3	4	7/30		S-15: Same as S-14.
		8.00-8.45						S-16: Dark Gray mf SAND, little(+) Silt (Wet).
		S-9	2	2	2	4/30		S-17: Same as S-16.
		9.00-9.45						S-18: Same as S-16.
		S-10	2	3	3	6/30		S-19: Gray mf(+) SAND, Some(-) Clayey Silt.
		10.00-10.45						
		S-11	2	2	3	5/30		
		11.00-11.45						
		S-12	2	3	4	7/30		
		12.00-12.45						
		S-13	3	3	5	8/30		
		13.00-13.45						
		S-14	6	28	10/5	36/20		
		14.00-14.45						
		S-15	15	22	-	37/30		
		15.00-15.45						
		S-16	22	13/5	-	35/20		
		16.00-16.45						
		S-17	17	20/10	-	37/25		
		17.00-17.45						
		S-18	18	20	-	36/30		
		18.00-18.45						
		S-19	2	4	5	4/30		
		19.00-19.45						
20								

Soils Engineer: <u>Dr. Julio Alencar</u>	Contractor: _____
Drilling Inspector: <u>Dr. Julio Alencar</u>	Driller: _____

VISUAL IDENTIFICATION TERMS USED							
Clayey Soils		At Ball Moisture		Relative Density(Dr) of Granular Soils		Consistency of Clayey Soils	
Clayey Silt	slight PL	Thread	1/4"	Very loose	0-15 %	soft (S)	0.1-0.5 tsf
SILT & CLAY	low PL	Thread	1/8"	Loose	15-35 %	firm (F)	0.5-1.0 tsf
CLAY & SILT	medium PL	Thread	1/16"	Medium	35-65 %	med.hard (MH)	1.0-2.0 tsf
SILTY CLAY	high PL	Thread	1/32"	Dense	65-85 %	hard (H)	2.0-4.0 tsf
CLAY	very high PL	Thread	1/64"	Very Dense	85-100%	very hard (VH)	Over 4.0 tsf
						Proportions Used	
						trace = 1-10 %	
						little = 10-20 %	
						some = 20-35 %	
						and = 35-50 %	

Table 2.0 Translated Soil Boring Log (Continued)

[illegible]

This machine is used for cast in place concrete piles. Jetting was used to erode the soil into a soil-water suspension. The soil was sampled at a depth of 10.7m from the ground surface using a 10.48 cm diameter brass shelby tube. The tube was then sealed with wax on both ends and stored horizontally submerged in water for a period of about one week. Once the sample arrived in the United States, it was stored vertically as sampled and enclosed in a water filled sealed container.

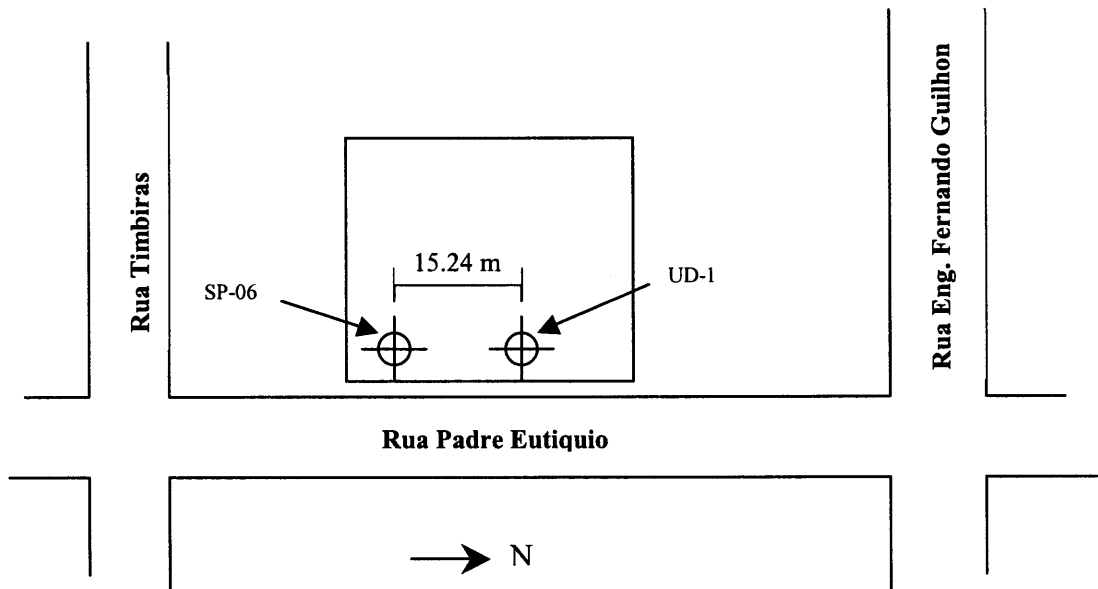


Figure 2.7 Boring location plan.

2.4 Strata Classification

The exact description of the Shelby tube contents can be seen in figure 2.8. The majority of the soil can be classified as Dark Gray SILT & CLAY, little fine Sand (varved).

Although it is difficult to determine the exact sedimentation processes that occurred with this soil it is possible to postulate this with the aid of the various cited works.

Rossetti, Truckenbrodt and Goes (1989) give the best representation and description of this soils age and sedimentation process. They specifically categorize this exact soil type as belonging to Association C of a Late Barreiras Formation.

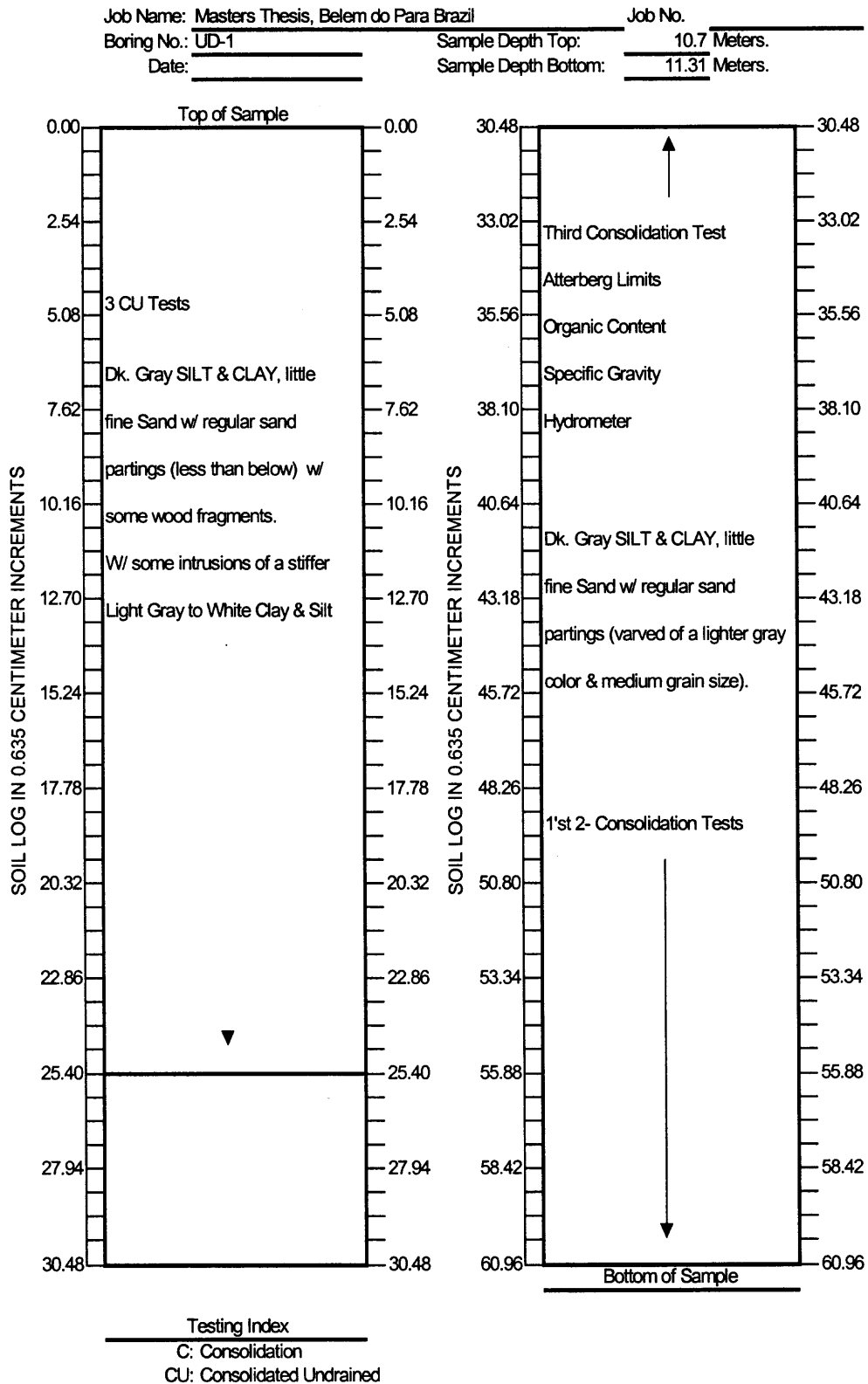


Figure 2.8 Shelby tube log.

CHAPTER 3

TESTING PROCEDURES AND RESULTS

3.1 General

Seven types of tests were performed on the sample to determine specific index properties and characteristics. These tests are ultimately what will help determine a recommendation for construction on or through this soil. A testing schedule was determined prior to the arrival of the soil. The following tests were performed on the soil; 1) Moisture Content, 2) Atterberg Limits, 3) Particle Size Analysis - Hydrometer, 4) Specific Gravity, 5) Organic Content, 6) Consolidation and 7) Triaxial - Consolidated Undrained.

A general visual classification of the soil was conducted using the Burmeister classification system. This was done each time the sample was pushed for testing. The general classification was a Dark Gray SILT & CLAY, little fine Sand with regular sand partings (varved of a lighter Gray coloration; & medium grain size). There are areas where the sand partings decrease and the consistency drops to soft. A White SILT & CLAY, trace fine Sand of stiff consistency was found in the last six inches of sample. It was imbedded within and around the previous dark gray varved material. This material was not tested due to small quantities that were encountered. It may be another area for future research.

3.3 Particle Size Analysis - Hydrometer Method

A particle size analysis was performed on two representative samples. The hydrometer method was used and the procedure was followed in accordance to the ASTM D422 method for determining an estimate of the distribution of soil particle sizes below the No. 200 sieve. The results of the two tests were very similar. Percentages of fine sand were between 9.0% and 9.6%, Silt were between 55% and 60.2% and clay were in the range of 3.4% to 7.5%. These results can be seen in Table 3.2, 3.3, Figure 3.1, 3.2.

Table 3.2 Hydrometer Test Data (S-1)

5.41 g retained on # 200 Sieve
% Passing # 200 = 91.0%

Mass of soil used = 60.0 g

Zero correction = 6.5 @ 20° C
Meniscus = 1.0
Dispersing Agent = NaPC3 @ 40g/gal
Gs = 2.664

Date	Time of Reading	Elapsed time, min	Temp. C	Actual Reading	Corr. Reading	Actual % Finer	Adjusted % Finer	Corr. For meniscus	L	L ^{1/2}	K	D, mm
09/08/2000	4:23 PM											
	4:25 PM	2	20.00	43	36.50	60.83	55.36	44.00	9.1	4.55	0.0134	0.028583
	4:27 PM	4	20.00	38	31.50	52.50	47.78	39.00	9.9	2.475	0.0134	0.021081
	4:31 PM	8	20.00	33.5	27.00	45.00	40.95	34.50	10.6	1.325	0.0134	0.015425
	4:39 PM	16	21.50	30	23.80	39.67	36.10	31.00	11.2	0.7	0.0132	0.011044
	4:53 PM	30	21.50	29	22.80	38.00	34.58	30.00	11.4	0.38	0.0132	0.008137
	5:23 PM	60	21.50	28	21.80	36.33	33.06	29.00	11.5	0.191666667	0.0132	0.005779
	6:23 PM	120	21.00	27	20.70	34.50	31.40	28.00	11.7	0.0975	0.0133	0.004153
	8:32 PM	249	21.00	26	19.70	32.83	29.88	27.00	11.9	0.047791165	0.0133	0.002908
09/09/2000	12:36 AM	493	21.00	26	19.70	32.83	29.88	27.00	11.9	0.024137931	0.0133	0.002066
	5:43 PM	1520	19.50	24	17.40	29.00	26.39	25.00	12.2	0.008026316	0.0135	0.001209
09/10/2000	8:10 PM	3107	20.00	23.5	17.00	28.33	25.78	24.50	12.3	0.003958803	0.0134	0.000843
09/11/2000	5:38 PM	4395	20.50	23	16.60	27.67	25.18	24.00	12.4	0.002821388	0.01335	0.000709
09/12/2000	5:22 PM	5819	20.50	23	16.60	27.67	25.18	24.00	12.4	0.00213095	0.01335	0.000616
09/13/2000	11:04 AM	6881	21.00	22	15.70	26.17	23.81	23.00	12.5	0.001816596	0.0133	0.000567

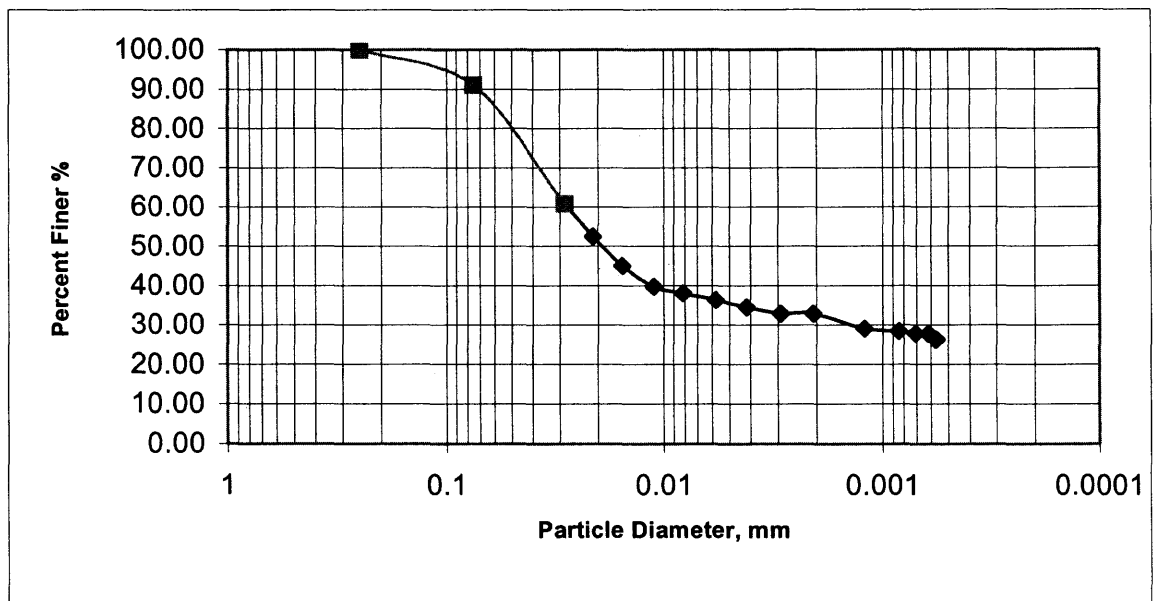


Figure 3.1 Hydrometer analysis (S-1).

Table 3.3 Hydrometer Test Data (S-2)

5.77 g retained on # 200 Sieve
 % Passing # 200 = 90.4%

Mass of soil used = 60.0 g

Zero correction = 6.5 @ 20° C
 Meniscus = 1.0
 Dispersing Agent = NaPO₃ @ 40g/gal
 G_s = 2.664

Date	Time of Reading	Elapsed time, min	Temp, C	Actual Reading	Corr. Reading	Actual % Finer	Adjusted % Finer	Corr. For meniscus	L	Lt	K	D, mm
09/08/2000	4:35 PM											
	4:37 PM	2	22.00	42	35.90	59.83	54.09	43.00	9.2	4.6	0.0134	0.02874
	4:39 PM	4	22.00	37	30.90	51.50	46.56	38.00	10.1	2.525	0.0134	0.021293
	4:43 PM	8	22.00	32.5	26.40	44.00	39.78	33.50	10.8	1.35	0.0134	0.015569
	4:51 PM	16	22.00	31	24.90	41.50	37.52	32.00	11.1	0.69375	0.0132	0.010994
	5:05 PM	30	21.50	28.5	22.30	37.17	33.60	29.50	11.45	0.381666667	0.0132	0.008155
	5:35 PM	60	21.50	27	20.80	34.67	31.34	28.00	11.7	0.195	0.0132	0.005829
	6:35 PM	120	21.50	26	19.80	33.00	29.83	27.00	11.9	0.099166667	0.0133	0.004188
	8:35 PM	240	21.00	26	19.70	32.83	29.68	27.00	11.9	0.049583333	0.0133	0.002962
09/09/2000	12:35 AM	480	21.00	26	19.70	32.83	29.68	27.00	11.9	0.024791667	0.0133	0.002094
	5:43 PM	1508	20.50	24.5	18.10	30.17	27.27	25.50	12.1	0.008023873	0.0135	0.001209
09/10/2000	8:10 PM	3095	20.50	24	17.60	29.33	26.52	25.00	12.2	0.003941842	0.0134	0.000841
09/11/2000	5:38 PM	4323	20.50	23	16.60	27.67	25.01	24.00	12.4	0.002868378	0.01335	0.000715
09/12/2000	5:22 PM	5807	20.50	23	16.60	27.67	25.01	24.00	12.4	0.002135354	0.01335	0.000617
09/13/2000	11:04 AM	6869	21.00	22	15.70	26.17	23.65	23.00	12.5	0.00181977	0.0133	0.000567
09/12/2000	5:22 PM	5819	20.50	23	16.60	27.67	25.18	24.00	12.4	0.00213095	0.01335	0.000616
09/13/2000	11:04 AM	6881	21.00	22	15.70	26.17	23.81	23.00	12.5	0.001816596	0.0133	0.000567

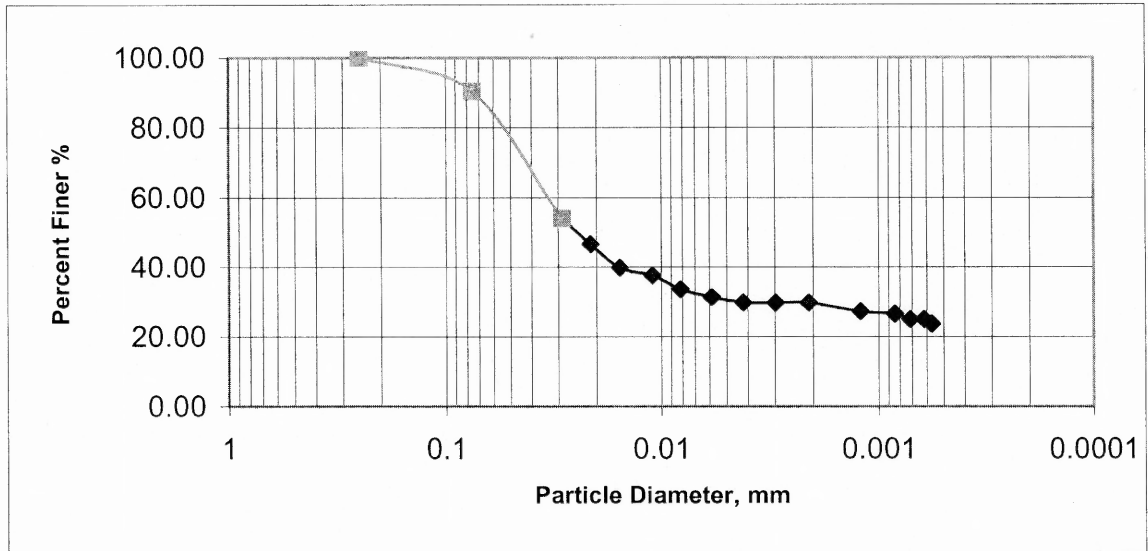


Figure 3.2 Hydrometer analysis (S-2).

3.4 Atterberg Limits & Organic Content

The Atterberg limits were determined using the standard test method for liquid limit, plastic limit, and plasticity index of soils D 4318-84 as specified by ASTM standards. A series of five tests were run at different conditions (Table 3.1). Samples were tested at natural or wet conditions and dry (at 60° C); some were allowed to soak for 16 hours and others were not. The data plotted as an Inorganic Clay of medium plasticity on the Plasticity chart (ASTM D4318). When comparing the results between the dry and wet prepared sample, the difference shows a 6% increase in water content for the wet sample. According to ASTM D2487, if the ratio between oven dry and wet is less than 0.75, then the soil is considered organic. The soil tested had a ratio of 0.82, which classifies it as inorganic. This sample is a borderline case where the water content falls just below the organic content criteria.

The organic content of this soil was determined using the ASTM D 2974 standard. A series of three organic content tests were run and showed that the organic content was on average 3% (Table 3.1). This percentage is lower than what was originally thought. According to Alencar (1999), the soils found in this stratum generally appear to have a higher organic content. In this area of Belem the organic content may change sporadically within the soil profile. What was sampled at the present site may change 500 feet down the road due to varying geologic settings.

3.5 Consolidation Analysis

The ASTM method D 2435 was used for the consolidation analysis. The principal objective of this test was to obtain the consolidation properties of the material used.

A series of three consolidation testes were run at different times. The first two tests were loaded from 7.77 kPa to a maximum load of 994.42 kPa where the last test was loaded to 1988.84 kPa and was then unloaded at $\frac{1}{4}$ load decrements. Load increments were doubled as required by ASTM standards. The first two tests used a time interval of three days between load increments. The third test used a time interval of 24 hours between load increments. The results for this test can be seen in Table 3.4.

The preconsolidation pressure (P_c) of this clay shows values, which range between 150-180 kPa. The average pressure shows to be about 165 kPa. The values for P_c shown on Table 3.4 were obtained using the Casagrande (1936) method as stated in Das (1994). The last value for P_c represented on Table 3.4 is 165 kPa, which was obtained using the Schmertmann (1955) method. This method was only used on S-3 because it requires a full unload cycle, which S-1 and S-2 did not have.

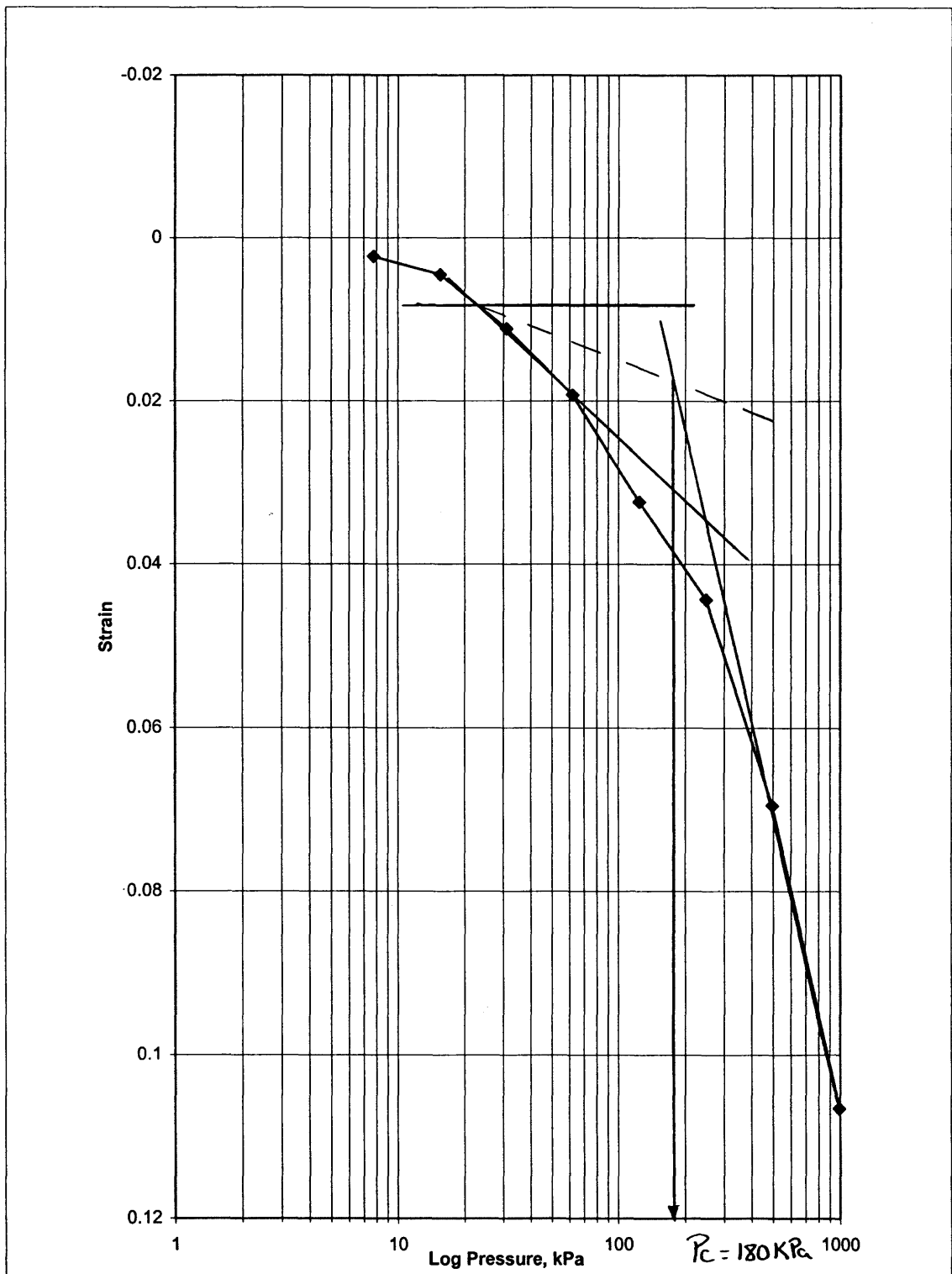


Figure 3.3 Strain vs. Log Pressure; 0.25 kg – 32 kg (S-1).

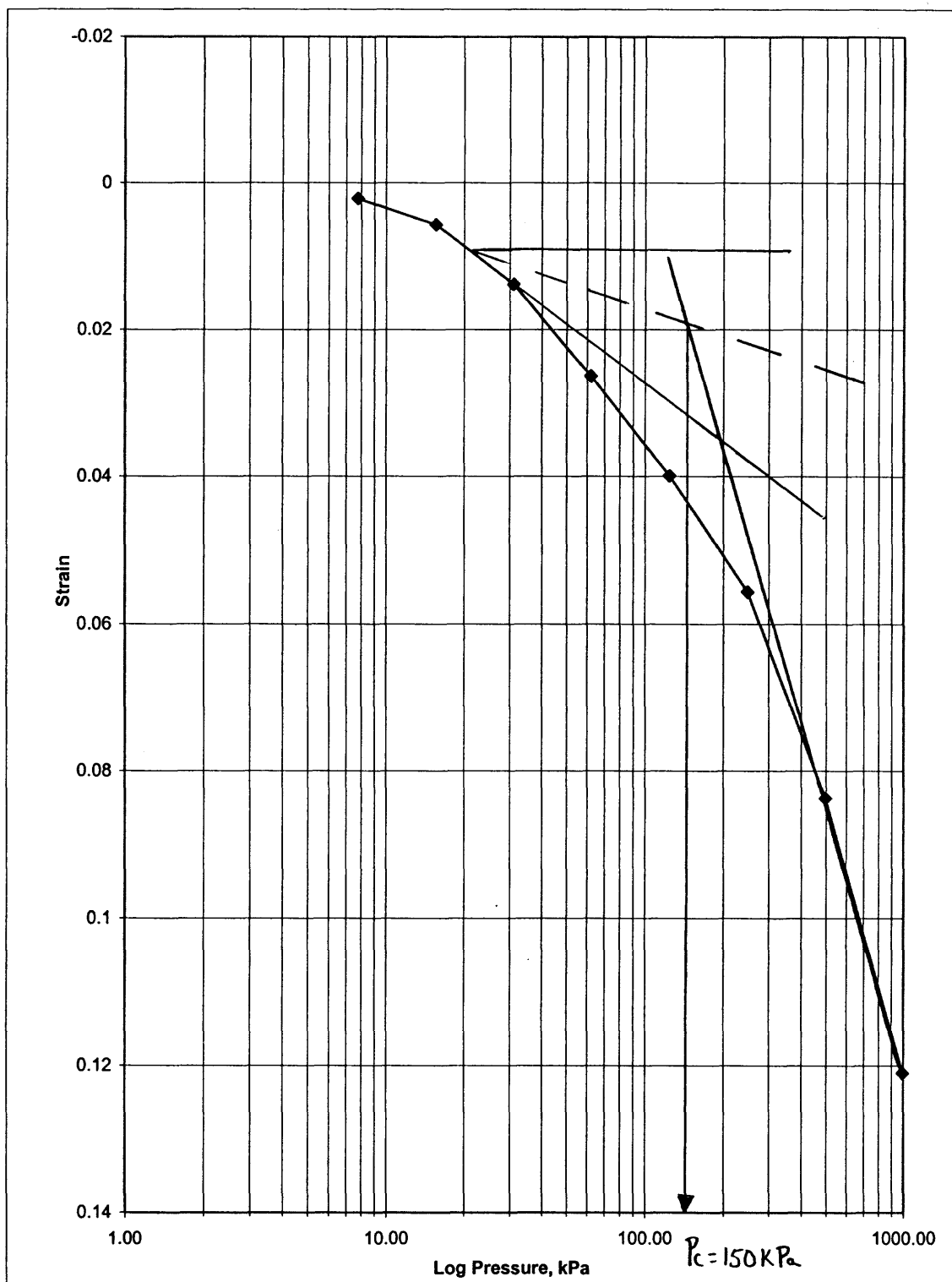


Figure 3.4 Strain vs. Log Pressure; 0.25 kg – 32 kg (S-2).

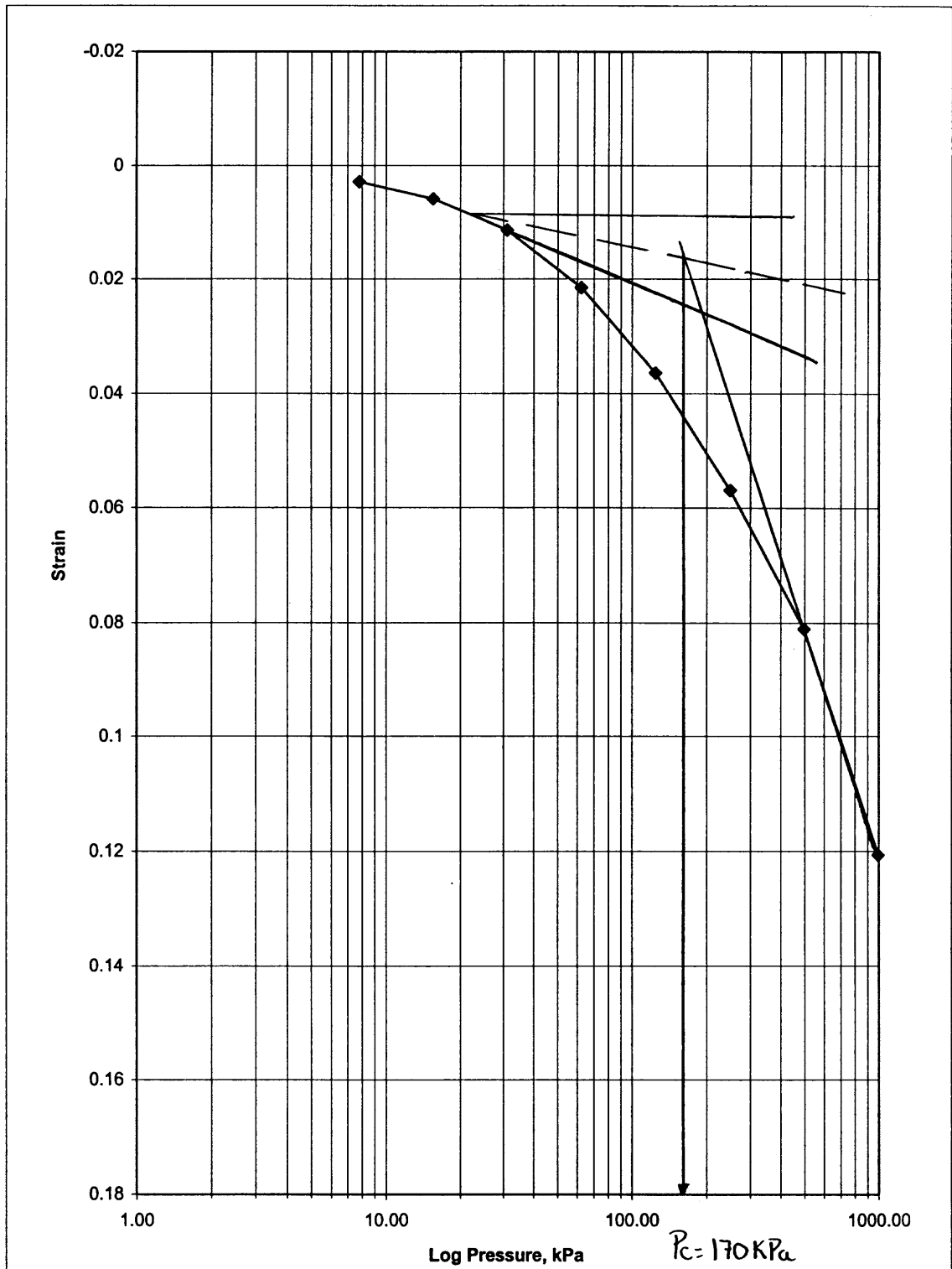


Figure 3.5 Strain vs. Log Pressure; 0.25 kg – 32 kg (S-3).

Table 3.4 Lab Test Summary Data #2Consolidation

C_α calculated for loads of 994.42 and 996.0 Kpa for S-1 & S-2.

For S-3 loads of 996.0 & 1992.0 Kpa were used.

Sample #	P_0 (Kpa)	P_c (Kpa)	OCR	C_α	C_c Graph	C_α/C_c
S-1	91.0	180.0	1.978	0.00272	0.123	0.022114
S-2	91.0	160.0	1.758	0.00265	0.123	0.021545
S-3	91.0	170.0	1.868	0.00262	0.132	0.019848
	91.0	150.0	1.648	0.002	0.122	0.016393
Schmert.	91.0	165.0	1.813		0.224	0.008929
Average			1.813			

Triaxial

Sample #	σ'_1 (psi)	σ'_3 (psi)	σ_1 (psi)	σ_3 (psi)	τ (psi)	t (min)	P (lb.)	U (psi)
S-1	11.60	2.07	38.15	28.62	4.765	1428.1	23.29	26.55
S-2	11.47	2.81	49.07	40.41	4.33	1428.2	23.11	37.6
S-3	11.99	2.48	59.12	49.61	4.755	1428.2	26.94	47.13

Sample #	σ'_1 (kPa)	σ'_3 (kPa)	σ_1 (kPa)	σ_3 (kPa)	τ (kPa)	t (min)	P (N)	U (kPa)
S-1	79.92	14.26	262.85	197.2	32.83	1428.1	10.56	182.93
S-2	79.03	19.36	338.09	278.42	29.83	1428.2	10.48	259.06
S-3	82.61	17.09	407.34	341.81	32.76	1428.2	12.22	324.72

Since the Schmertmann method represents the field curve conditions; a conservative estimate of 165 kPa was used as the preconsolidation pressure. The graphical construction of P_c can be seen in Figures 3.3-3.7. Figure 3.8 shows all three samples on one graph.

The effective overburden pressure (σ'_0) for this clay layer was approximated at 91.0 kPa. This value was estimated by using the unit weight values that were presented in Joao Luiz Castro Sampaio Junior's thesis of consolidation for the overlying soils and the calculated unit weight for the Belem clay. In comparison, since both studies are from

the same region, the soil profile analyzed in Sampaio Jr. (1995) is very similar to this research. The main difference in research is the two types of clays that lie at similar depths. This soil classifies as a slightly overconsolidated clay with an average overconsolidation ratio (OCR) of 1.8. Since the OCR is rather low, this soil may also be classified as a nearly normally consolidated clay.

The coefficient of consolidation, C_v , was found by two graphical procedures, the logarithm of time and square root of time fitting method. The results of the three tests can be seen in Appendix A, Figures A.1-A.29. The summary of values can be seen in Table 3.5. Both methods were used for comparison. Most of the values deviate by approximately 5%. Some deviate higher due to the difficulty in locating the end of primary consolidation. The graphs representing C_v vs. pressure can be seen in Figures B.1-B.3.

Table 3.5 Summary of C_v (Graphical Procedure)

Test #	S-1		S-2		S-3	
Load (kPa)	Log Time C_v (cm ² /s)	Sqrt. Time C_v (cm ² /s)	Log Time C_v (cm ² /s)	Sqrt. Time C_v (cm ² /s)	Log Time C_v (cm ² /s)	Sqrt. Time C_v (cm ² /s)
7.78	0.018601	0.006006	0.008430	0.004461	0.005058	0.007391
15.56	0.006490	0.015601	0.006091	0.004875	0.001635	0.005987
31.13	0.004293	0.015601	0.007509	0.003776	0.007224	0.007391
62.25	0.008587	0.012258	0.012451	0.006536	0.006576	0.014171
124.50	0.006566	0.016685	0.006091	0.012040	0.010496	0.014171
249.00	0.007249	0.008313	0.007615	0.013964	0.011126	0.016623
498.00	0.003189	0.006655	0.004386	0.007283	0.006953	0.014171
996.00	0.002536	0.004171	0.003916	0.005900	0.012354	0.016623
1992.00	-	-	-	-	0.003973	0.007247
498.00	-	-	-	-	0.007948	-
124.50	-	-	-	-	0.002419	-
31.13	-	-	-	-	0.001391	-
7.78	-	-	-	-	0.000397	-

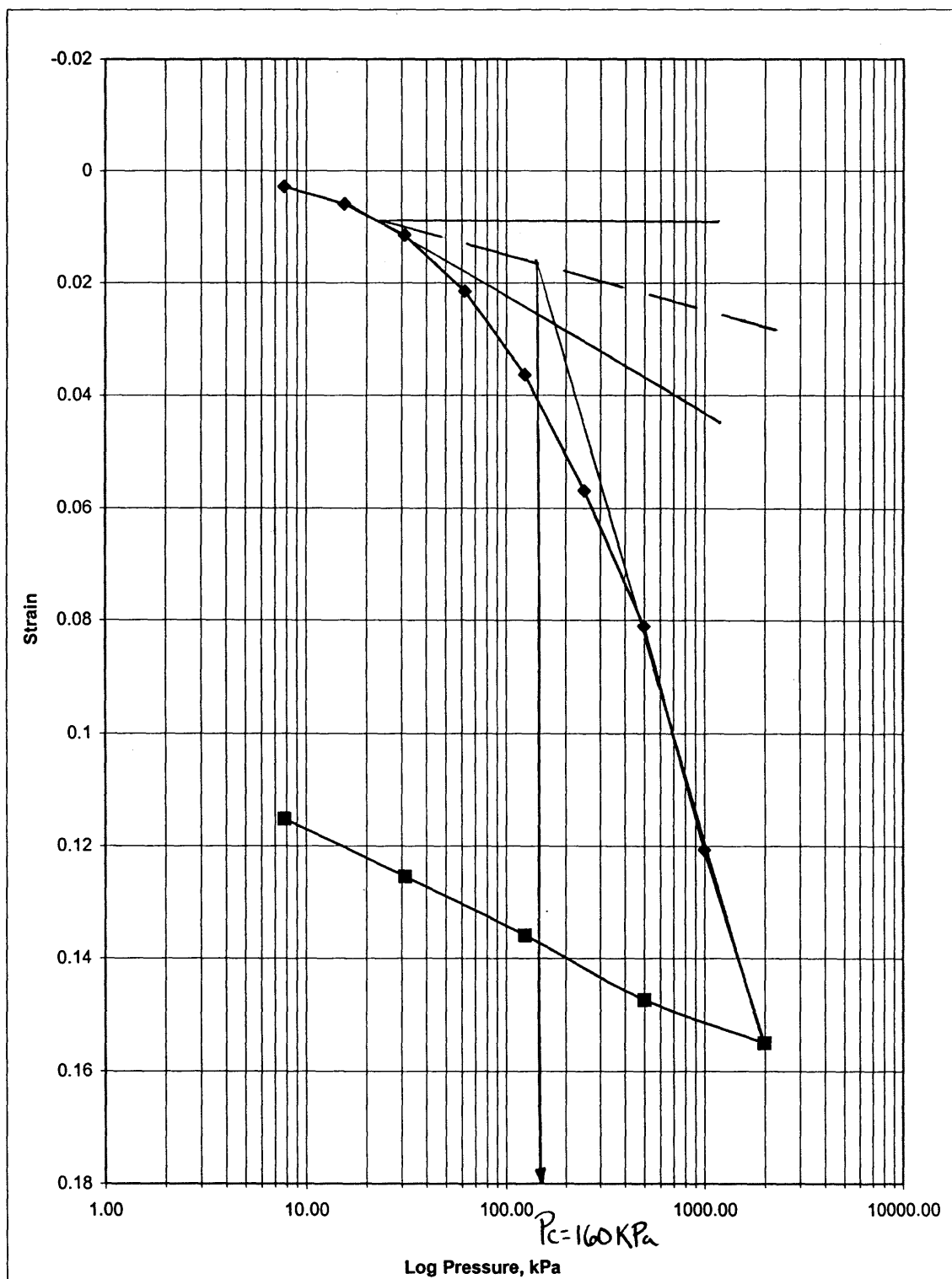


Figure 3.6 Strain vs. Log Pressure; 0.25 kg – 64 kg (S-3).

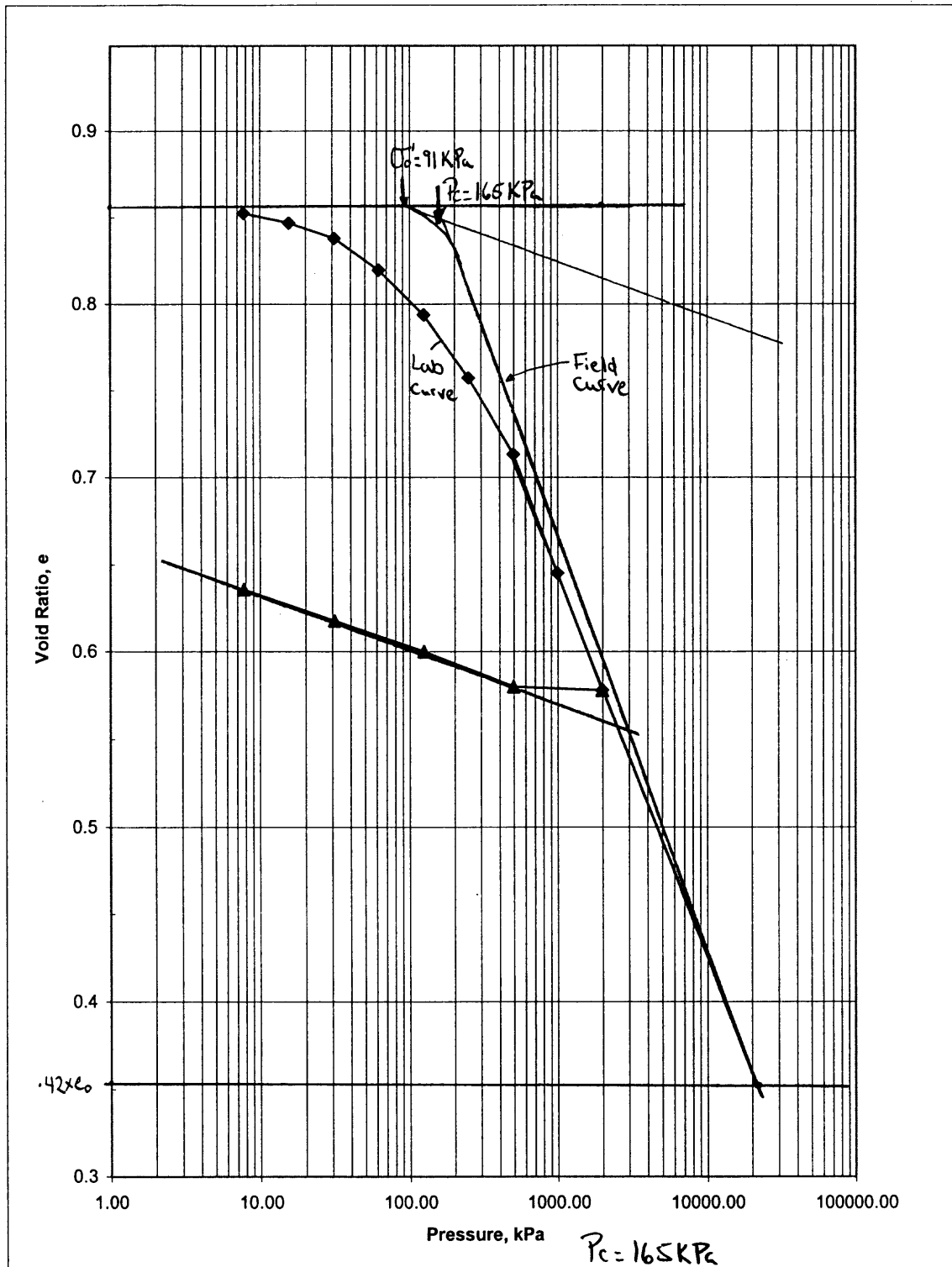


Figure 3.7 Void ratio vs. Log Pressure; Schmertman Method (S-3).

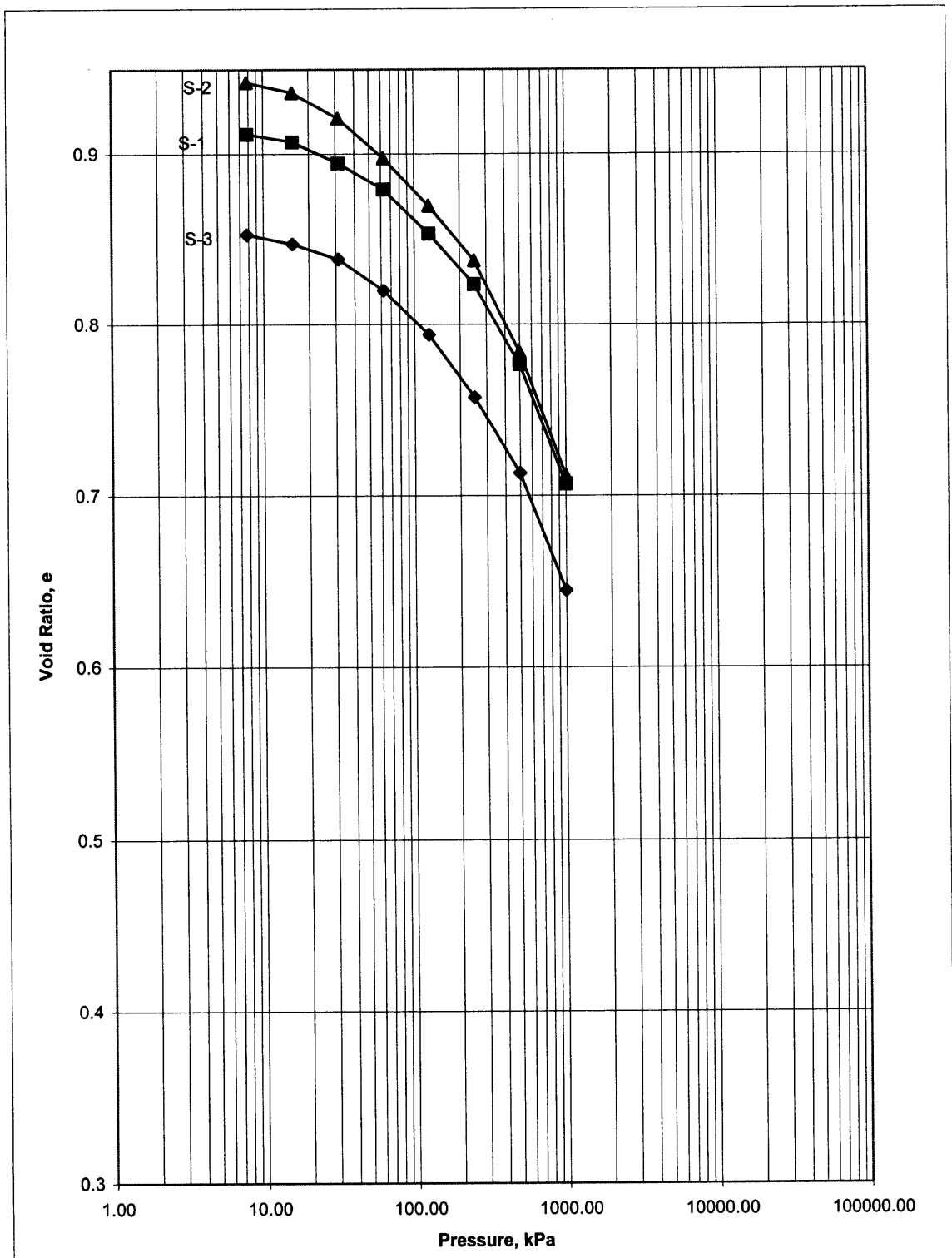


Figure 3.8 Void Ratio vs. Log Pressure (S-1, S-2, S-3).

The third method for calculating C_v , which can be considered to be the most accurate, uses values from the logarithm of time method such as D_{50} , D_{100} , and t_{50} . These values are used together with void ratio and strain data to calculate a more accurate value of C_v (Table 3.6 & 3.7). The average range for these values is between $0.003 - 0.006 \text{ cm}^2/\text{s}$. Holtz and Kovacs illustrate typical values of C_v in Table 3.8. The Belem clay most closely resembles the Boston blue clay (CL) with a C_v value of $0.004 \pm 0.002 \text{ cm}^2/\text{s}$. Figures 3.9 – 3.11 (Appendix B) represents the data from Table 3.6 and 3.7 as C_v vs. log pressure.

Table 3.6 Consolidation Raw Data (S-1 and S-2)**Sample # 1**H_i = 1.0267 inches e_o = 0.916H_{vi} = 0.4908 inches e_f = 0.7331H_s = 0.5358 inches Added deformation for D100 & D50 to account for test disturbar 0.0362

Load Increment kPa	D50 Inches	D100 Inches	Equipment deform. ΔH_e Inches	Void Ratio e	Strain e	Average sample ht. H in.	H used for cv in.	t50 min	cv in ² /min	cv cm ² /s
0.00	0	0	0	0	0	0	0	0	0	0
7.77	0.00108	0.00154	0.00075	0.911726	0.0007695	1.02562	0.51281	0.3	0.17269	0.01857
15.54	0.00321	0.0038	0.00095	0.907135	0.0027759	1.02349	0.511745	0.86	0.05999	0.00645
31.08	0.00843	0.01007	0.00145	0.894499	0.0083958	1.018275	0.5091375	1.3	0.03928	0.00422
62.15	0.0159	0.0177	0.0021	0.879046	0.0151943	1.0108	0.5054	0.65	0.07741	0.00832
124.3	0.02733	0.0308	0.003	0.852917	0.027077	0.99937	0.499685	0.85	0.05787	0.00622
248.61	0.0053	0.00948	0.0039	0.891028	0.0054349	1.0214	0.5107	0.77	0.06673	0.00717
497.21	0.02485	0.0338	0.0048	0.843958	0.0282458	1.00185	0.500925	1.75	0.02825	0.00304
994.42	0.0554	0.07	0.00585	0.774436	0.0624817	0.9713	0.48565	2.2	0.02112	0.00227

Sample # 2H_i = 1.0175 inches e_o = 0.9462H_{vi} = 0.4947 inches e_f = 0.7524H_s = 0.5228 inches Added deformation for D100 & D50 to account for test disturbar 0.0424

Load Increment kPa	D50 Inches	D100 Inches	Equipment deform. ΔH_e Inches	Void Ratio e	Strain e	Average sample ht. H in.	H used for cv in.	t50 min	cv in ² /min	cv cm ² /s
0.00	0	0	0	0	0	0	0	0	0	0
7.78	0.00117	0.0015	0.0005	0.912267	0.000974	1.02553	0.512765	0.65	0.07969	0.00857
15.56	0.00365	0.0044	0.0008	0.906295	0.0035064	1.02305	0.511525	0.9	0.05727	0.00616
31.13	0.01035	0.01196	0.0012	0.891439	0.0104802	1.01635	0.508175	0.73	0.06969	0.00749
62.25	0.02149	0.02398	0.0015	0.868445	0.0218954	1.00521	0.502605	0.44	0.1131	0.01216
124.50	0.03532	0.03836	0.0018	0.841047	0.0356092	0.99138	0.49569	0.9	0.05378	0.00578
249.00	0.05065	0.0549	0.0021	0.809617	0.0514269	0.97605	0.488025	0.72	0.06517	0.00701
498.00	0.07415	0.0821	0.0028	0.757545	0.0772378	0.95255	0.476275	1.25	0.03575	0.00384
996.00	0.10505	0.1186	0.0039	0.68737	0.1117172	0.92165	0.460825	1.4	0.02988	0.00321

The compression index, C_c, was calculated using the graphical method for Figures 3.3 - 3.7. The slope of the virgin compression curve represents the value C_c. The value of C_c for this clay ranges from 0.12 - 0.23 (refer to Table 3.4). These results are compared to typical values shown in Table 3.9 (Holtz and Kovacs). The Belem clay most closely resembles the Chicago silty clay (CL) with C_c range of 0.15 – 0.3. It also borderlines normally consolidated medium sensitive clays with a C_c range of 0.2 – 0.5.

Table 3.7 Consolidation Raw Data (S-3)

Sample # 3

H_i = 1.025 inches e_o = 0.8569
 H_v = 0.473 inches e_f = 0.6675
 H_s = 0.5519 inches

Load Incr., kPa	D50 Inches	D100 Inches	Equipment deform. ΔH_e Inches	Void Ratio e	Strain ϵ	Average sample ht. H In.	H used for cv in.	t50 min	cv in ² /min	cv cm ² /s
0.00	0	0	0	0	0	0	0	0	0	0
7.78	0.001315	0.00199	0.0005	0.852388	0.001454	1.023685	0.511843	1.1	0.046919	0.00504
15.56	0.003855	0.00471	0.0008	0.846916	0.003815	1.021145	0.510573	3.4	0.015104	0.00162
31.13	0.00773	0.00927	0.0012	0.837929	0.007873	1.01727	0.508635	0.77	0.066189	0.00712
62.25	0.01636	0.01905	0.0015	0.819665	0.017122	1.00864	0.50432	0.73	0.068637	0.00738
124.50	0.029625	0.033	0.0018	0.793845	0.030439	0.995375	0.497688	0.53	0.092067	0.0099
249.00	0.0479	0.053	0.0021	0.757063	0.049659	0.9771	0.48855	0.5	0.09404	0.01011
498.00	0.0688	0.0766	0.0028	0.713033	0.072	0.9562	0.4781	0.8	0.056288	0.00605
996.00	0.09965	0.113	0.0039	0.645086	0.106439	0.92535	0.462675	0.45	0.093714	0.01008
1992.00	0.13705	0.1484	0.0056	0.577864	0.139317	0.88795	0.443975	1.4	0.027737	0.00298
498	0.151225	0.1501	0.0028	0.579857	0.143707	0.873775	0.436888	0.7	0.053716	0.00578
124.5	0.1435	0.14	0.0018	0.599969	0.134829	0.8815	0.44075	2.3	0.016639	0.00179
31.13	0.134775	0.1308	0.0012	0.617726	0.126439	0.890225	0.445113	4	0.009758	0.00105
7.78	0.12525	0.1216	0.0005	0.635664	0.118146	0.89975	0.449875	14	0.002848	0.00031

Table 3.4 also shows values of the secondary compression index, C_α ranging between 0.002 – 0.0027. This was calculated using graphical data from the logarithm of time method. This is computed as the slope of the secondary consolidation portion of the graph. The values for C_α represented in Figure 3.4 were calculated for loads of 994.42 kPa and 996.0 kPa.

Table 3.8 Typical Values of the Coefficient of Consolidation, C_v (Holtz & Kovacs, 1981)

Soil	C_v	
	$\text{cm}^2/\text{s}, \times 10^{-4}$	m^2/yr
Boston blue clay (CL) (Ladd and Luscher, 1965)	40 ± 20	12 ± 6
Organic silt (OH) (Lowe, Zaccheo, and Feldman, 1964)	2–10	0.6–3
Glacial lake clays (CL) (Wallace and Otto, 1964)	6.5–8.7	2.0–2.7
Chicago silty clay (CL) (Terzaghi and Peck, 1967)	8.5	2.7
Swedish medium sensitive clays (CL-CH) (Holtz and Broms, 1972)		
1. laboratory	0.4–0.7	0.1–0.2
2. field	0.7–3.0	0.2–1.0
San Francisco Bay Mud (CL)	2–4	0.6–1.2
Mexico City clay (MH) (Leonards and Girault, 1961)	0.9–1.5	0.3–0.5

Table 3.9 Typical Values of the Compression Index, C_c (Holtz & Kovacs, 1981)

Soil	C_c
Normally consolidated medium sensitive clays	0.2 to 0.5
Chicago silty clay (CL)	0.15 to 0.3
Boston blue clay (CL)	0.3 to 0.5
Vicksburg buckshot clay (CH)	0.5 to 0.6
Swedish medium sensitive clays (CL-CH)	1 to 3
Canadian Leda clays (CL-CH)	1 to 4
Mexico City clay (MH)	7 to 10
Organic clays (OH)	4 and up
Peats (Pt)	10 to 15
Organic silt and clayey silts (ML-MH)	1.5 to 4.0
San Francisco Bay Mud (CL)	0.4 to 1.2
San Francisco Old Bay clays (CH)	0.7 to 0.9
Bangkok clay (CH)	0.4

Figure 3.12 plots modified secondary compression index (%) versus natural water content after Mesri, 1973 (as cited in Holtz and Kovacs, 1981) for several clays. The Belem soil falls on the boundary line between Boston blue clay and Chicago blue clay with $C'_\alpha(\%)=1.9$ and $w(\%)=31$. In Table 3.10 (Values of C_α/C_c for natural soils) the Belem soil (0.008 – 0.022) comes close to Sensitive clay, Portland, ME (0.025 – 0.055) and Soft blue clay (0.026), but does not fall within the range.

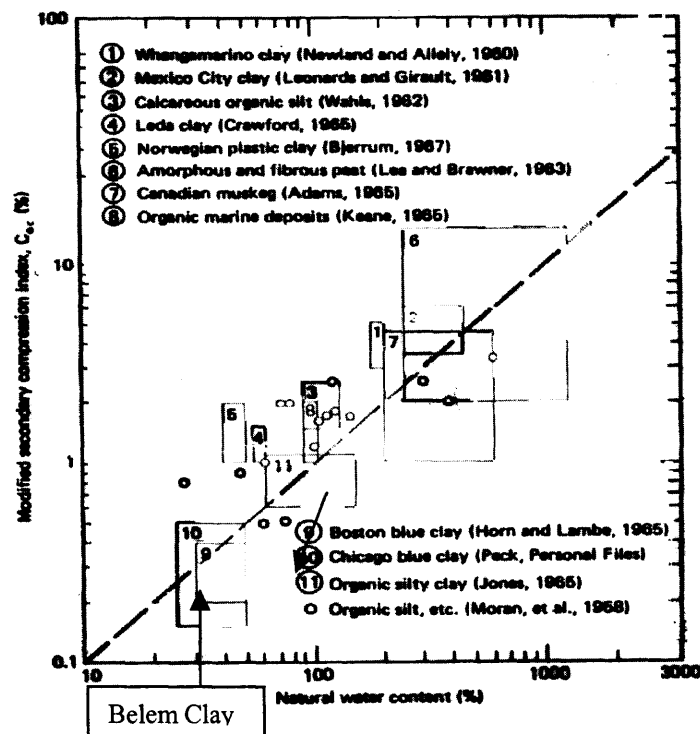


Figure 3.12 Modified secondary compression index versus natural water content. (Holtz & Kovacs, 1981)

Table 3.10 Values of C_α/C_c for Natural Soils (Holtz & Kovacs, 1981)

Soil	C_α/C_c
Organic silts	0.035–0.06
Amorphous and fibrous peat	0.005–0.085
Canadian muskeg	0.09–0.10
Leda clay (Canada)	0.03–0.06
Post-glacial Swedish clay	0.05–0.07
Soft blue clay (Victoria, B.C.)	0.026
Organic clays and silts	0.04–0.06
Sensitive clay, Portland, ME	0.025–0.035
San Francisco Bay Mud	0.04–0.06
New Lakeard (Canada) varved clay	0.03–0.06
Mexico City clay	0.03–0.035
Hudson River silt	0.03–0.06
New Haven organic clay silt	0.04–0.075

*Modified after Mesri and Godlewski (1977).

As mentioned before, this soil possesses some signs of a borderline normally consolidated soil. Another indication to this statement is the shape of the consolidation curves. Figures 3.3 – 3.7 show curves that lack some shape. There is no real flat section and so no distinct break after P'_c has been reached. Some consideration must be given to sample disturbance. The disturbance is mainly attributed to transport time and storage during travel. This sample disturbance may have caused the graphs to take the shape they possess. It may also be possible that this soil holds some characteristics of a normally consolidated clay. Additional consolidation tests are recommended with the proper sampling and testing conditions in order to rule out sample disturbances and possible equipment failure or error.

3.6 Triaxial Test

The undrained shear strength parameters of the specimen were determined using the ASTM D 4767-88 procedures for a consolidated –undrained test with pore pressure measurements.

Three samples were trimmed from an 8” section of the Shelby tube. The trimming became very tedious due to the soft consistency of the clay. The first sample had an approximate 1” intrusion of a stiffer light gray CLAY & SILT. The next two samples were consistent with the rest of the tube with the exception of less sand seams and a few wood fragments embedded in the sample.

Head (1981) discusses that the confining pressures should be $\frac{1}{2}$, 1 and 2 time the effective overburden pressure of the sample. The effective overburden pressure used for this test was calculated to be 84.0 kPa. The confining pressure for the first sample was set to 55.16 kPa. This pressure was so low that the saturation stage of the test was lasting for a longer period than previously expected. As a result, the backpressures for the test were changed to 206.84, 275.80 and 344.74 kPa respectively. The saturation period thus dropped from a week to approximately 2 days. A 27.58 kPa pressure differential was used in the consolidation stage of the test. Complete consolidation was reached in approximately one day. This 27.58 kPa consolidation pressure was used for all three tests. Shear strength parameter results can be found in Table 3.4. These values ranged from 29.83 kPa to 32.83 kPa.

This test was not conducted with great consistency due to inexperience. The three tests were run at different conditions. The first was run with a rubber membrane and filter strips. The second was run with a condom and no filter strips. The rubber

membrane in the first sample proved to be too thick. The third was run with a condom and filter strips. The proper membrane compliance adjustments were calculated according to ASTM D 4767. Lack of sufficient soil resulted in the inability to repeat the test. The results showed that the consolidation pressure was too low. Table 3.4 shows that the maximum value for σ'_1 (82.6 kPa) did not exceed the true overburden pressure of approximately 91 kPa. This makes it difficult to properly estimate the internal angle of friction and the cohesion. The indication that the test had not been performed properly was in the construction of the Mohr circles (Figure B.15). They did not follow the normal textbook pattern or anything close to that. They overlapped each other and thus made it impossible to use. This essentially produced an average value of 4.61 psi or 31.81 kPa for the undrained shear strength parameter. The reason for this is that the normal stress at failure for both S-1 and S-2 were nearly equal. The graphs for the three samples tested can be found in Appendix B and the summary of results in Table 3.4.

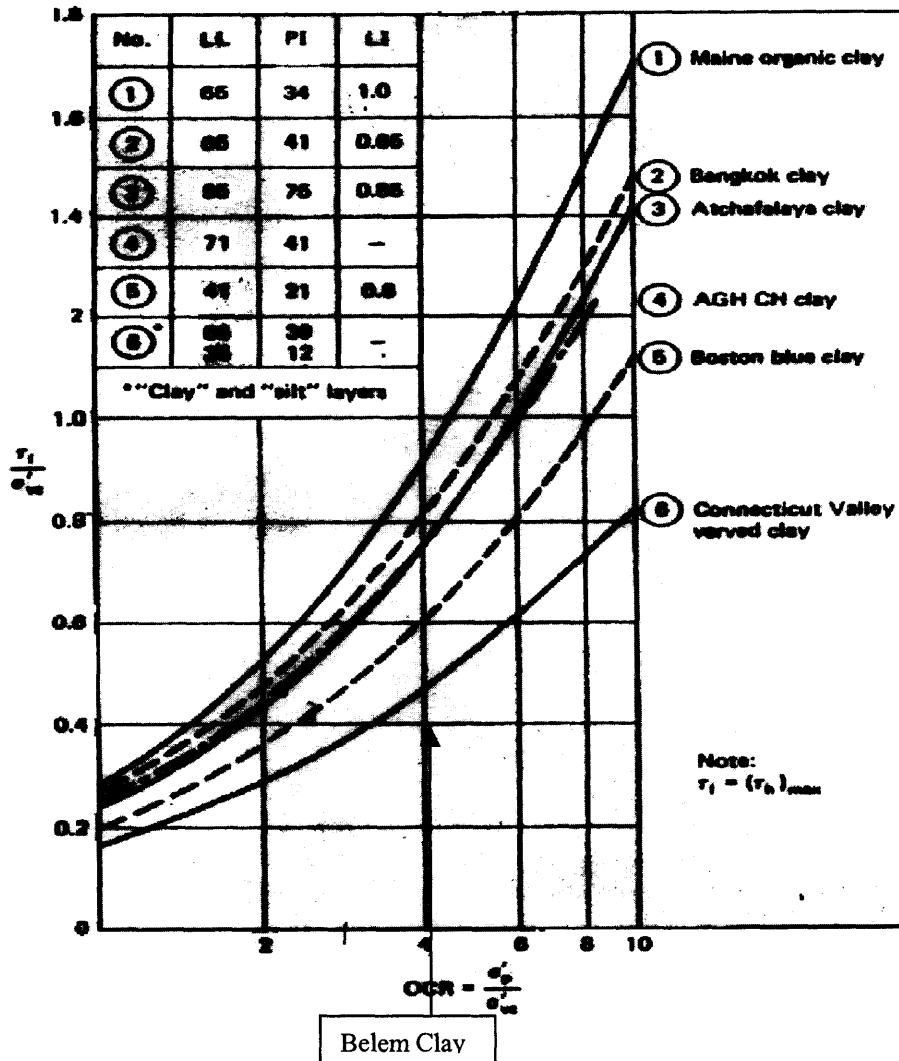


Figure 3.13 Undrained strength ratio versus overconsolidation ratio from direct simple shear tests on six clays. (Holtz and Kovacs, 1981)

According Ladd and Edgers, 1972, and Ladd, et al., 1977, Figure 3.13 represents the undrained strength ratio versus overconsolidation ratio from direct-simple shear tests on six clays (as cited in Holtz and Kovacs, 1981). The Belem clay analyzed falls close to the Boston blue Clay.

CHAPTER 4

CONCLUSIONS AND RECOMMENDATIONS

4.1 Conclusions

The present work has the principal objective to study the characteristics of compressibility of an argilous stratum that can be found in large areas of the metropolitan region of Belem in the state of Para, Brazil,

The argilous material that makes up this stratum is alluvial in origin with possible marine intrusions. The geologic time setting refers to the Tertiary/Quaternary period pertaining to the Barreiras Group. The Belem clay is varved in nature, which is characteristic of its complex depositional setting. The consistency of this material varies from soft to medium according to N-SPT. The material varies in color, but is predominantly dark gray.

The study of this material is based on the results obtained from an experimental program involving characterization, compression and triaxial tests using undisturbed samples.

The characterization tests demonstrate that the soil is of medium plasticity with an average plasticity index (PI) of 18.5% and liquid limit of 35.5%. It can be classified under the Burmeister classification system as a Dark Gray SILT & CLAY, little fine Sand with regular sand partings (varved of a lighter Gray coloration; & medium grain size). The Unified System classifies the soil as an inorganic clay of medium plasticity (CL).

The compression tests characterize the Belem clay as a slightly overconsolidated clay with some characteristics of a normally consolidated clay. Its preconsolidation pressure was estimated to be approximately 165 kPa and its effective overburden pressure as 91 kPa. Other properties such as the overconsolidation ratio $OCR = 1.8$, compression index $C_c = 0.23$, coefficient of consolidation $C_v = 0.003-0.006$ and the secondary compression index $C_\alpha = 0.002$ were calculated and used to better understand the clay characteristics. According to the sources utilized in this paper, the Belem clay is most similar to the Boston blue clay. Further research on this clay is recommended for possible links between the two soil characteristics and to properly determine and classify its stress history. Table 3.11 shows typical values for the clay layer analyzed by Sampaio Jr. It is important to notice that even though both clay layers analyzed (by myself and Sampaio Jr.) lie at similar depths, have been virtually exposed to the same geologic conditions and are found quite frequently throughout the city of Belem, they still possess distinct characteristics. These differences may be mainly attributed to the laterization process, due to quantities of iron oxide that occur in the clay analyzed by Sampaio Jr.

Table 3.11 Consolidation Test Results for Sampaio Jr. Clay Analysis

TEST #	CONV1	CONV2	CONV3	CONV4
Depth (m)	11.36	11.33	11.3	10.69
C_c	0.7	0.7	0.5	0.35
C_r	0.04	0.04	0.02	0.02
C_s	-	-	-	0.06
P_o (kPa)	83.5	83.3	83.1	78.5
P'_c (kPa) (Casag.)	385	380	288	315
OCR (Casag.)	4.6	4.5	3.4	4
P'_c (kPa) (Janbu)	500	500	325	500
OCR (Janbu)	5.9	6	3.9	6.3
E_t (kPa)	6700	6600	6750	4800
P'_c (kPa) (Pac. Sil.)	-	-	-	250
OCR (Pach. Silva)	-	-	-	3.1

The triaxial tests for the most part were unsuccessful. The sample was not consolidated past its preconsolidation pressure and so the results essentially yielded undrained shear strength. The only valuable information was the shear strength of the soil with an average shear strength of 31.8 kPa. The graphs representing the values on Table 3.4 are found in Appendix B. Further research is needed to obtain the proper information.

4.2 Recommendations

It is highly recommended that this soil be analyzed in a series of triaxial test. The triaxial test is the most reliable and the closest method to mimic field stress conditions in a laboratory. Geotechnical engineers should use this data in conjunction the consolidation test to calculate immediate, primary and secondary consolidation settlement that can occur when buildings are founded on the dense 4 m thick sand layer that lies on top of this varved clay. Due to the soft consistency of this clay, it is often recommended with higher loads to drive piles past this layer to the very dense sand layer located approximately 14 m (42 ft.) below the ground surface. Regardless of the general geology, a subsurface exploration should be mandatory even when dealing with residential structures. Most failures have occurred in residential areas, where a subsurface exploration was not performed and construction not supervised.

Belem is a fairly young city as far as high-rise buildings are concerned. Thus the data obtained from this analysis can be used to see where these buildings lie in a time/consolidation spectrum. Buildings that were constructed thirty to forty years ago

may not have taken into account long-term settlements. This leaves an open end to what the future of these structures hold (Alencar, 1999).

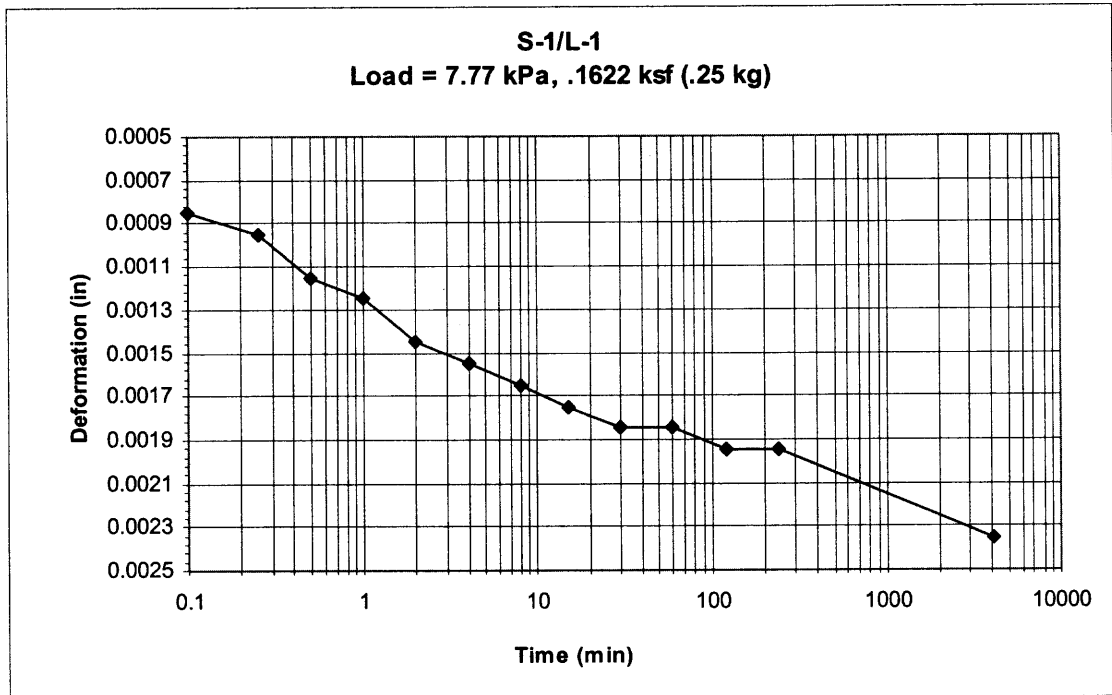
It is also highly recommended that more consolidation tests be run in order to determine its accurate stress history. Proper sampling and testing conditions must be met to rule out any erroneous data. The answer to whether this clay is normally consolidated or overconsolidated is very important information to the designing engineer.

APPENDIX A
TIME RATE OF CONSOLIDATION
GRAPHS

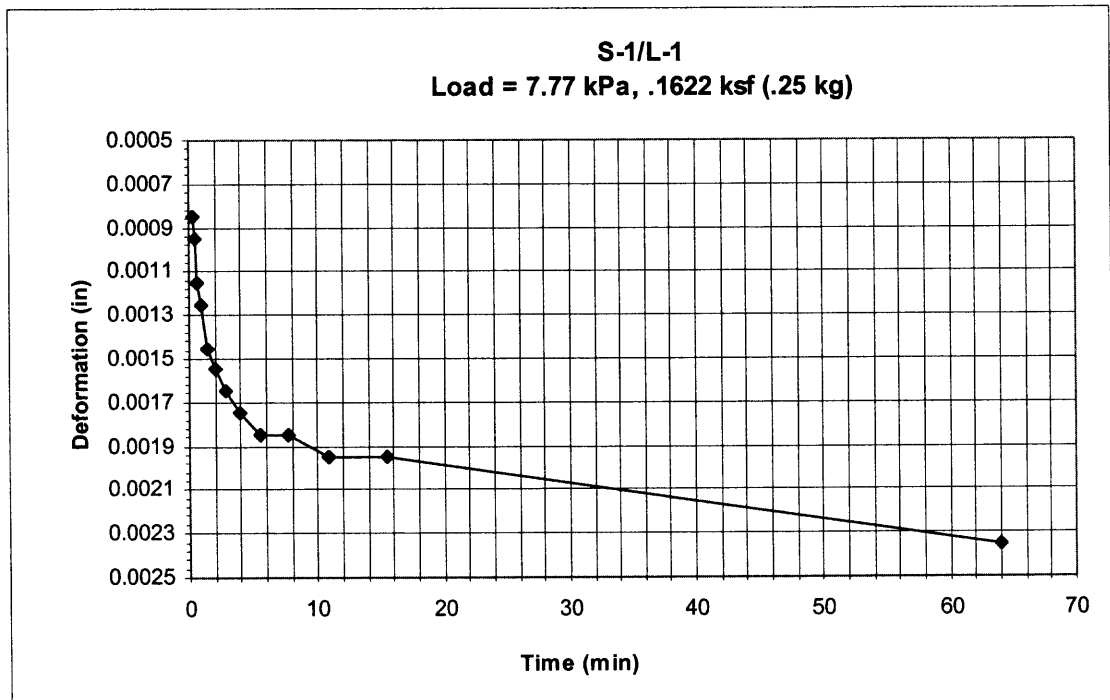
The following graphs represent the time rate of consolidation curves for samples 1-3.

The first two samples (S-1 and S-2) were loaded from 7.77 kPa to 994.42 kPa where the last sample (S-3) was loaded to 1988.84 kPa and unloaded at $\frac{1}{4}$ load decrements. Each

Figure is represented by two graphs that are later used to calculate and compare values of the coefficient of consolidation C_v . The two graphs show the logarithm of time method (a) and the square root of time method (b). The graph titles are interpreted as for example sample #1, load #1 (S-1/L-1). The last three graphs represent C_v vs. pressure.

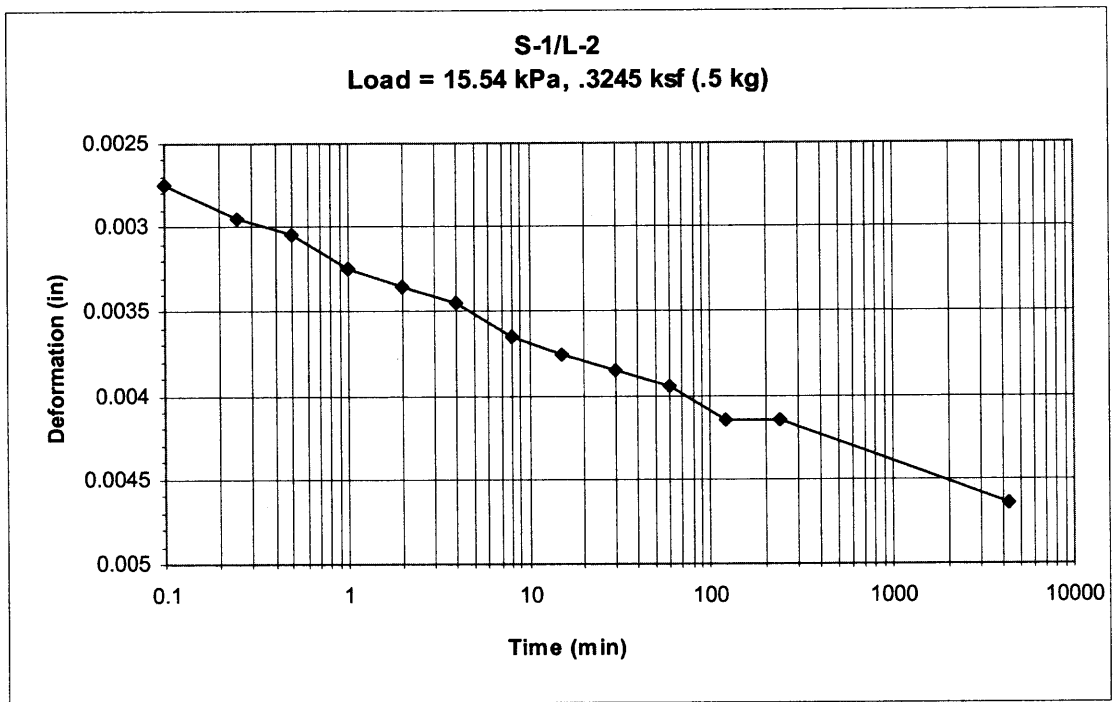


(a)

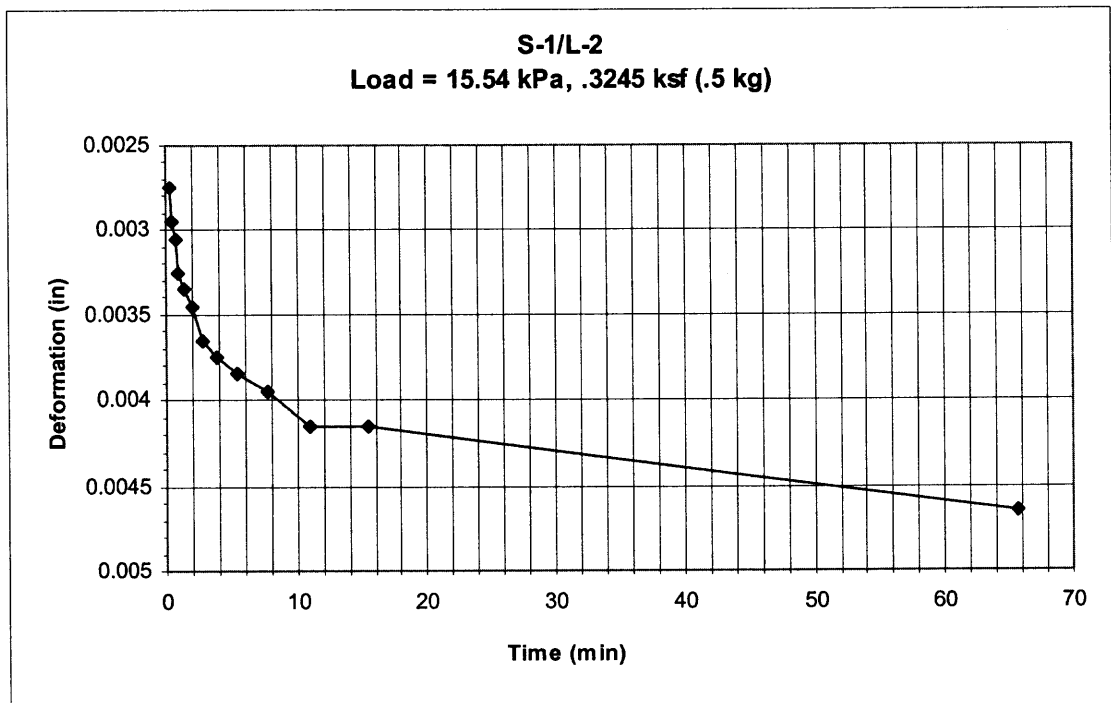


(b)

Figure A.1 Logarithm of time method (a) and square root of time method (b) for S-1/L-1.

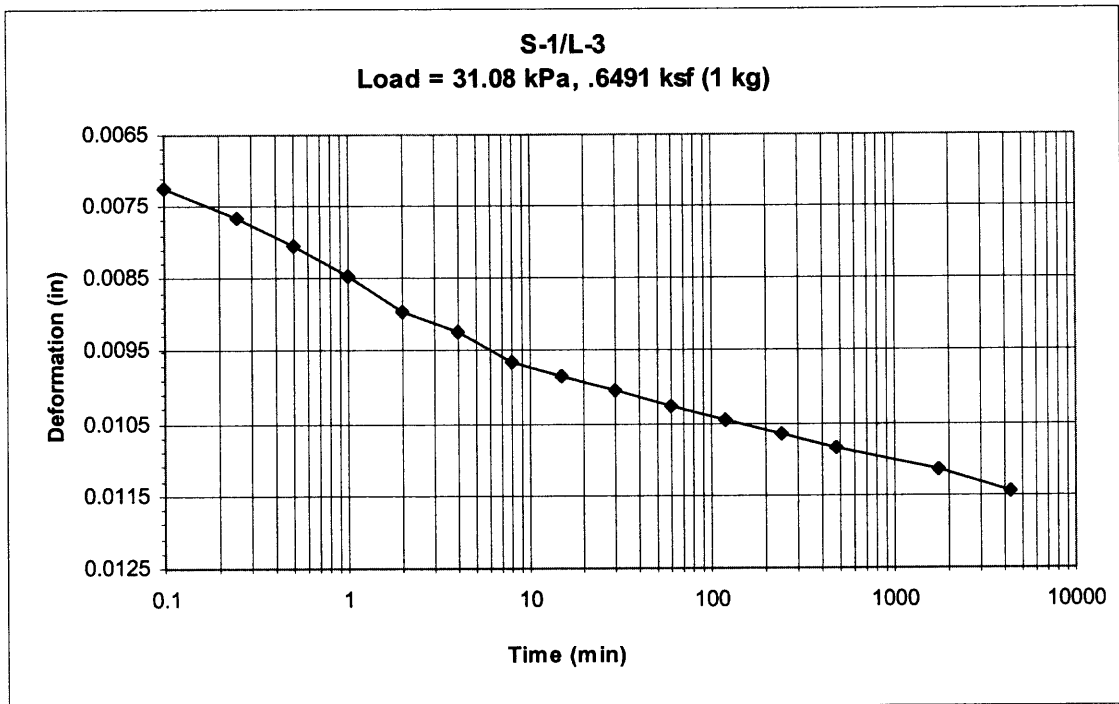


(a)

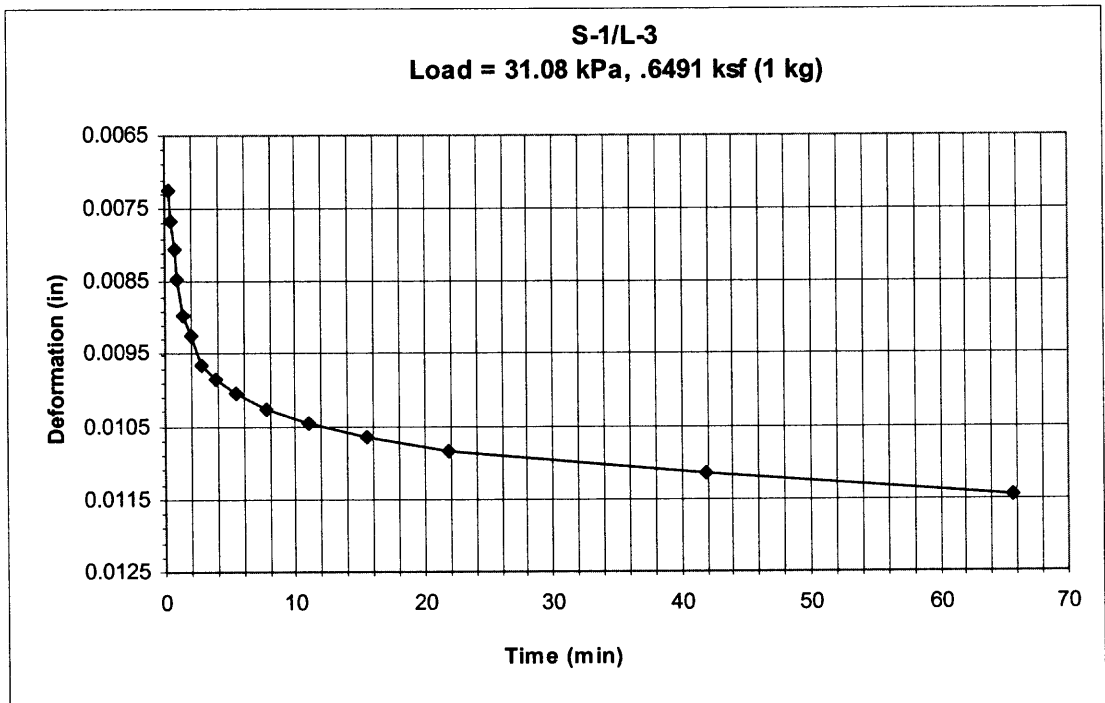


(b)

Figure A.2 Logarithm of time method (a) and square root of time method (b) for S-1/L-2.

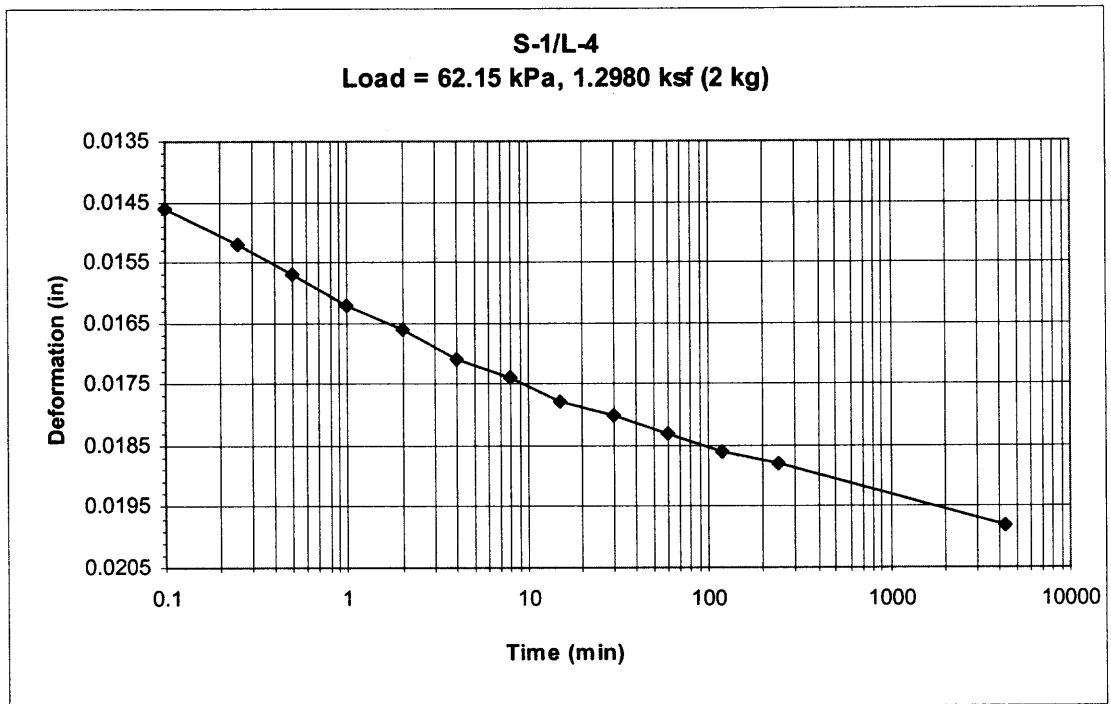


(a)

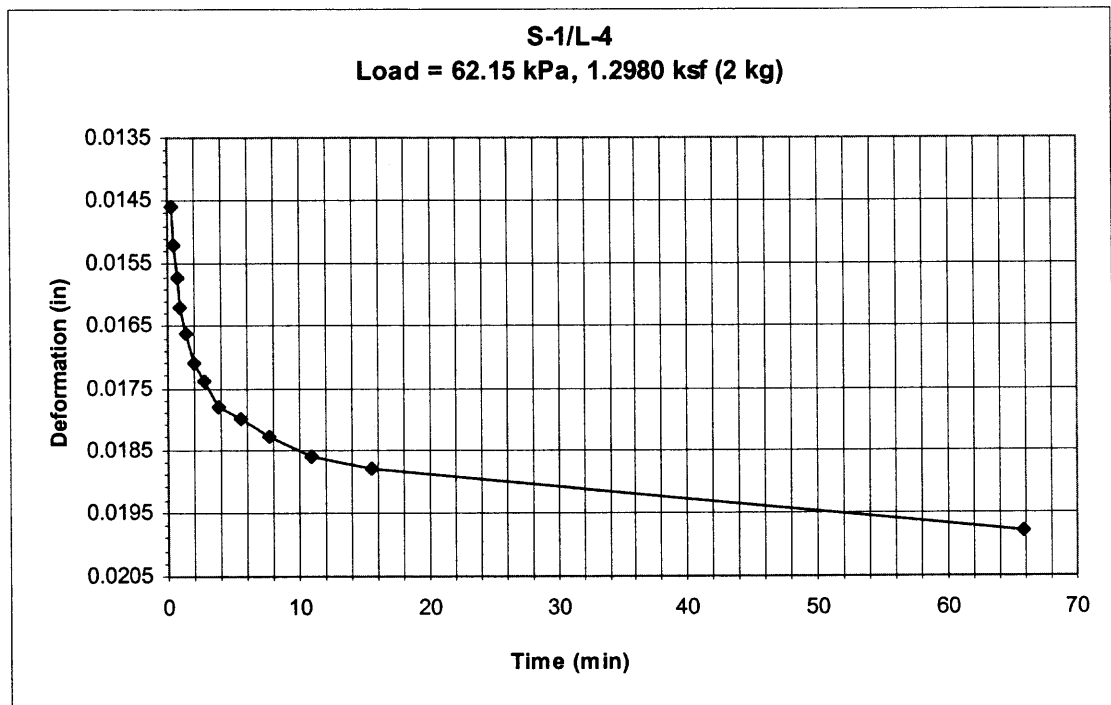


(b)

Figure A.3 Logarithm of time method (a) and square root of time method (b) for S-1/L-3.

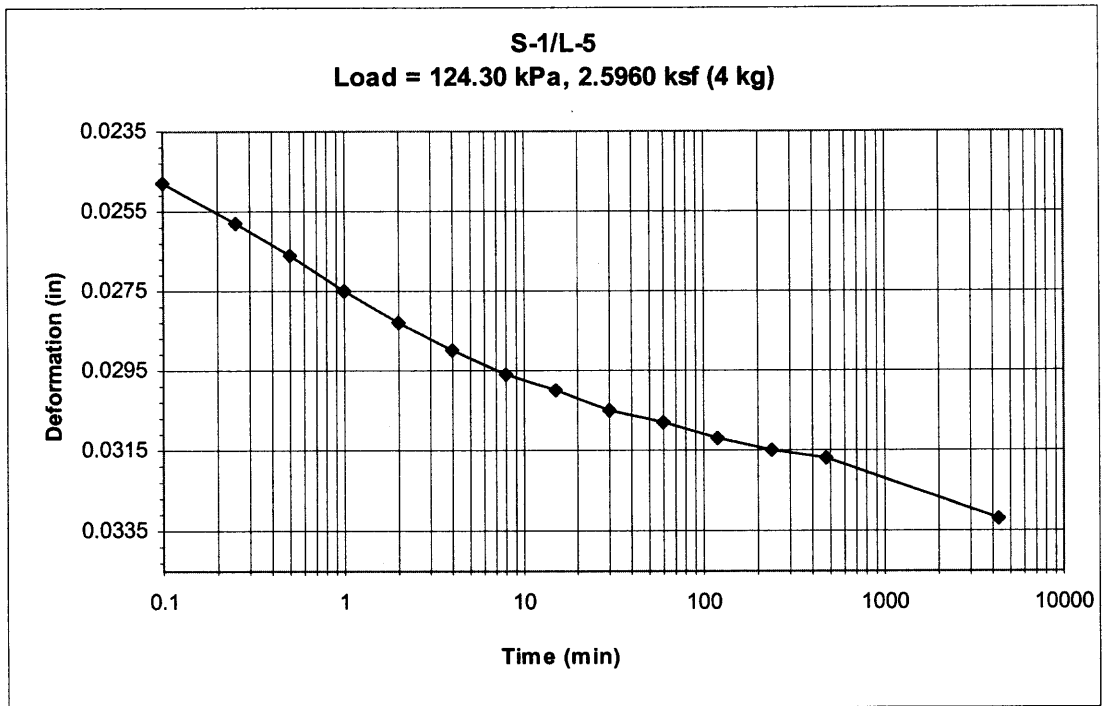


(a)

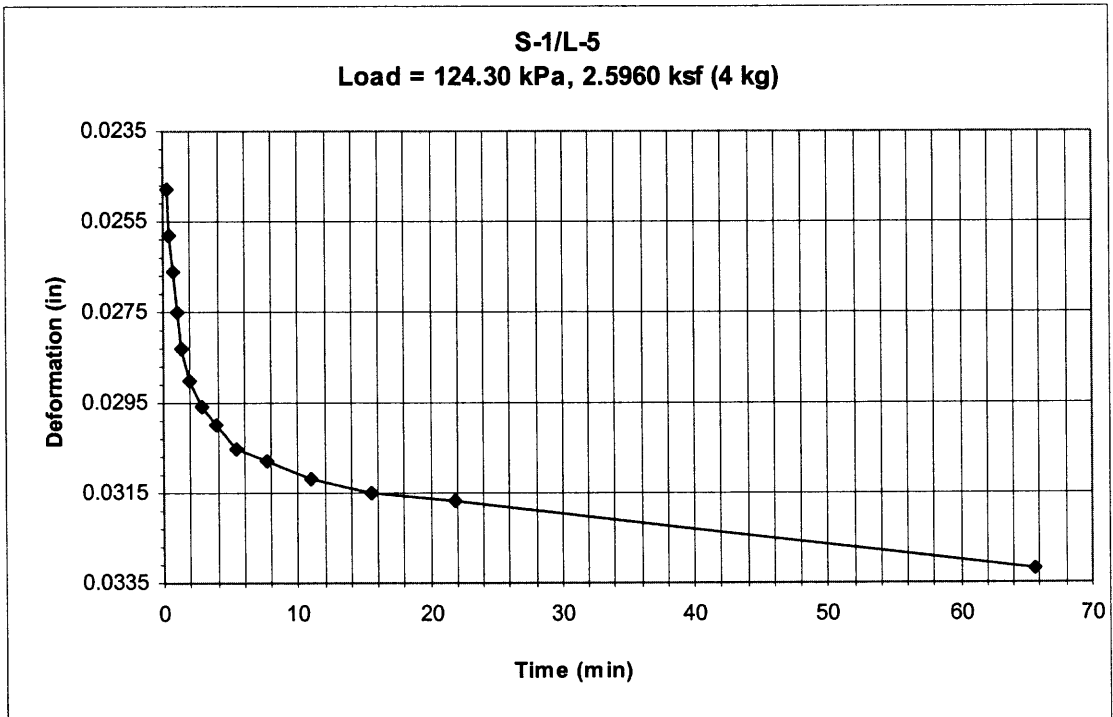


(b)

Figure A.4 Logarithm of time method (a) and square root of time method (b) for S-1/L-4.

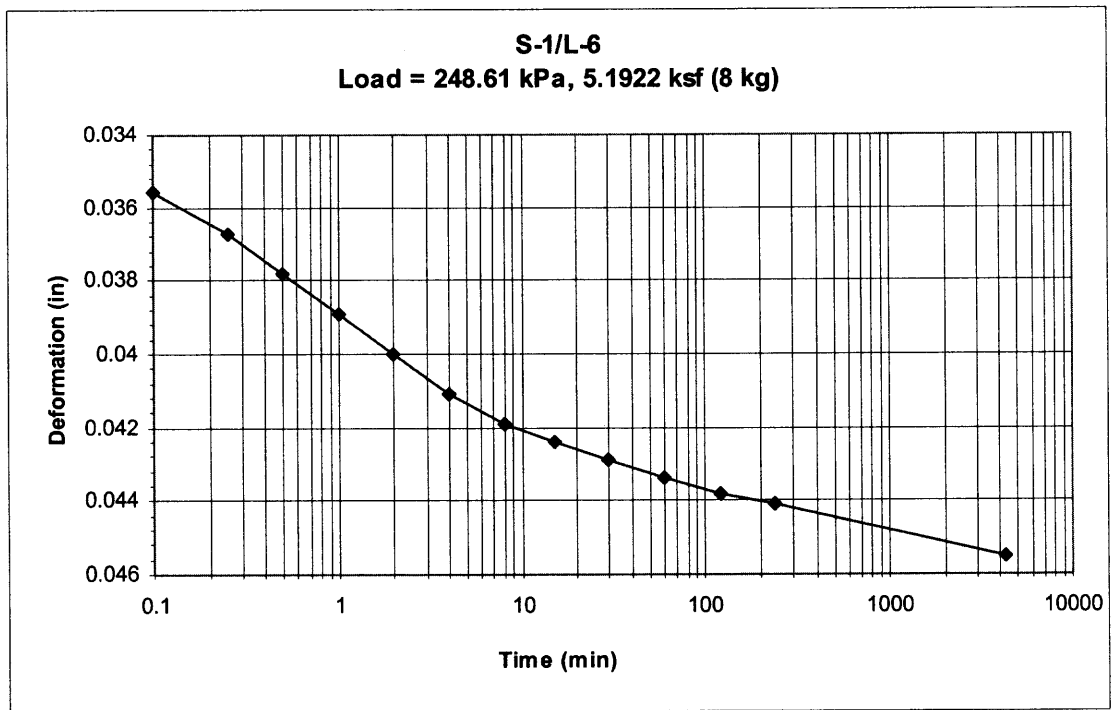


(a)

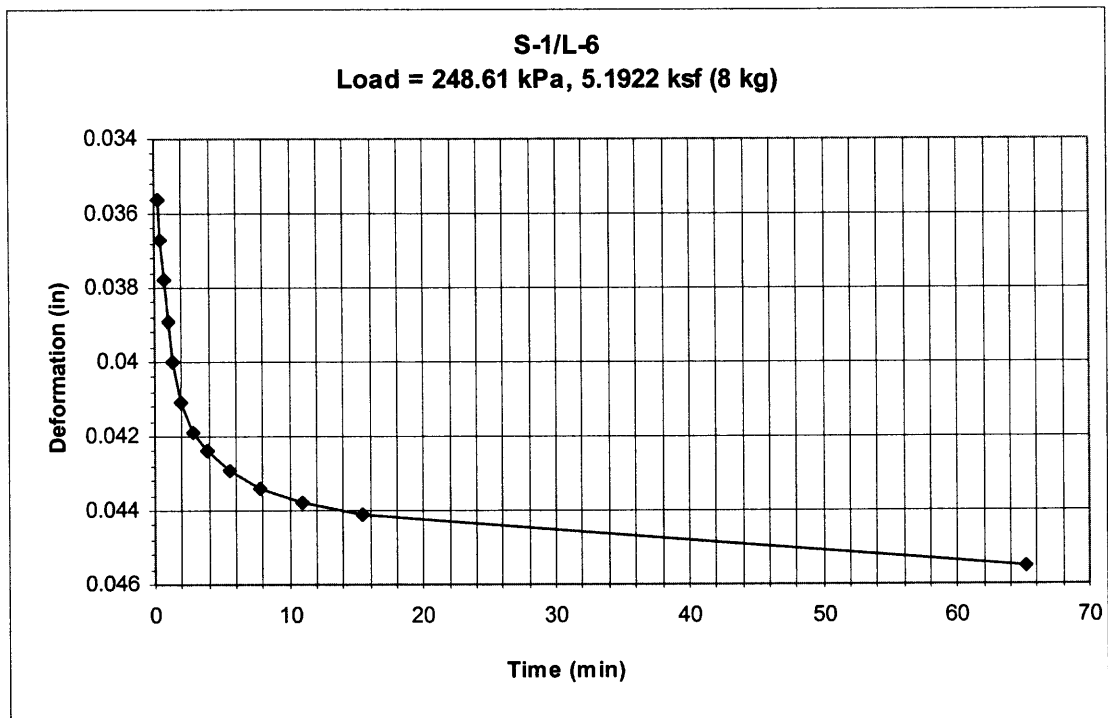


(b)

Figure A.5 Logarithm of time method (a) and square root of time method (b) for S-1/L-5.

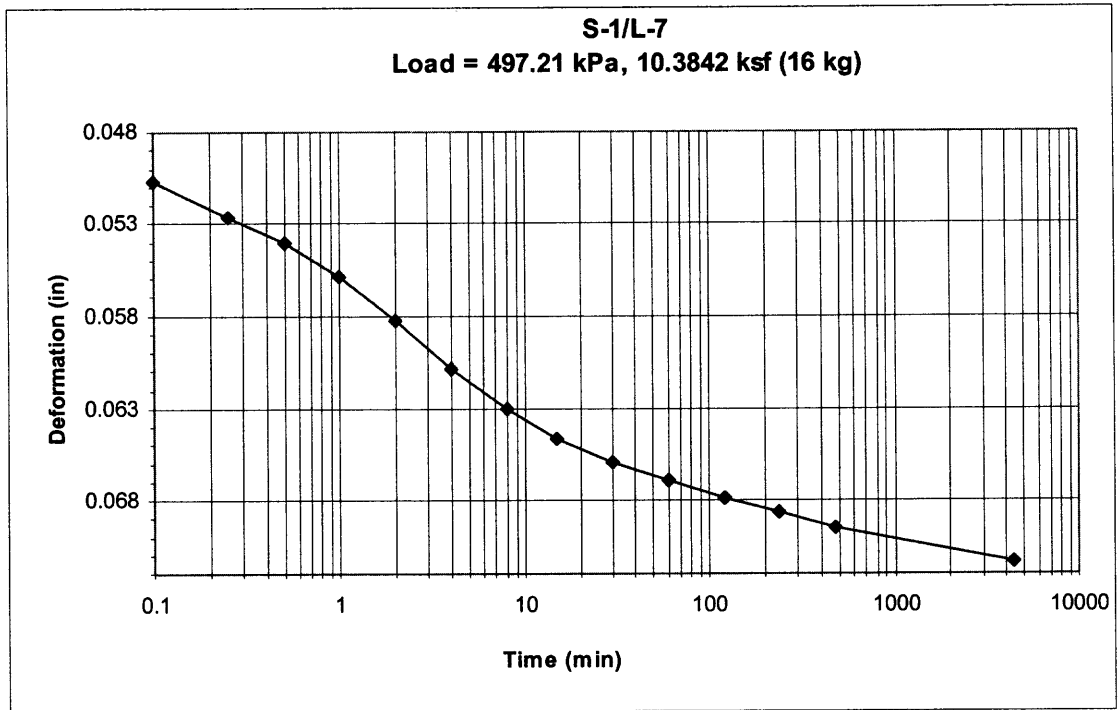


(a)

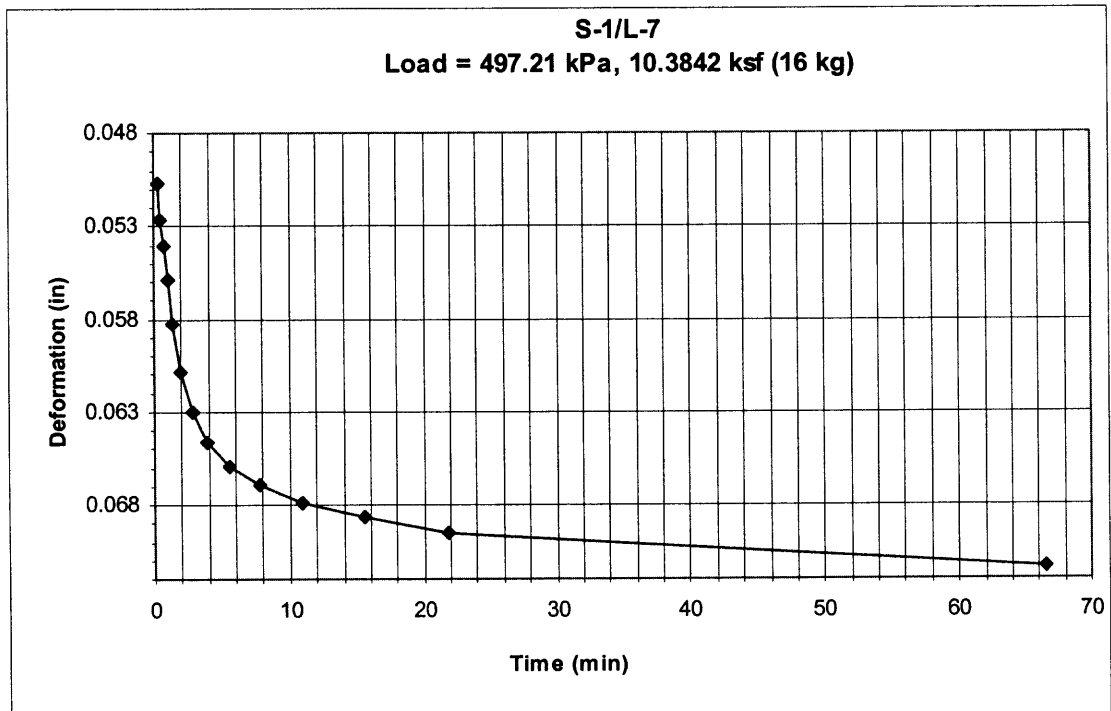


(b)

Figure A.6 Logarithm of time method (a) and square root of time method (b) for S-1/L-6.

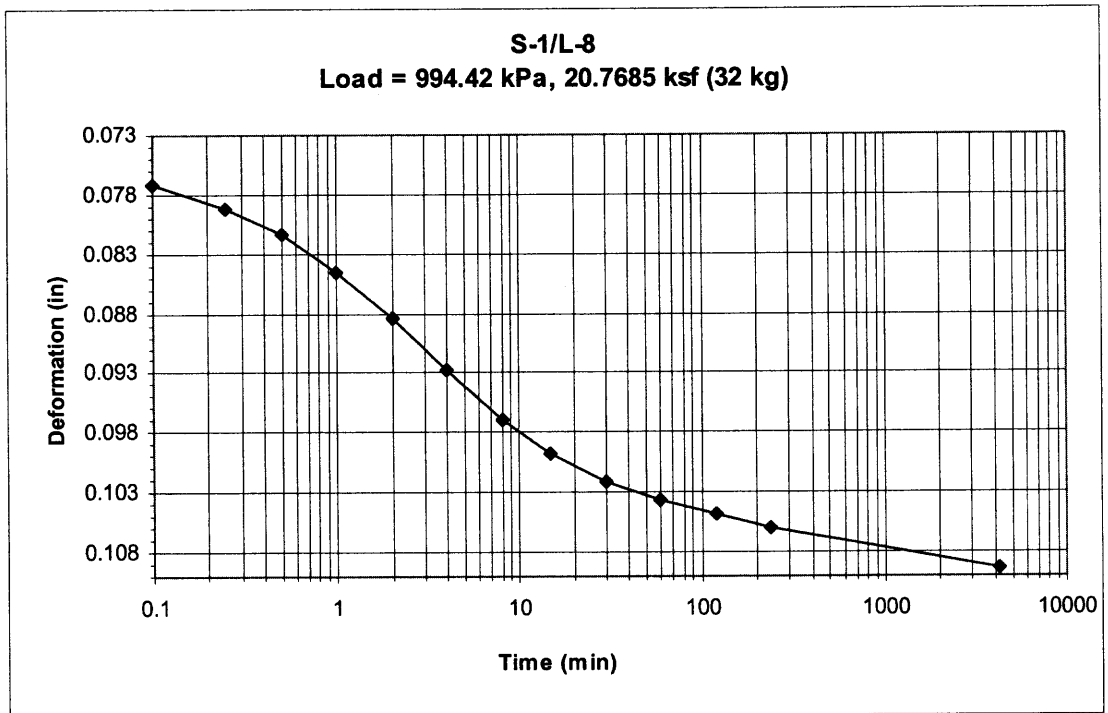


(a)

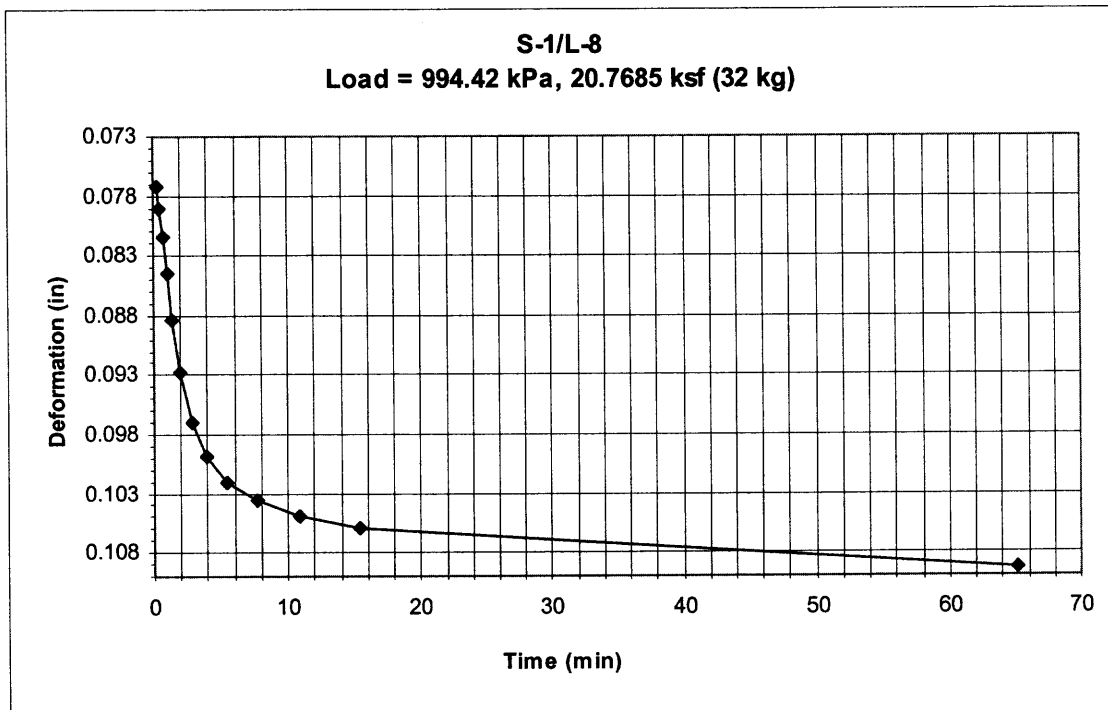


(b)

Figure A.7 Logarithm of time method (a) and square root of time method (b) for S-1/L-7.

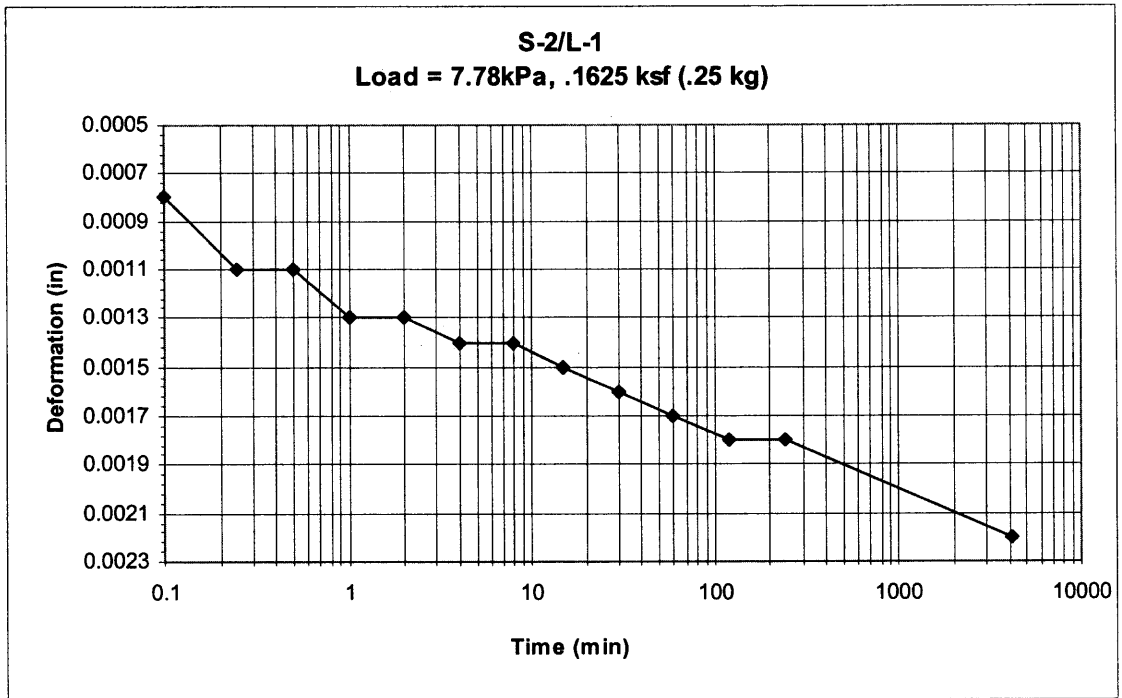


(a)

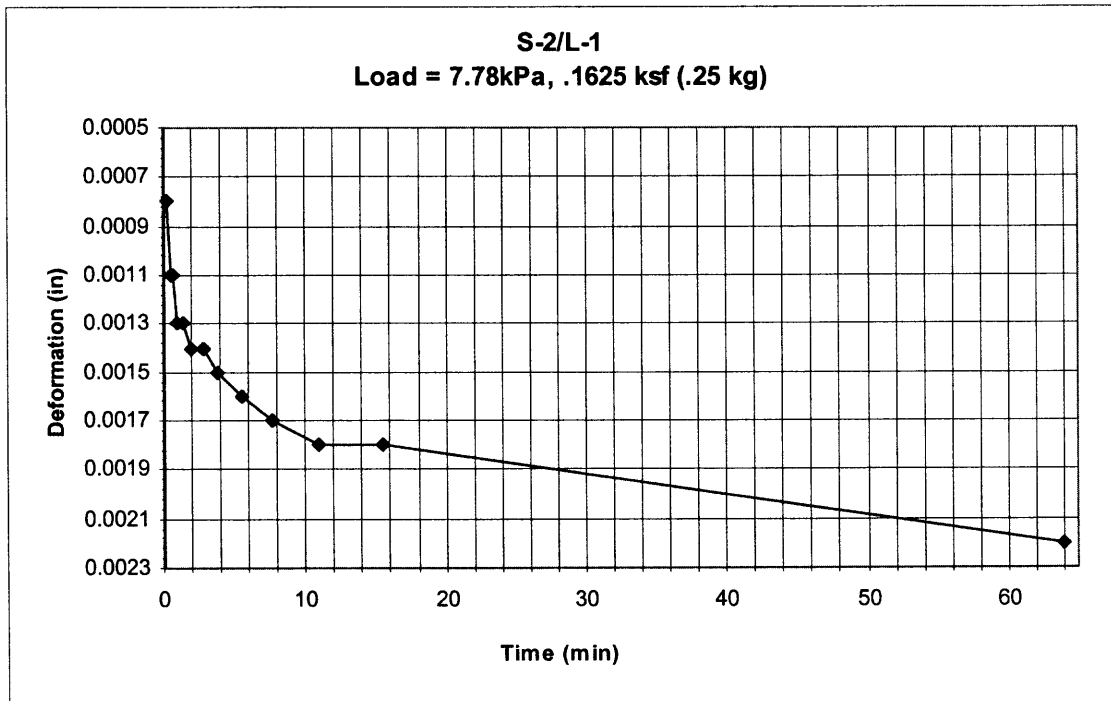


(b)

Figure A.8 Logarithm of time method (a) and square root of time method (b) for S-1/L-8.

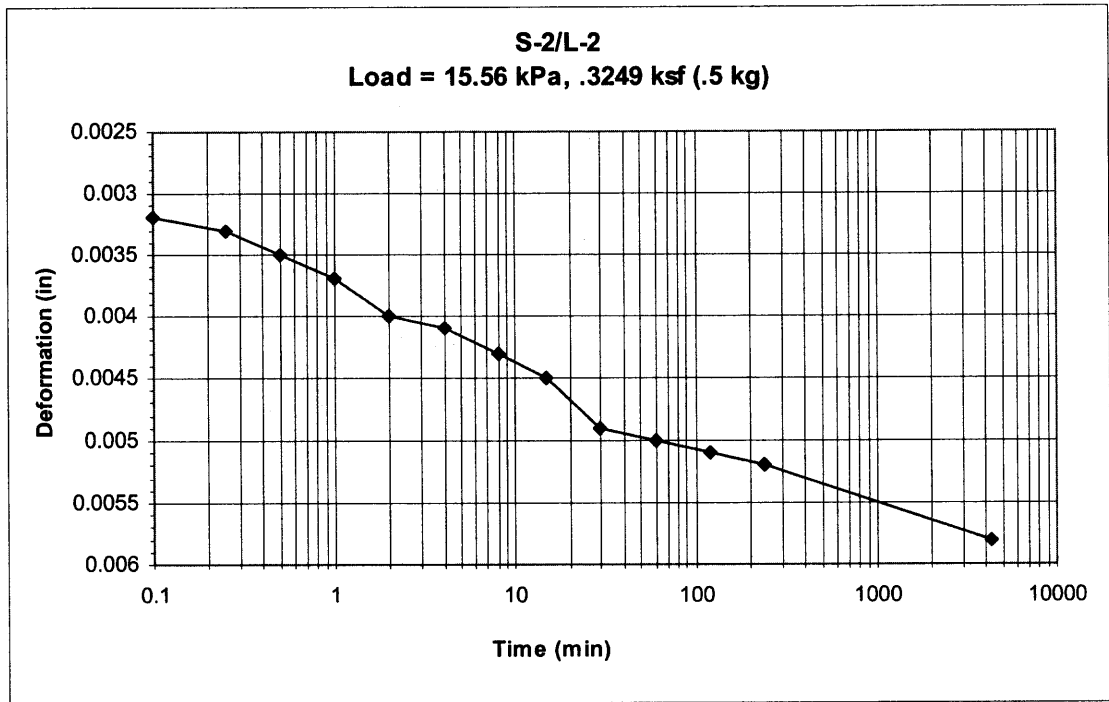


(a)

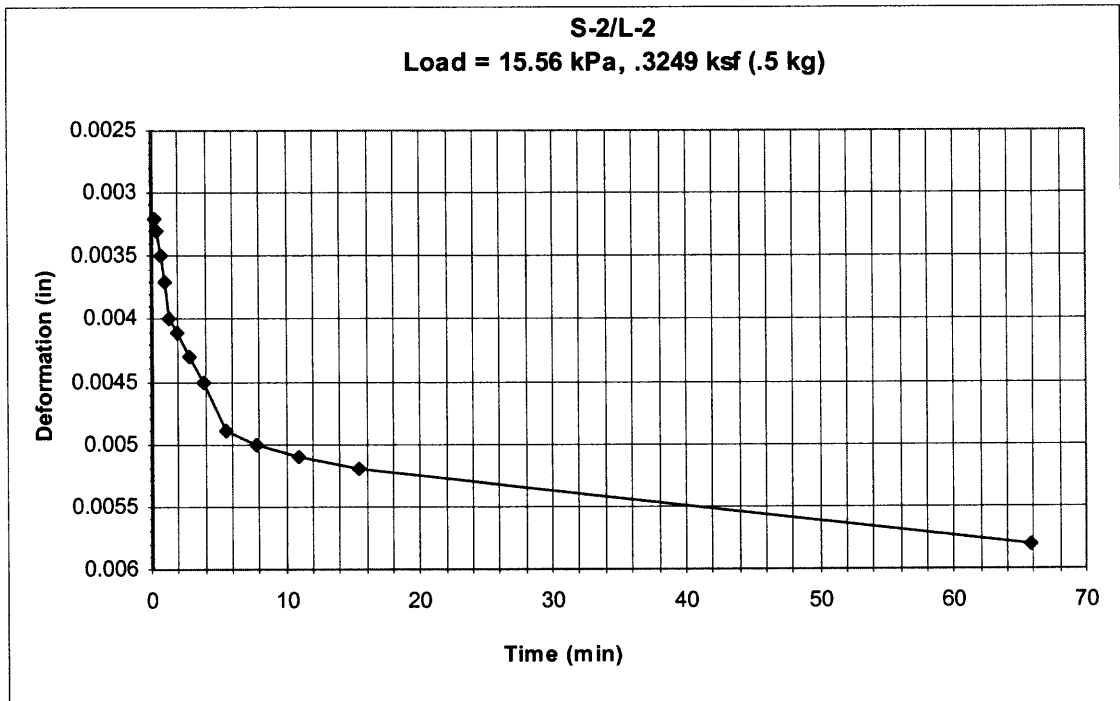


(b)

Figure A.9 Logarithm of time method (a) and square root of time method (b) for S-2/L-1.

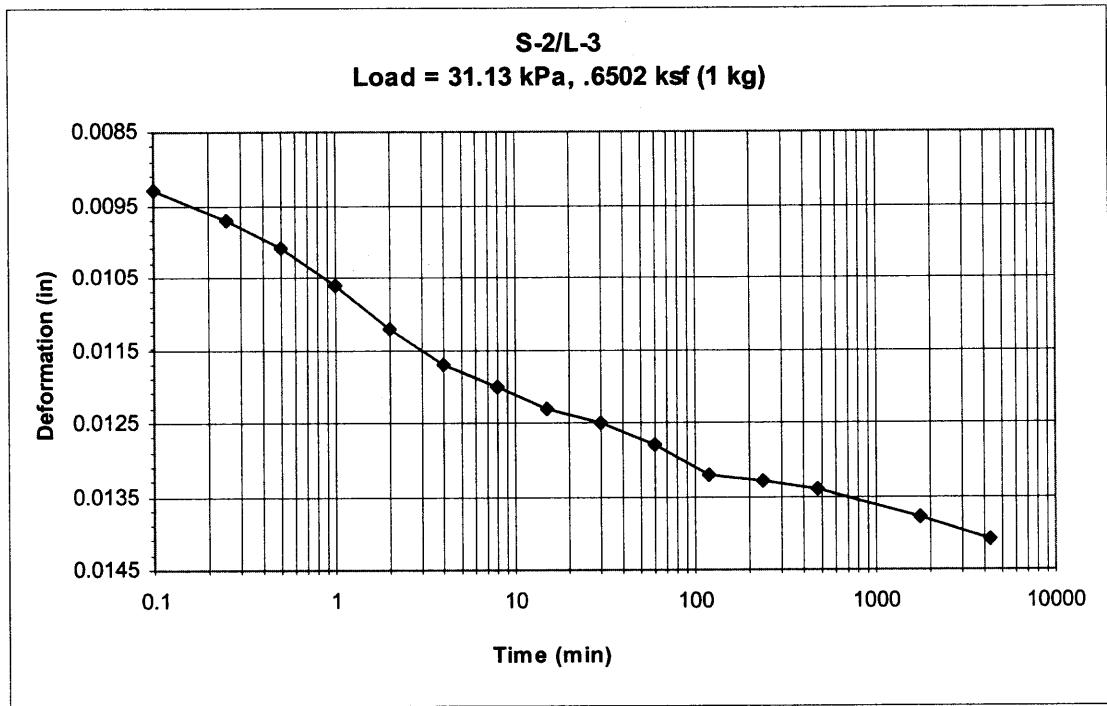


(a)

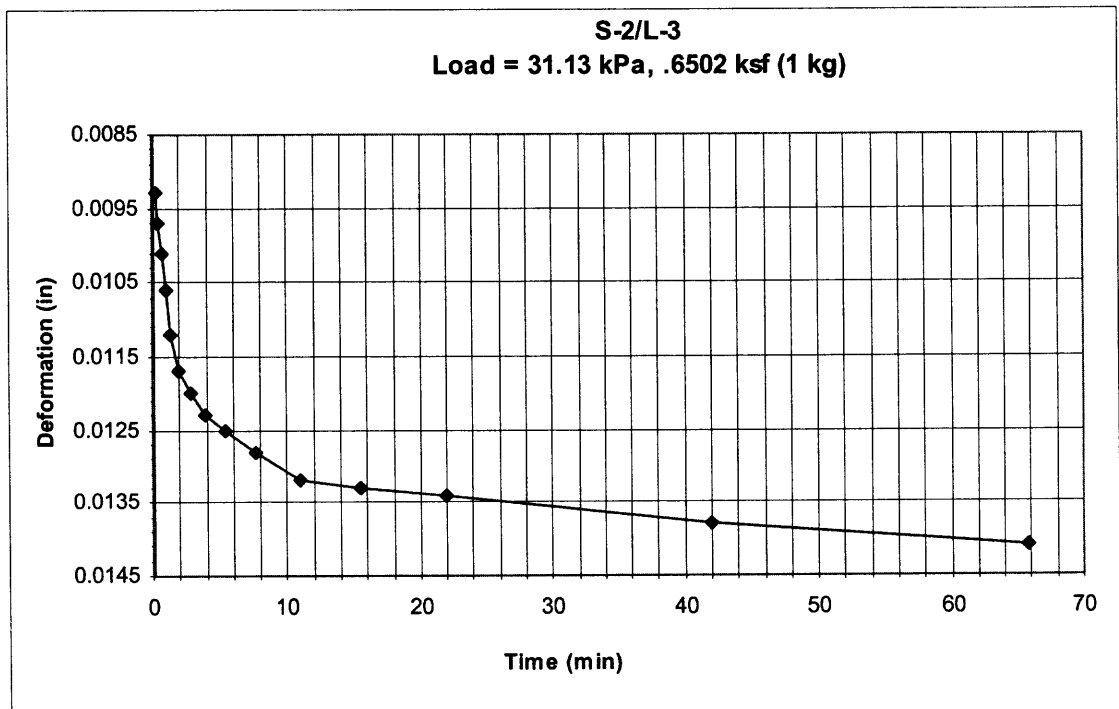


(b)

Figure A.10 Logarithm of time method (a) and square root of time method (b) for S-2/L-2.

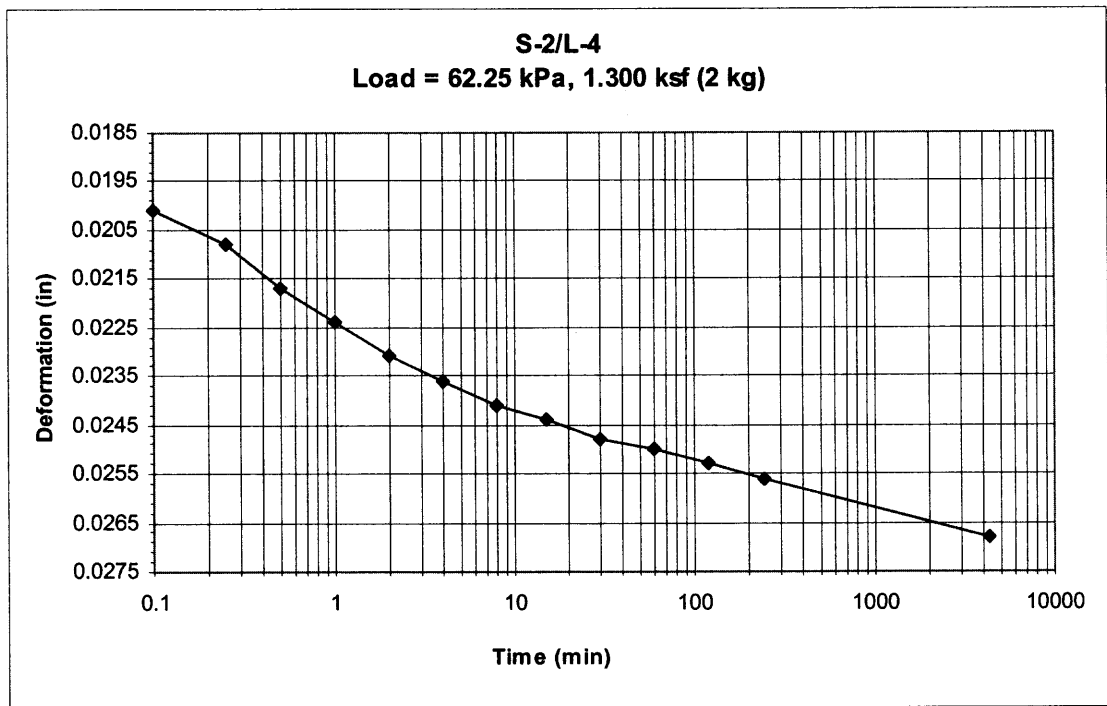


(a)

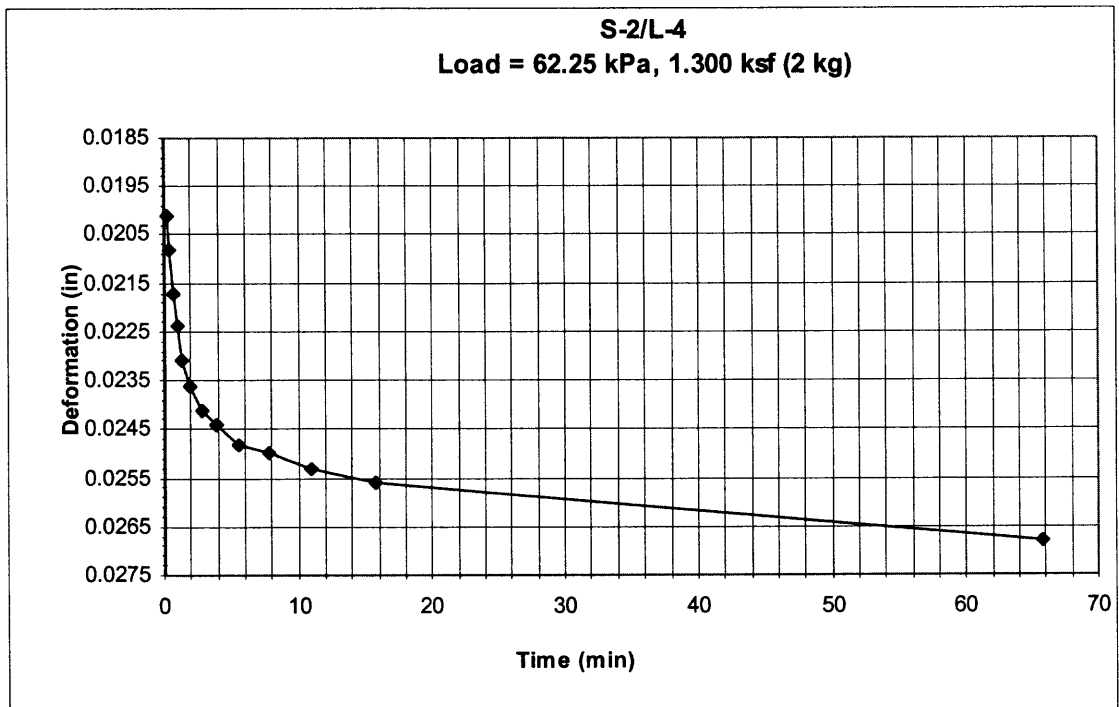


(b)

Figure A.11 Logarithm of time method (a) and square root of time method (b) for S-2/L-3.

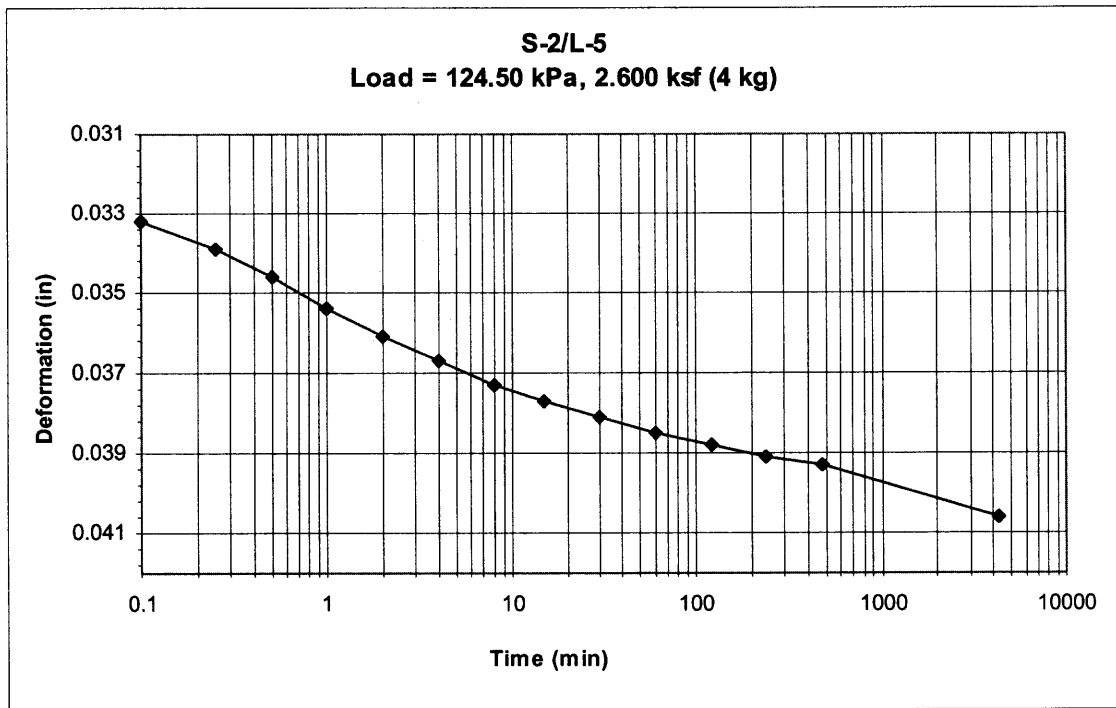


(a)

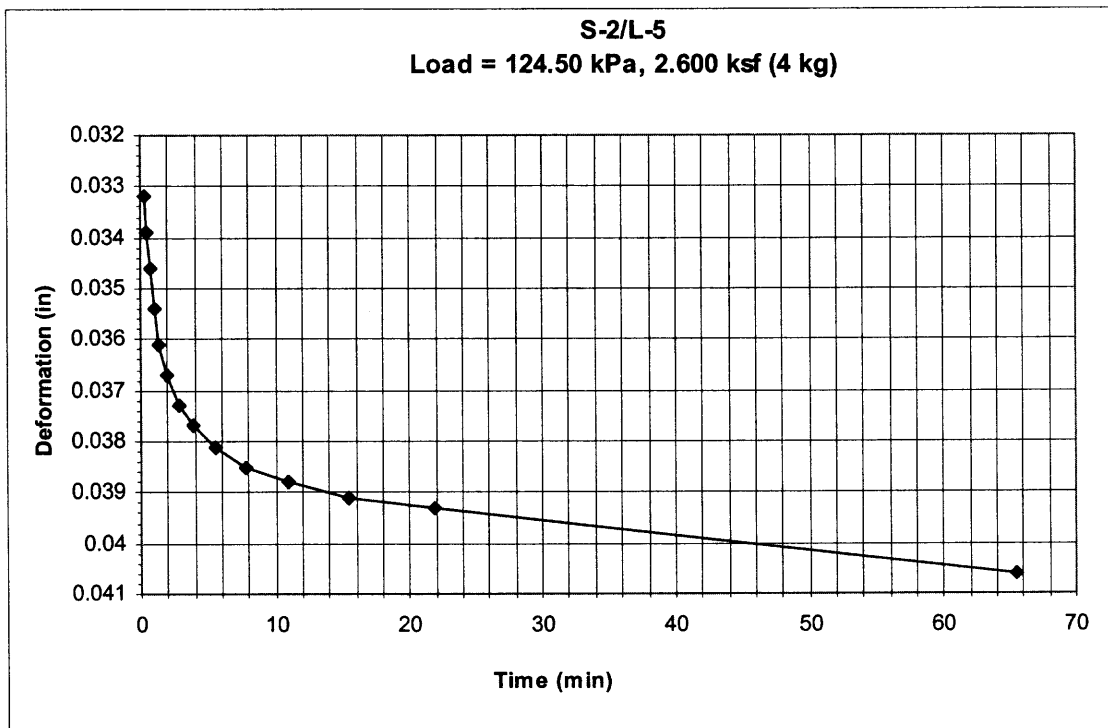


(b)

Figure A.12 Logarithm of time method (a) and square root of time method (b) for S-2/L-4.

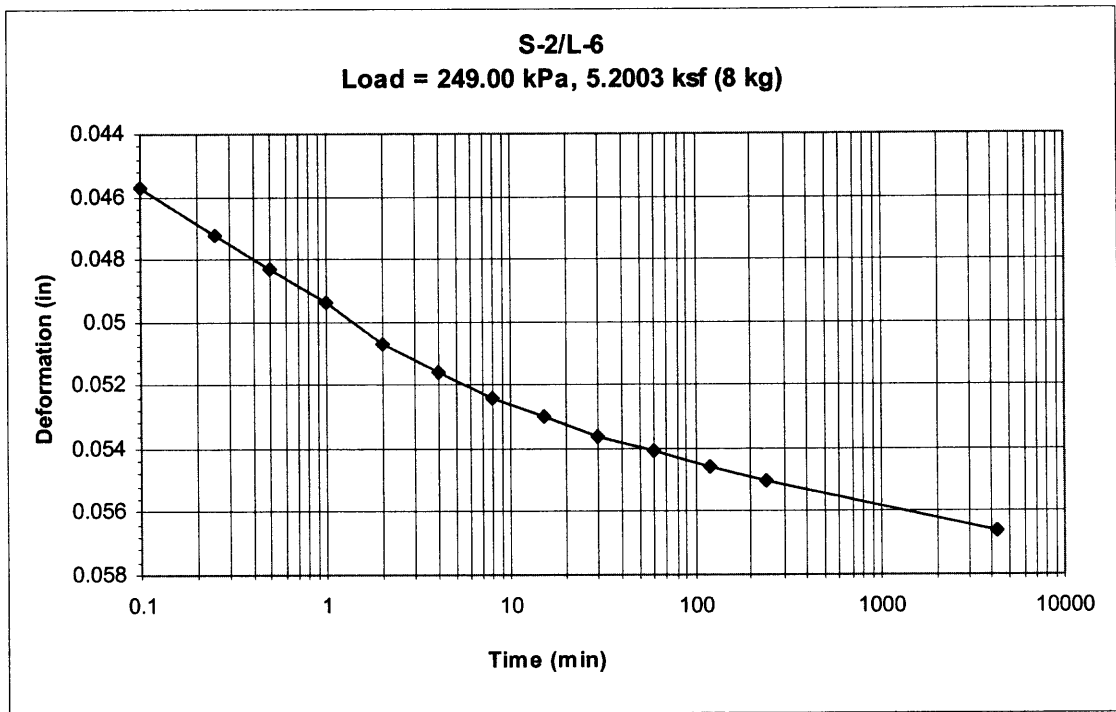


(a)

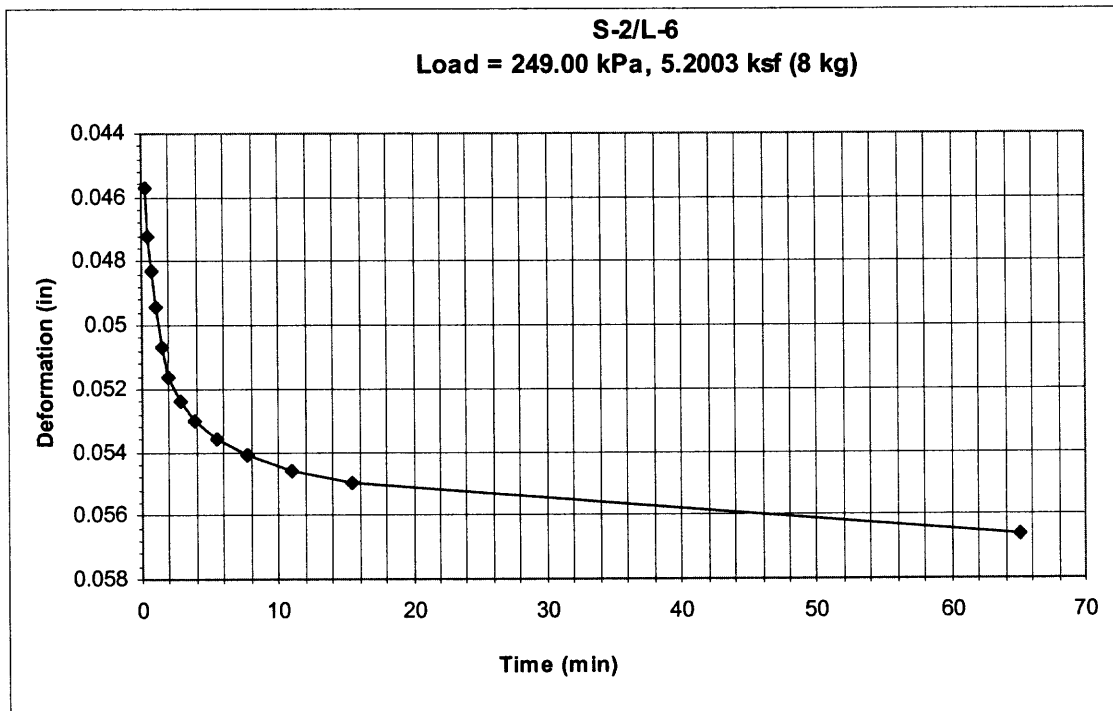


(b)

Figure A.13 Logarithm of time method (a) and square root of time method (b) for S-2/L-5.

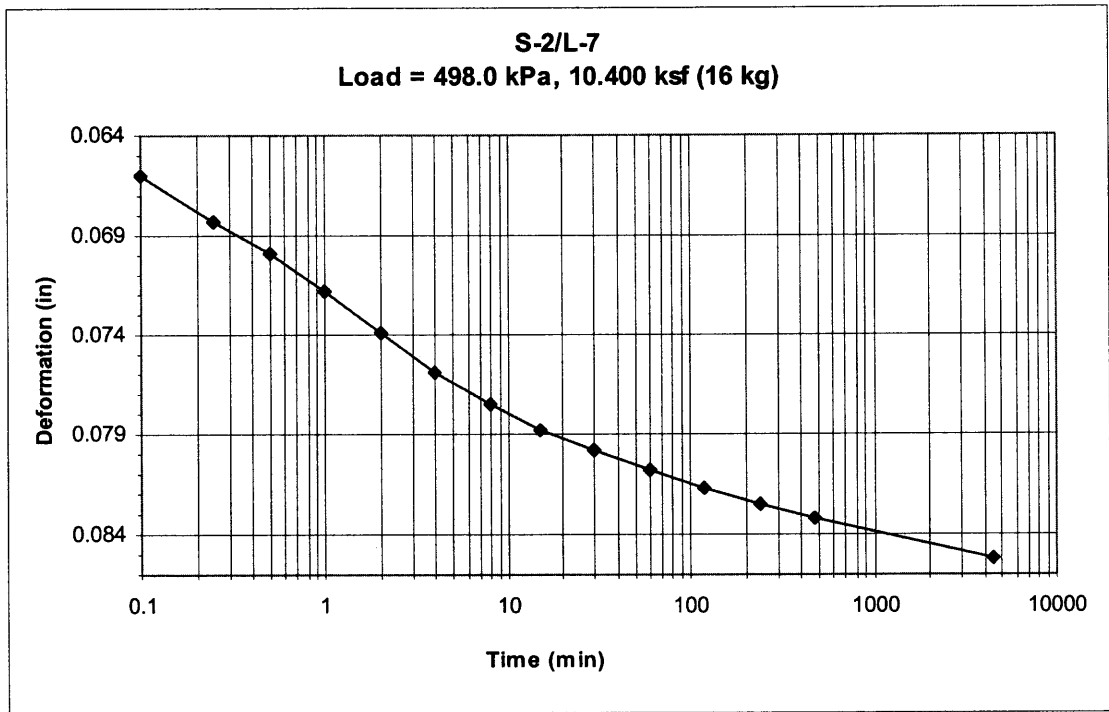


(a)

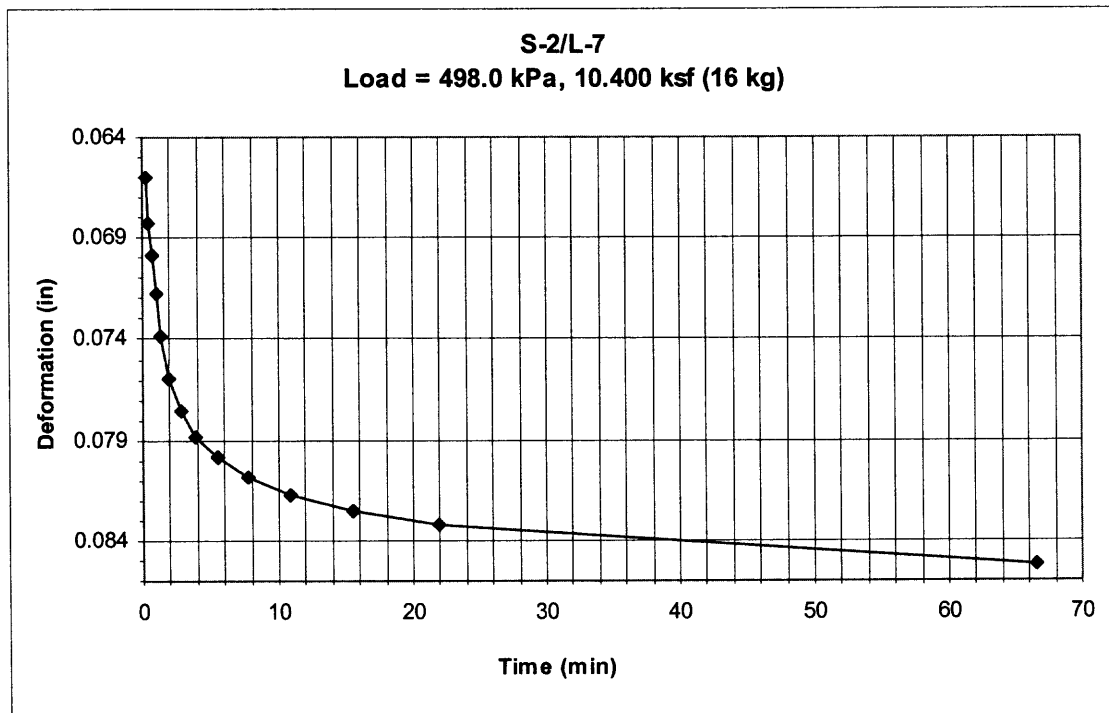


(b)

Figure A.14 Logarithm of time method (a) and square root of time method (b) for S-2/L-6.

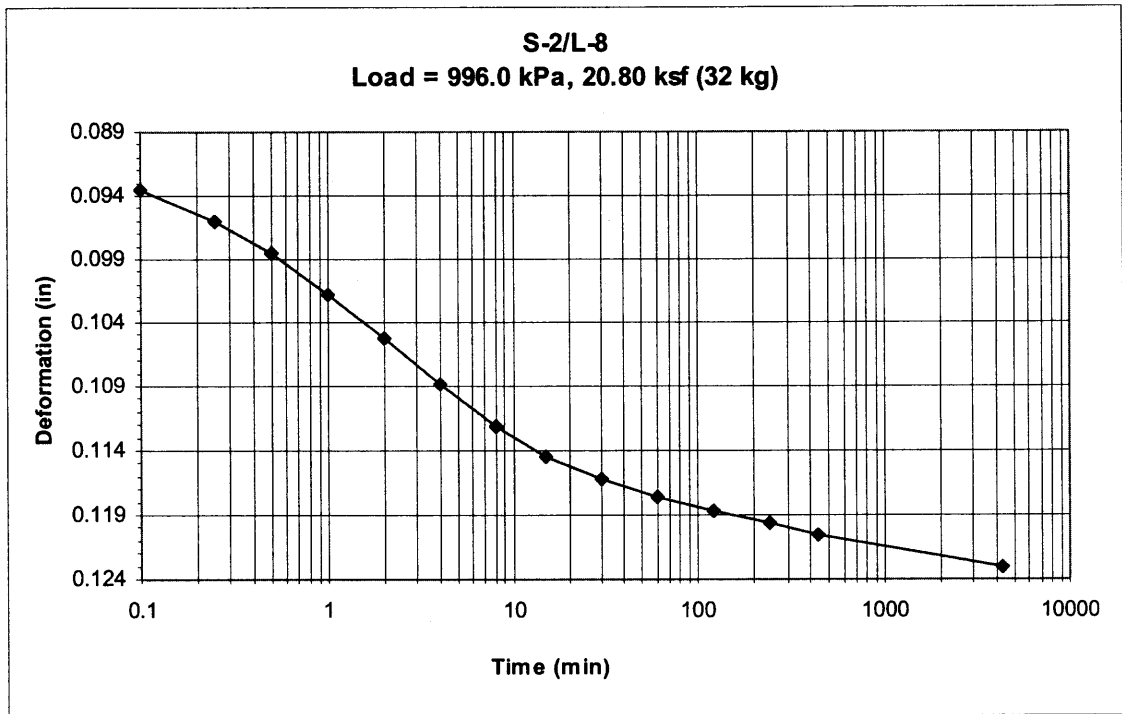


(a)

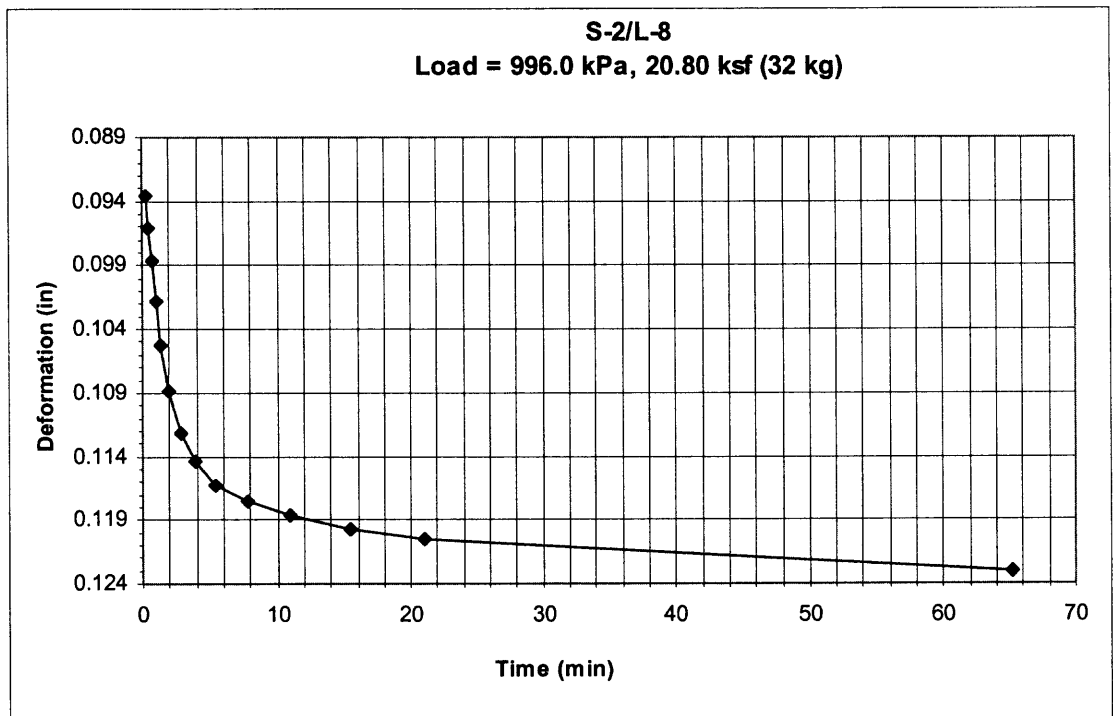


(b)

Figure A.15 Logarithm of time method (a) and square root of time method (b) for S-2/L-7.

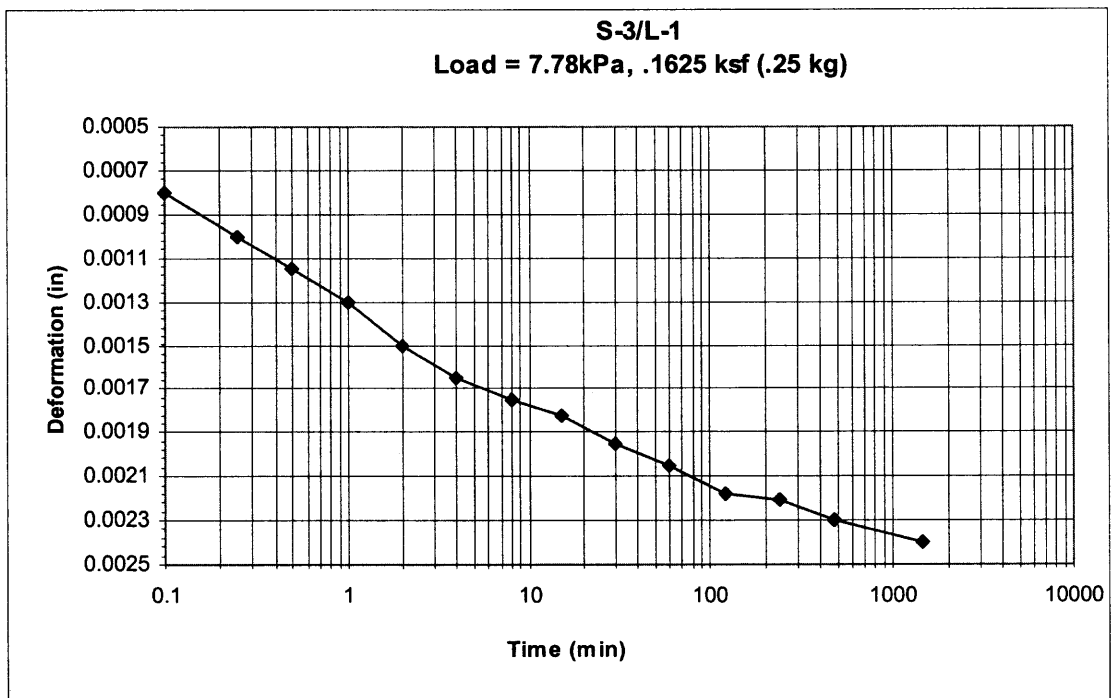


(a)

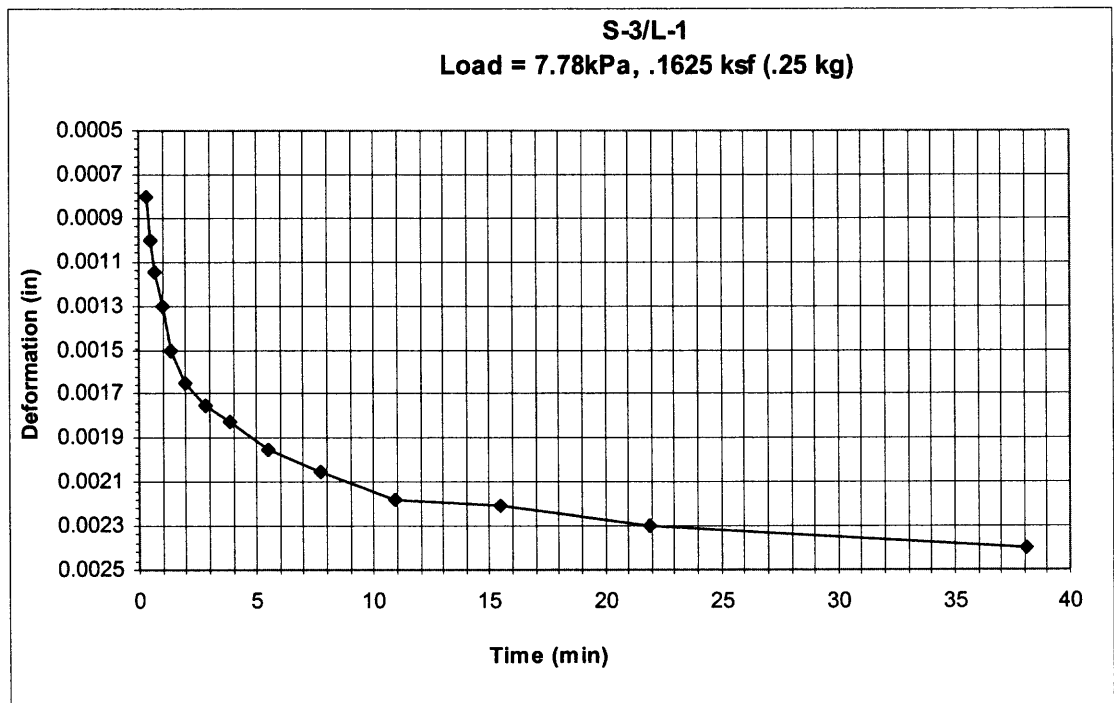


(b)

Figure A.16 Logarithm of time method (a) and square root of time method (b) for S-2/L-8.

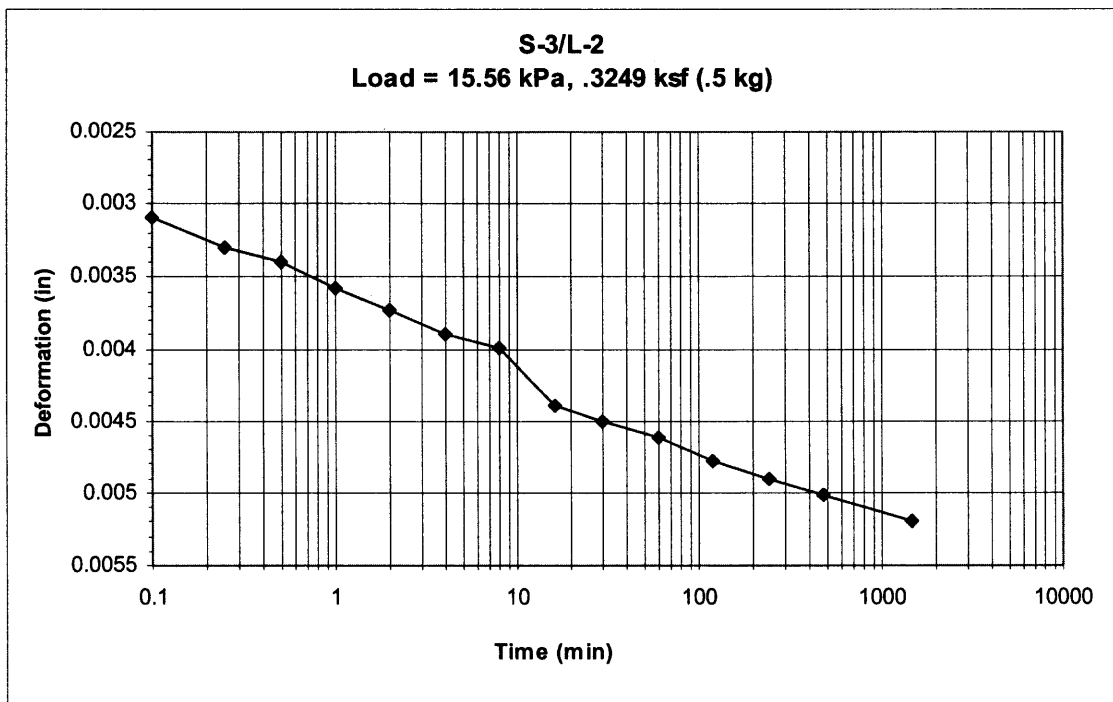


(a)

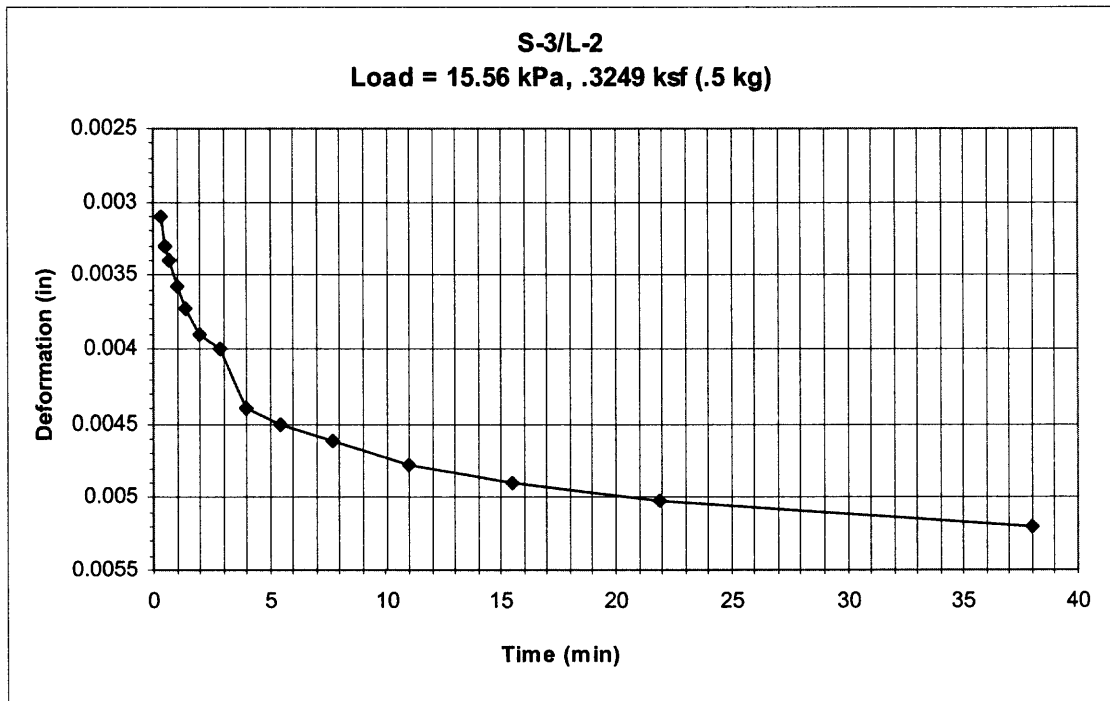


(b)

Figure A.17 Logarithm of time method (a) and square root of time method (b) for S-3/L-1.

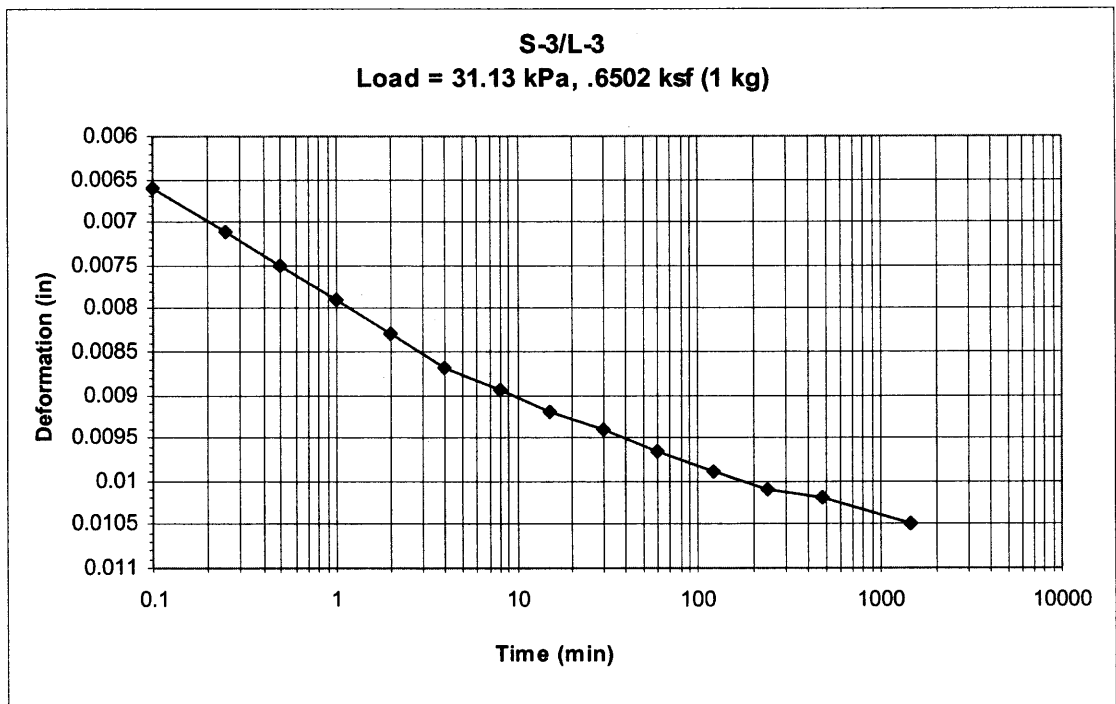


(a)

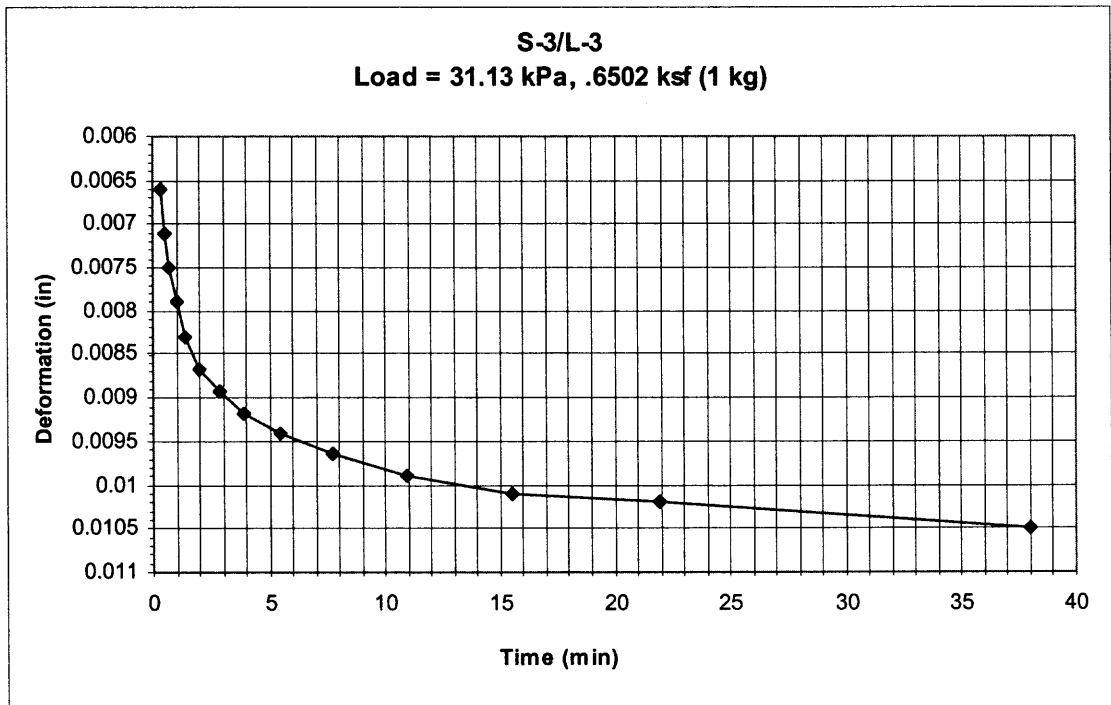


(b)

Figure A.18 Logarithm of time method (a) and square root of time method (b) for S-3/L-2.

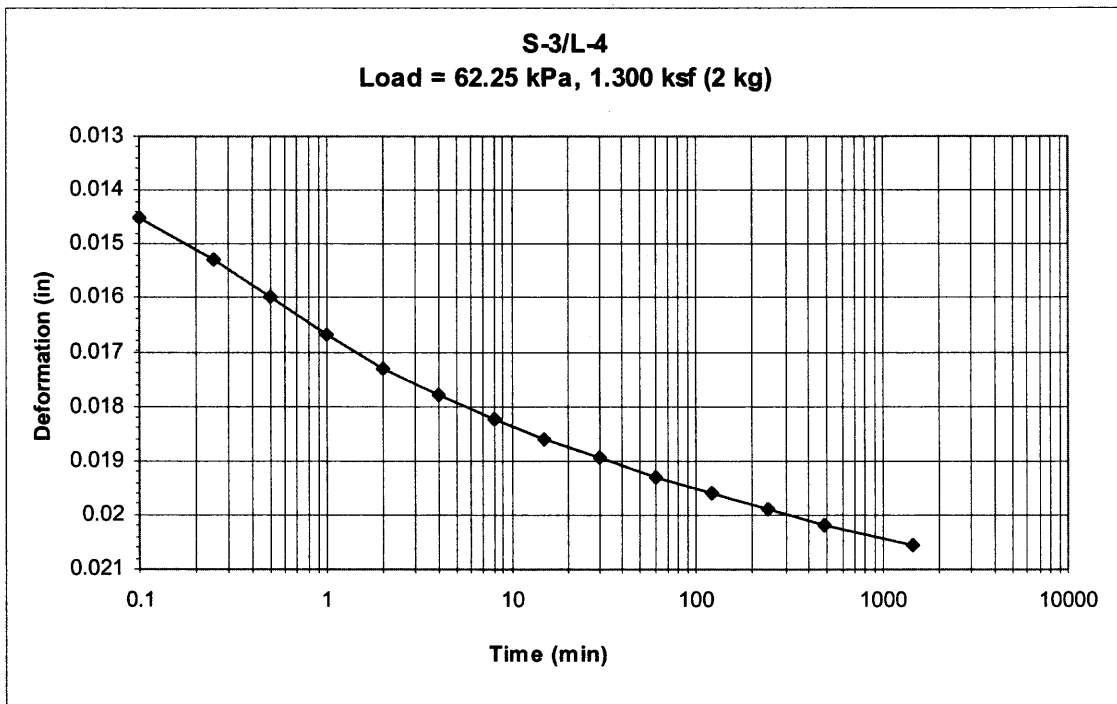


(a)

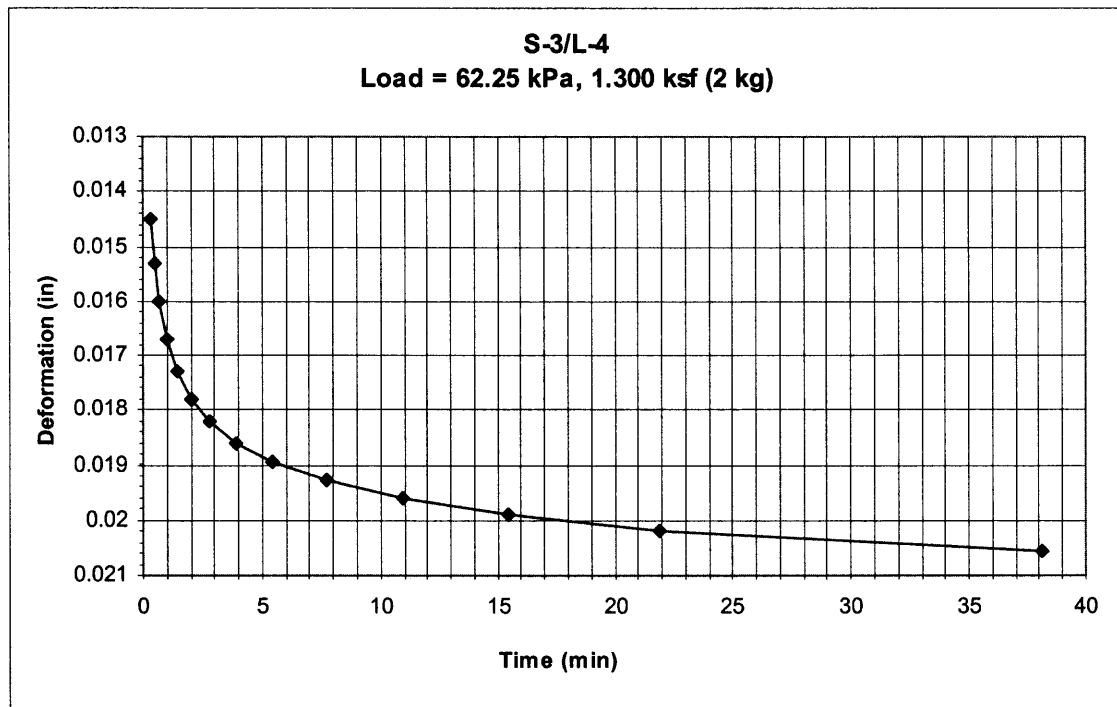


(b)

Figure A.19 Logarithm of time method (a) and square root of time method (b) for S-3/L-3.

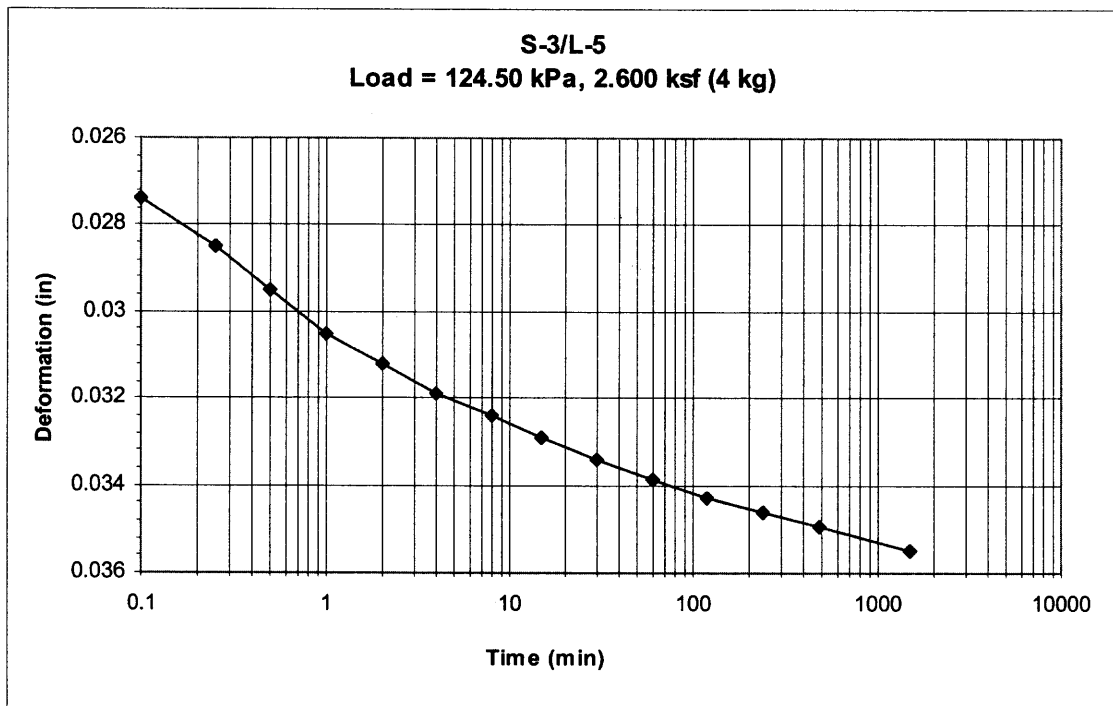


(a)

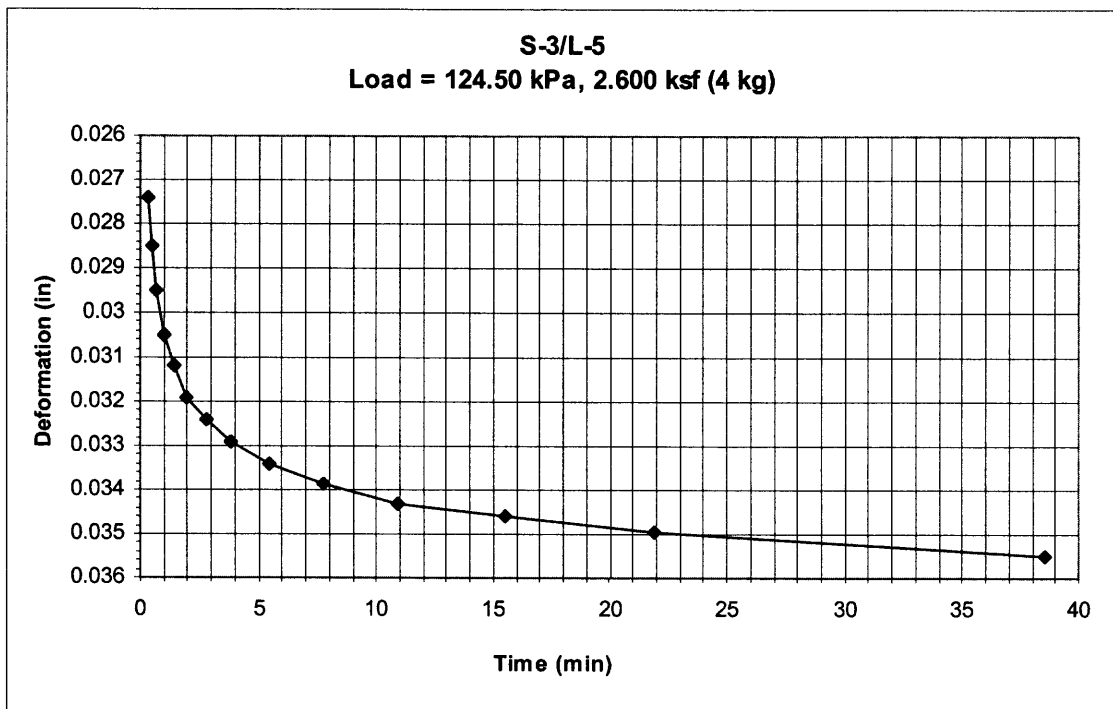


(b)

Figure A.20 Logarithm of time method (a) and square root of time method (b) for S-3/L-4.

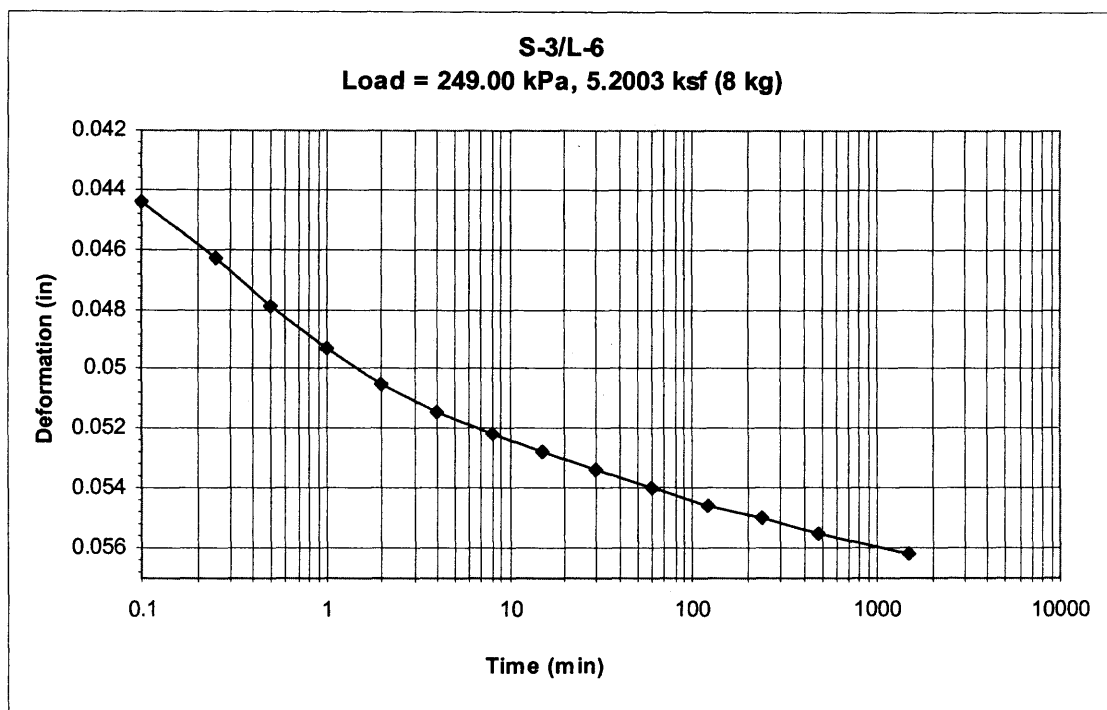


(a)

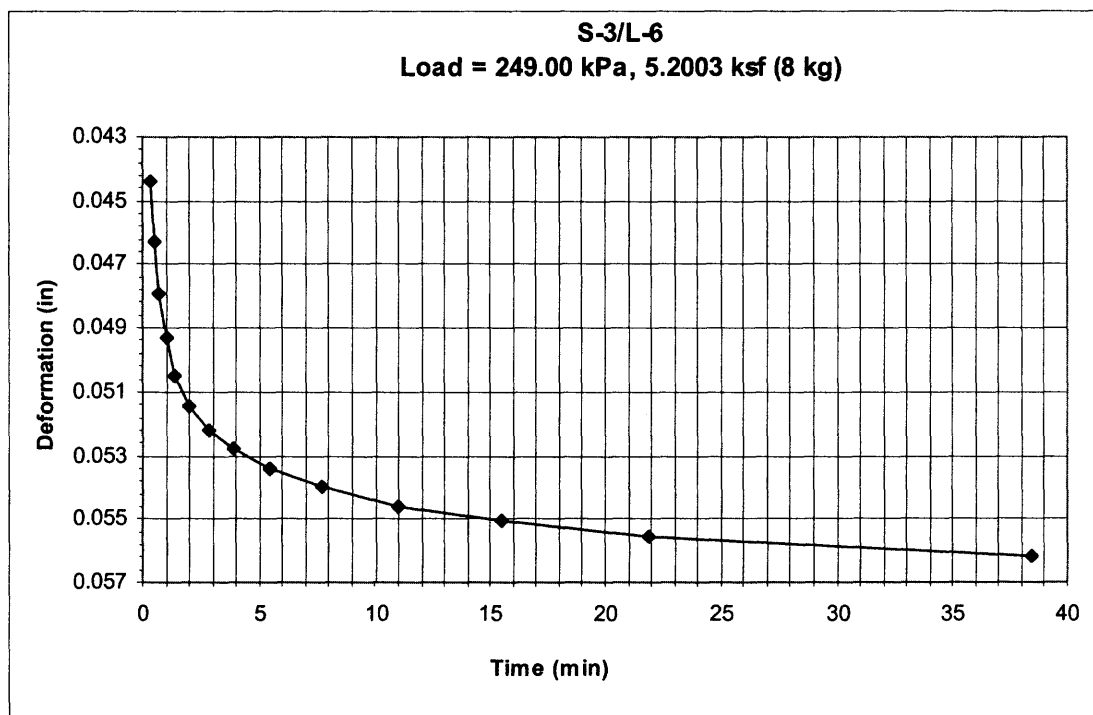


(b)

Figure A.21 Logarithm of time method (a) and square root of time method (b) for S-3/L-5.

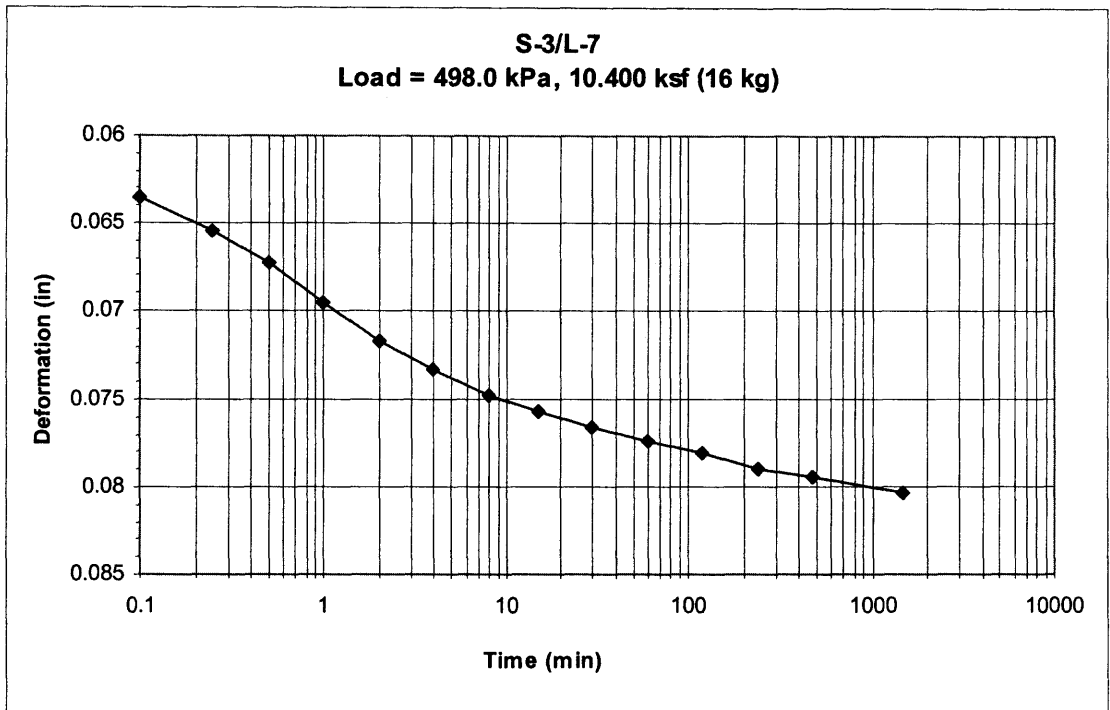


(a)

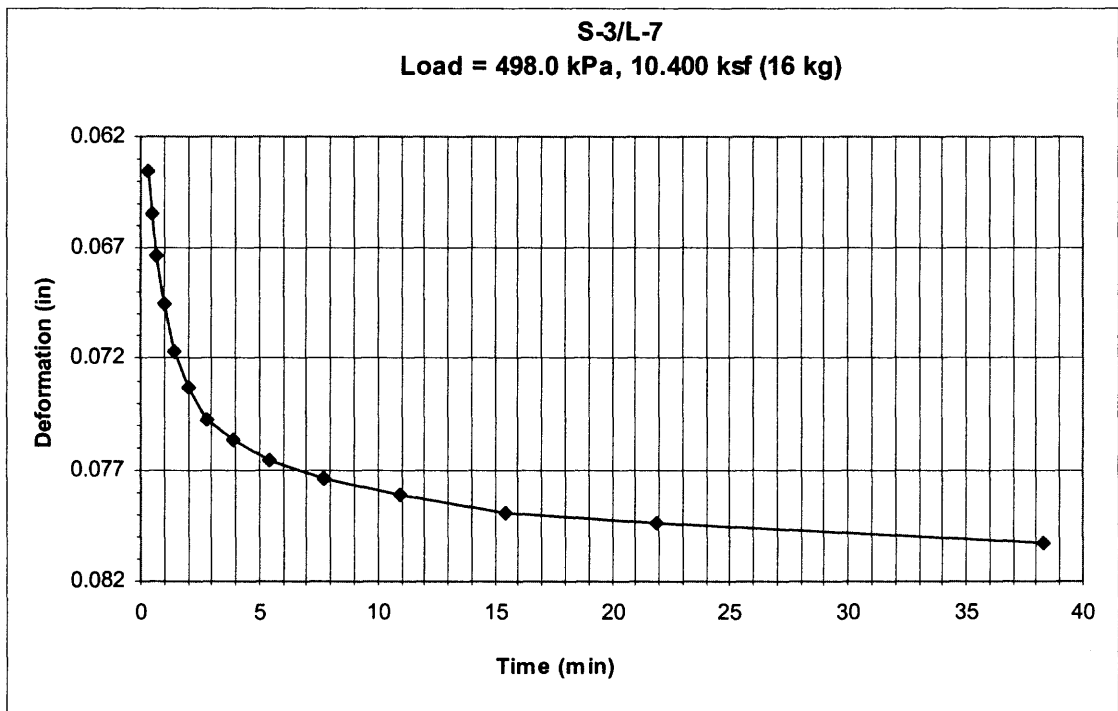


(b)

Figure A.22 Logarithm of time method (a) and square root of time method (b) for S-3/L-6.

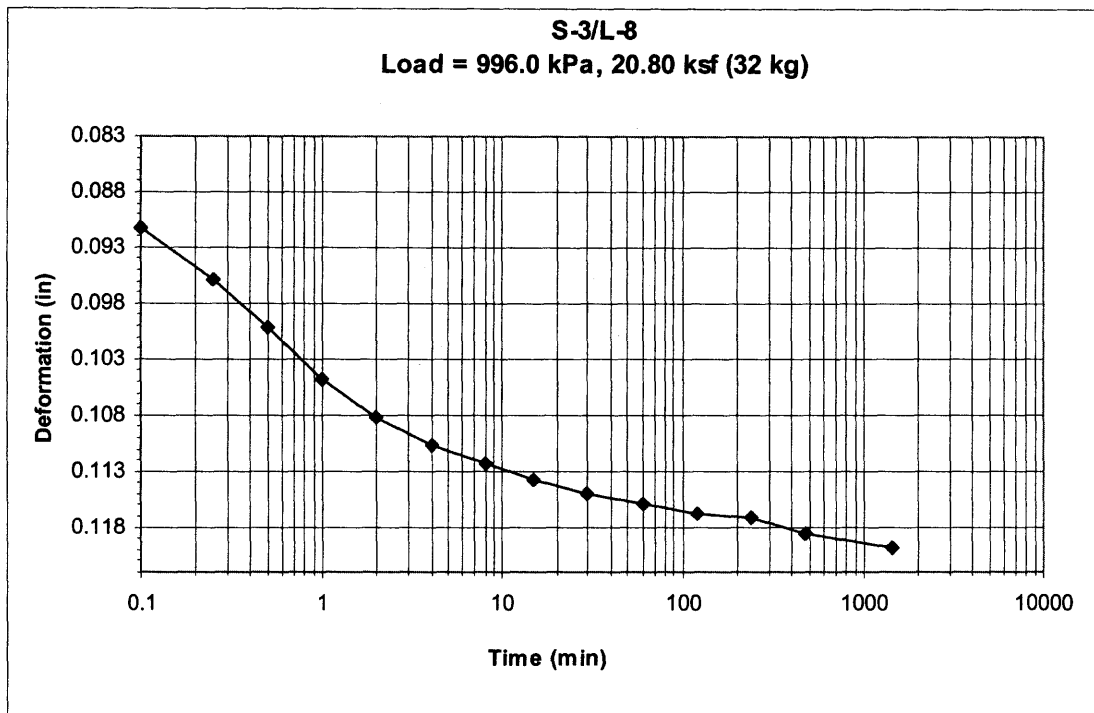


(a)

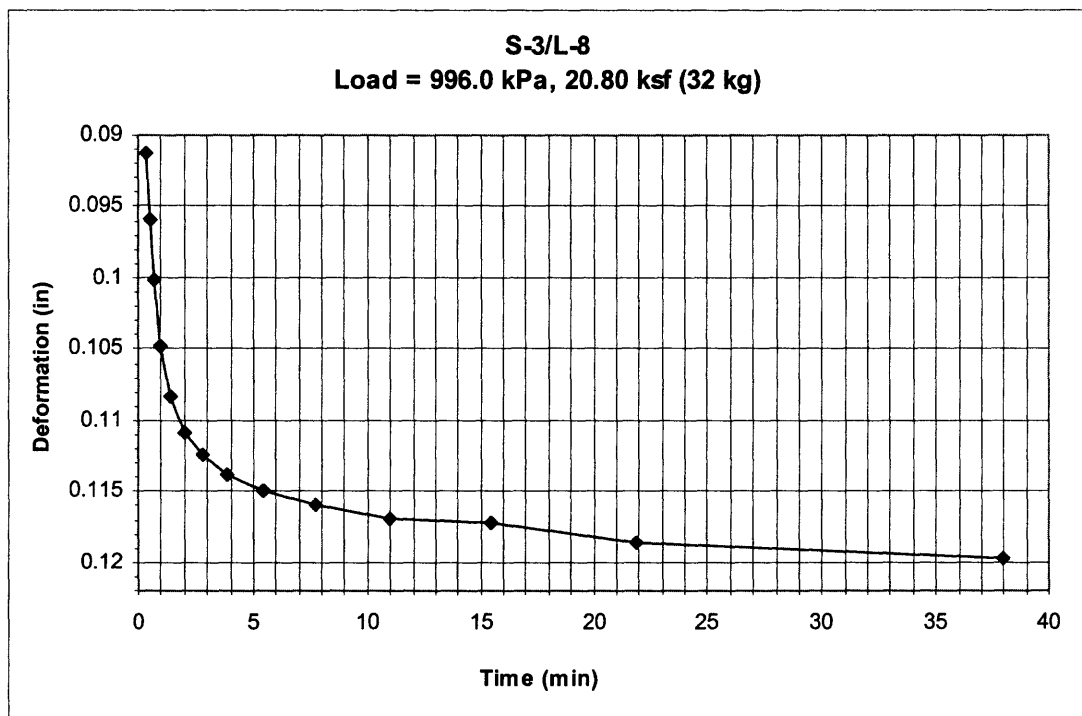


(b)

Figure A.23 Logarithm of time method (a) and square root of time method (b) for S-3/L-7.

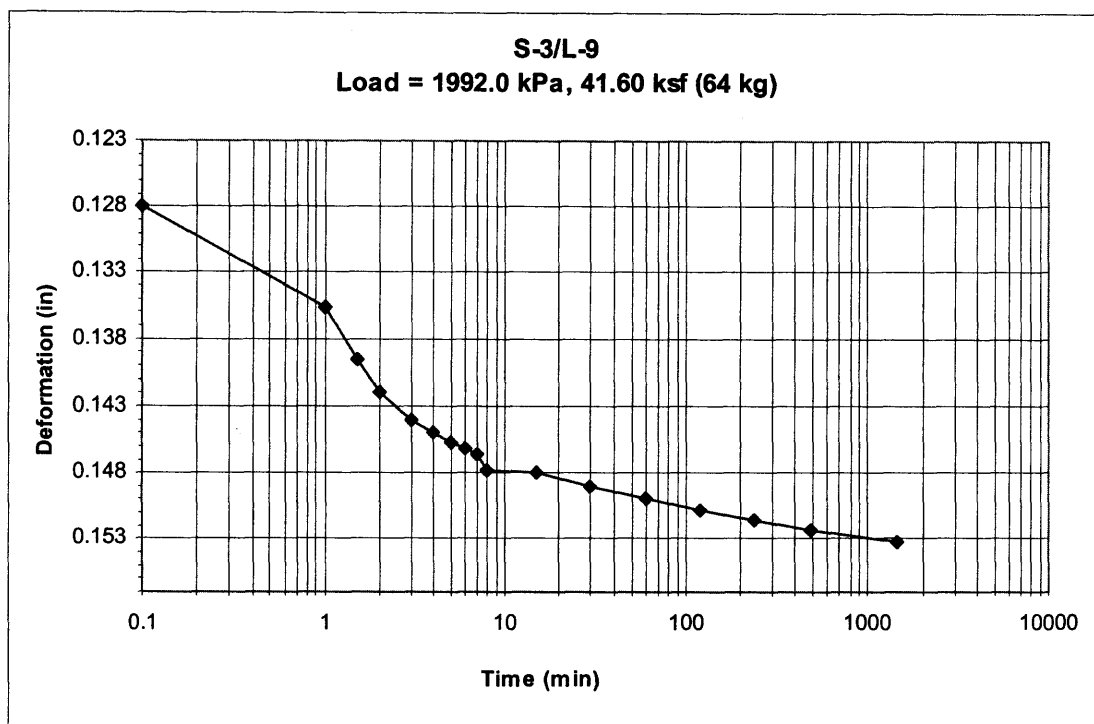


(a)

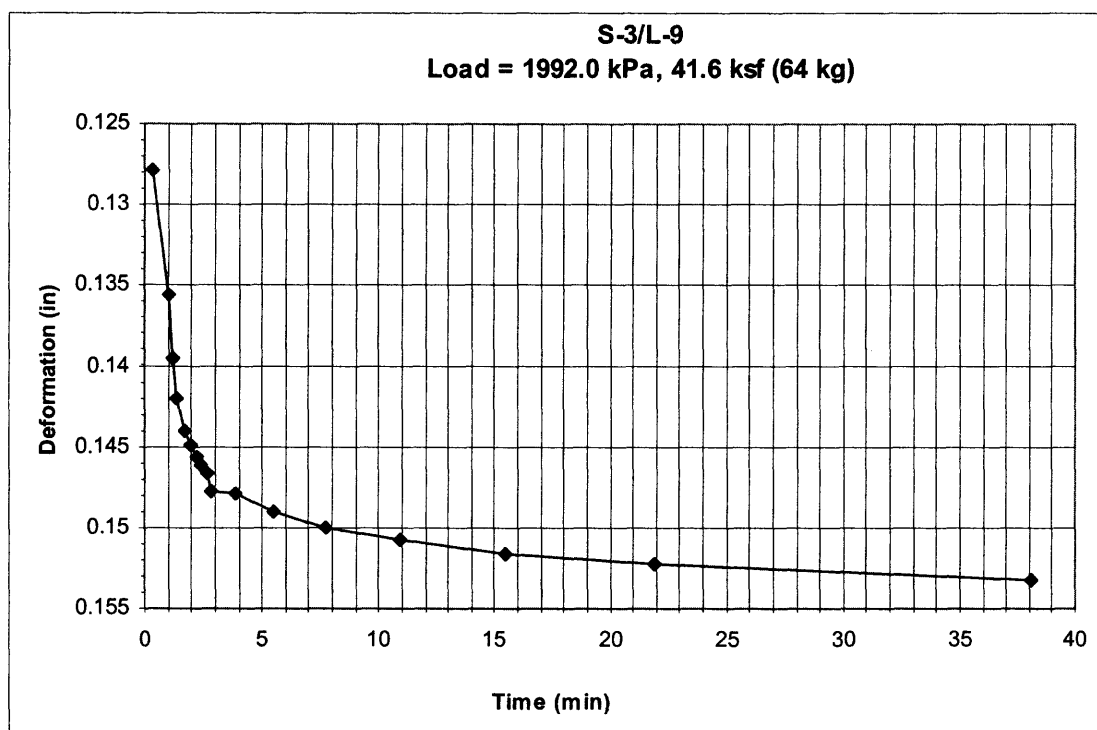


(b)

Figure A.24 Logarithm of time method (a) and square root of time method (b) for S-3/L-8.

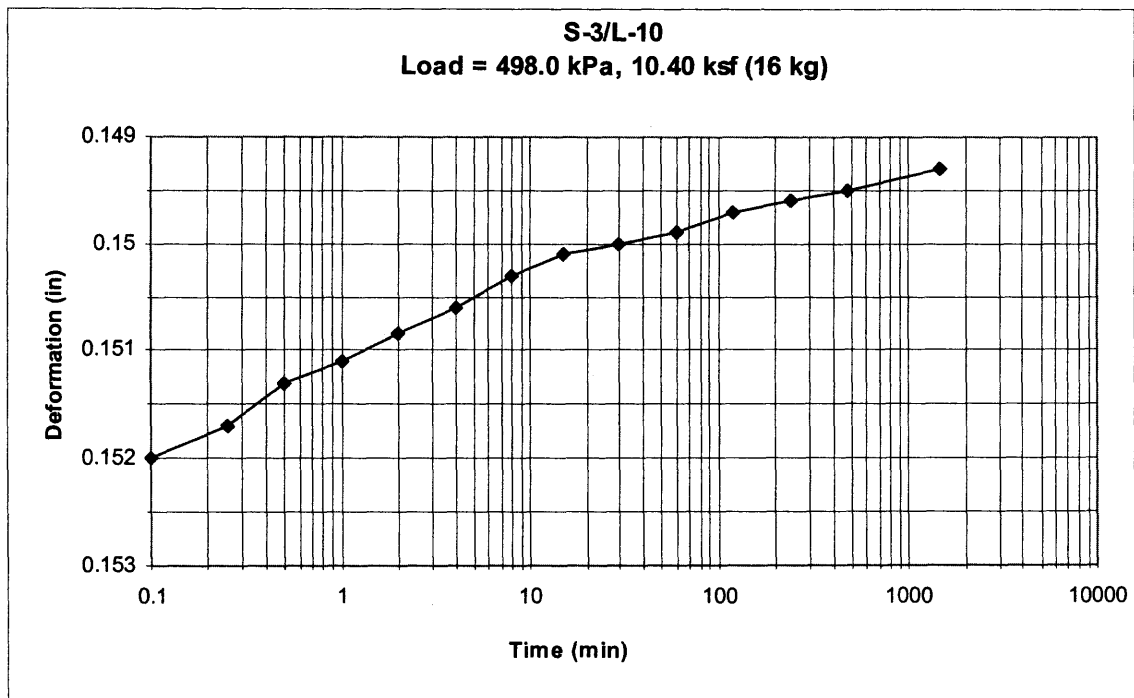


(a)

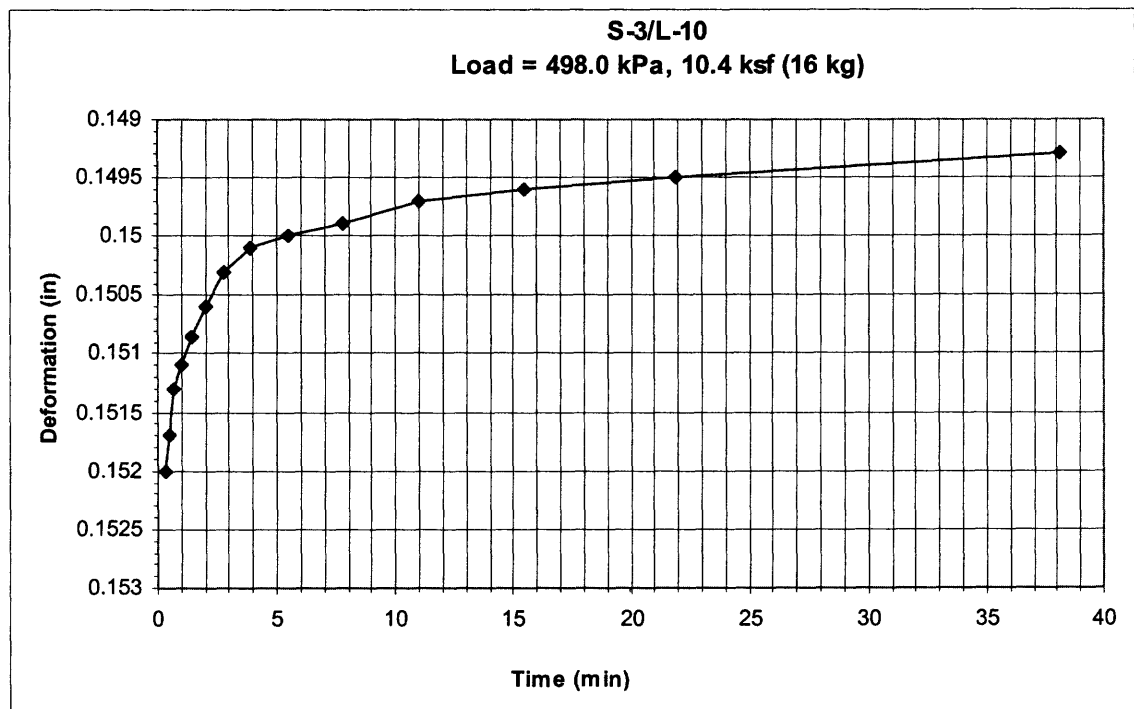


(b)

Figure A.25 Logarithm of time method (a) and square root of time method (b) for S-3/L-9.

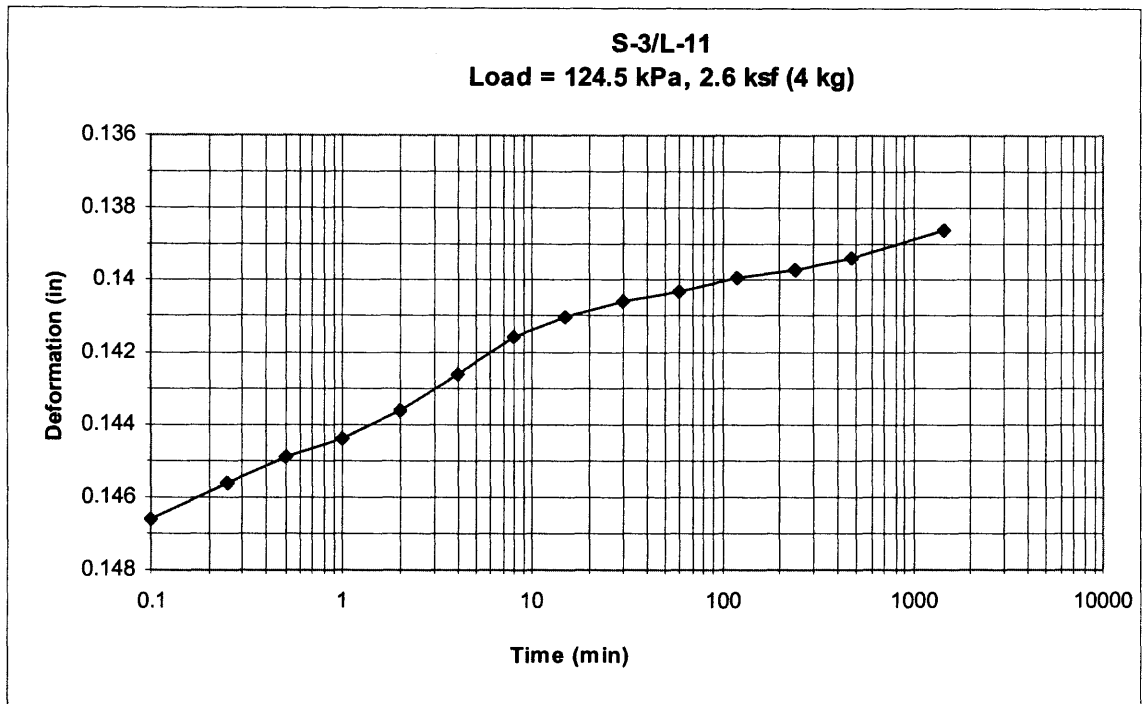


(a)

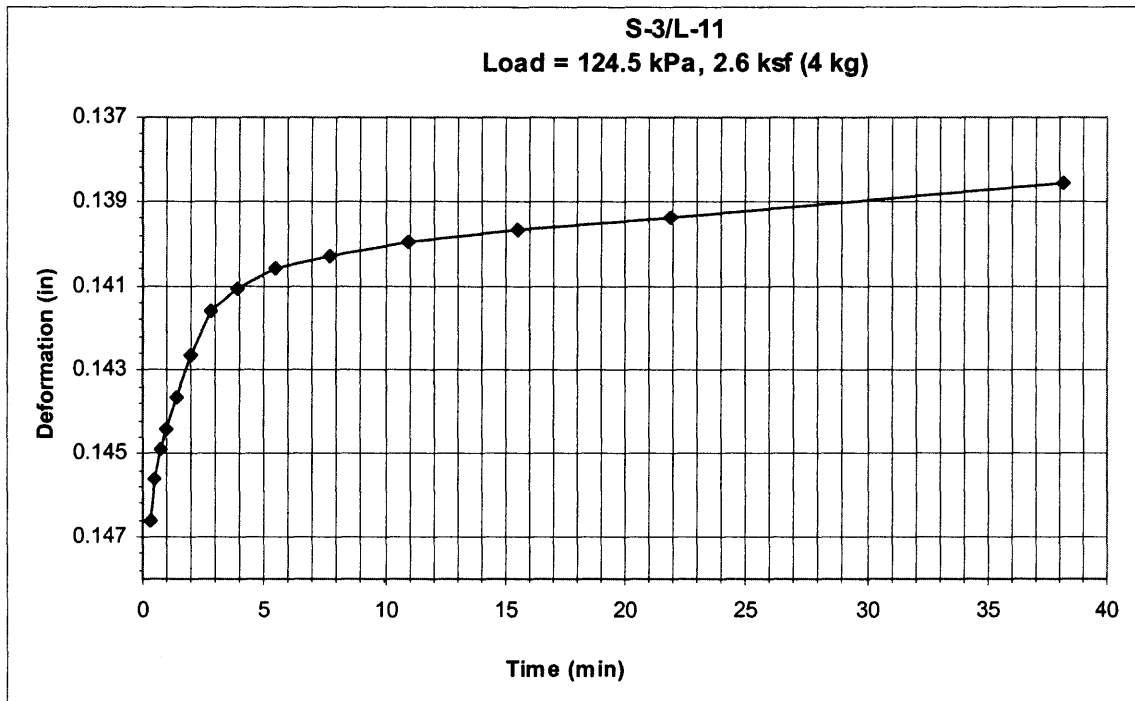


(b)

Figure A.26 Logarithm of time method (a) and square root of time method (b) for S-3/L-10.

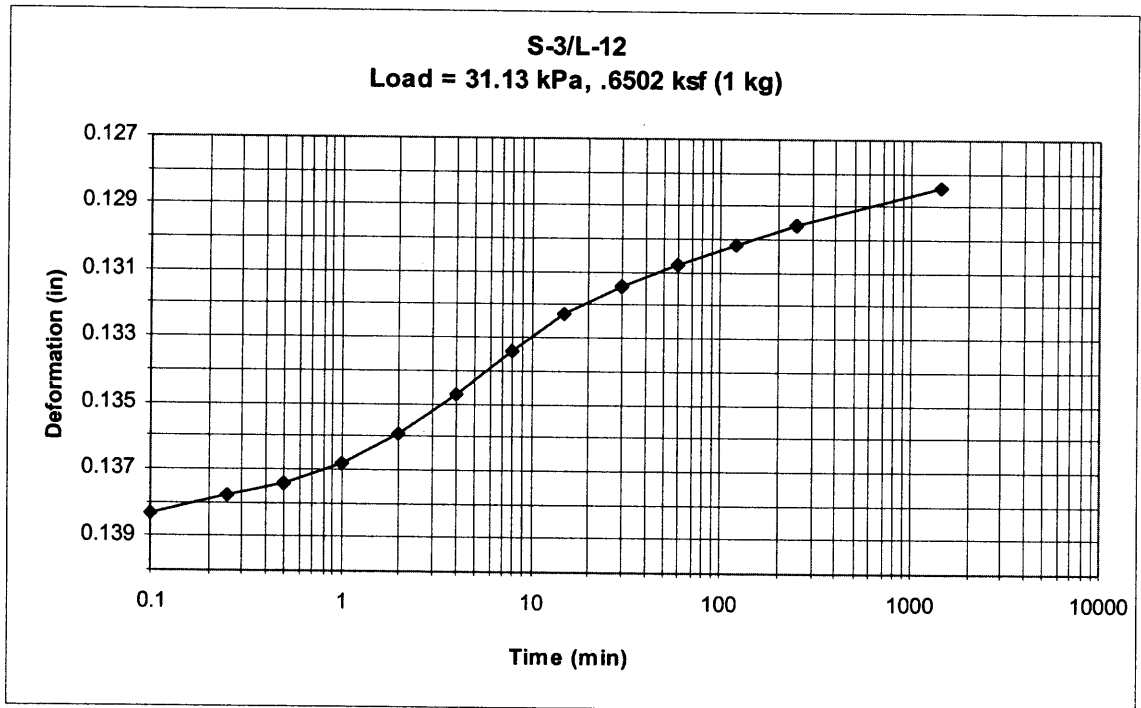


(a)

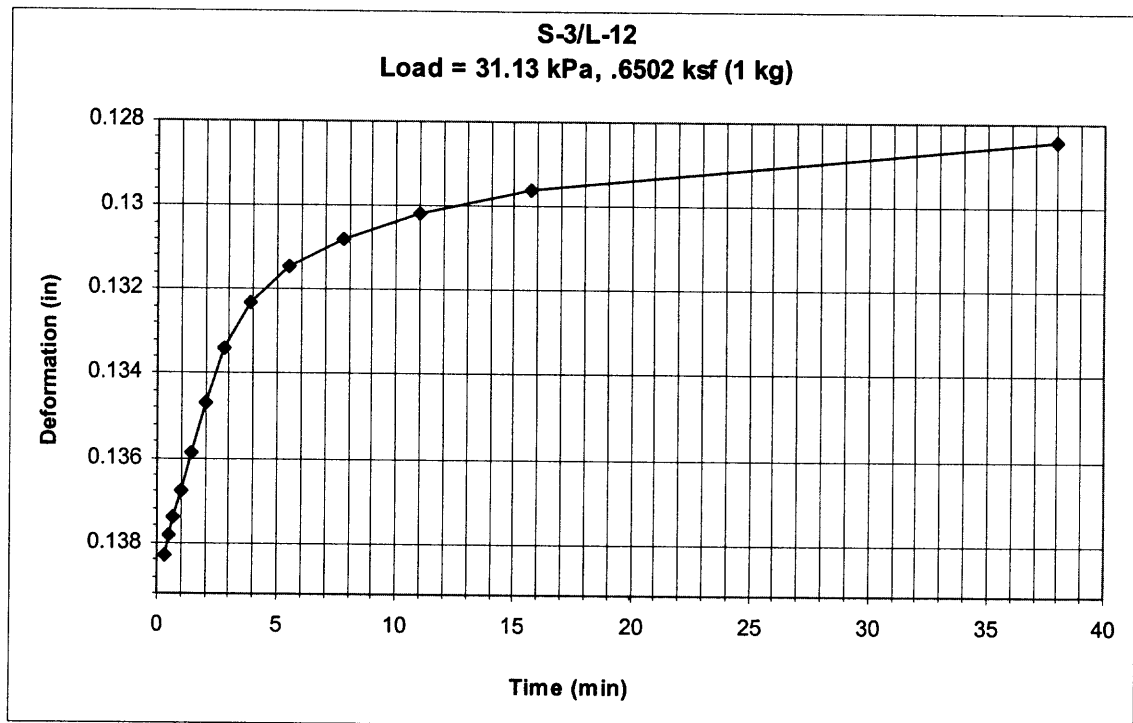


(b)

Figure A.27 Logarithm of time method (a) and square root of time method (b) for S-3/L-11.

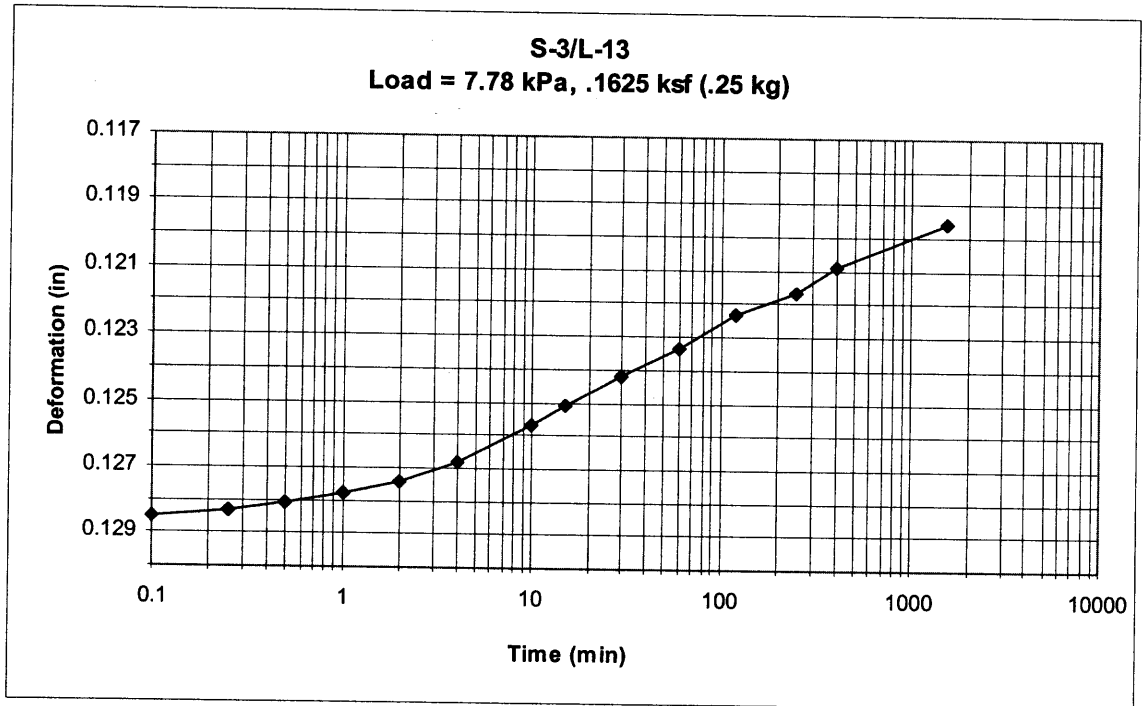


(a)

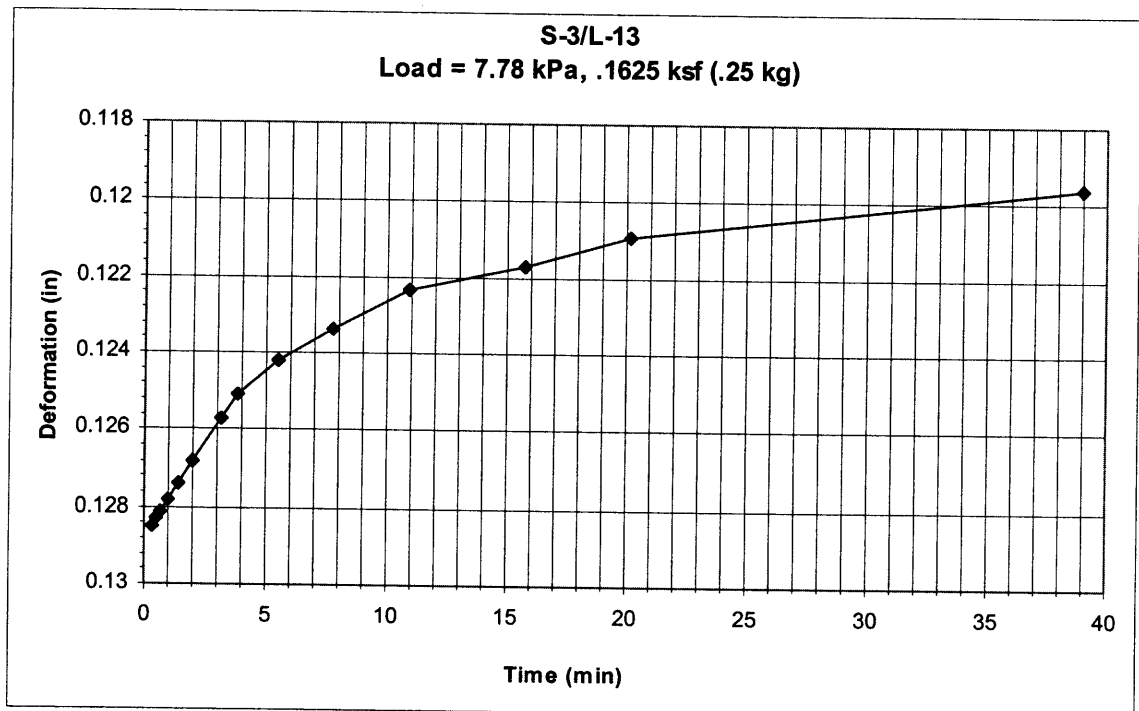


(b)

Figure A.28 Logarithm of time method (a) and square root of time method (b) for S-3/L-12.



(a)



(b)

Figure A.29 Logarithm of time method (a) and square root of time method (b) for S-3/L-13.

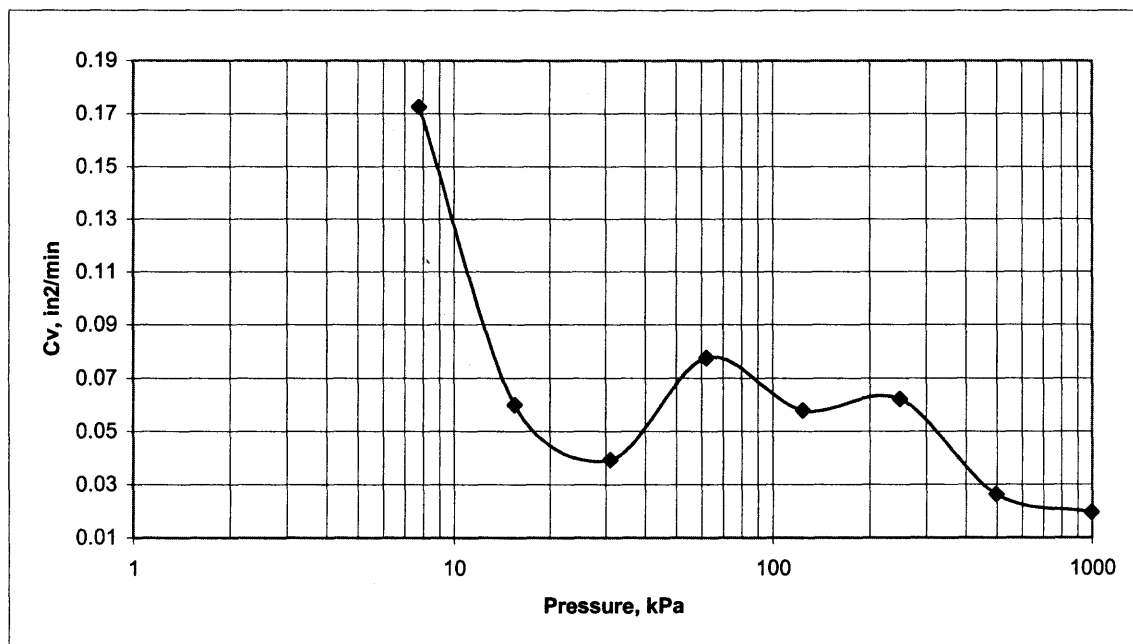


Figure A.30 Cv vs. Pressure (S-1).

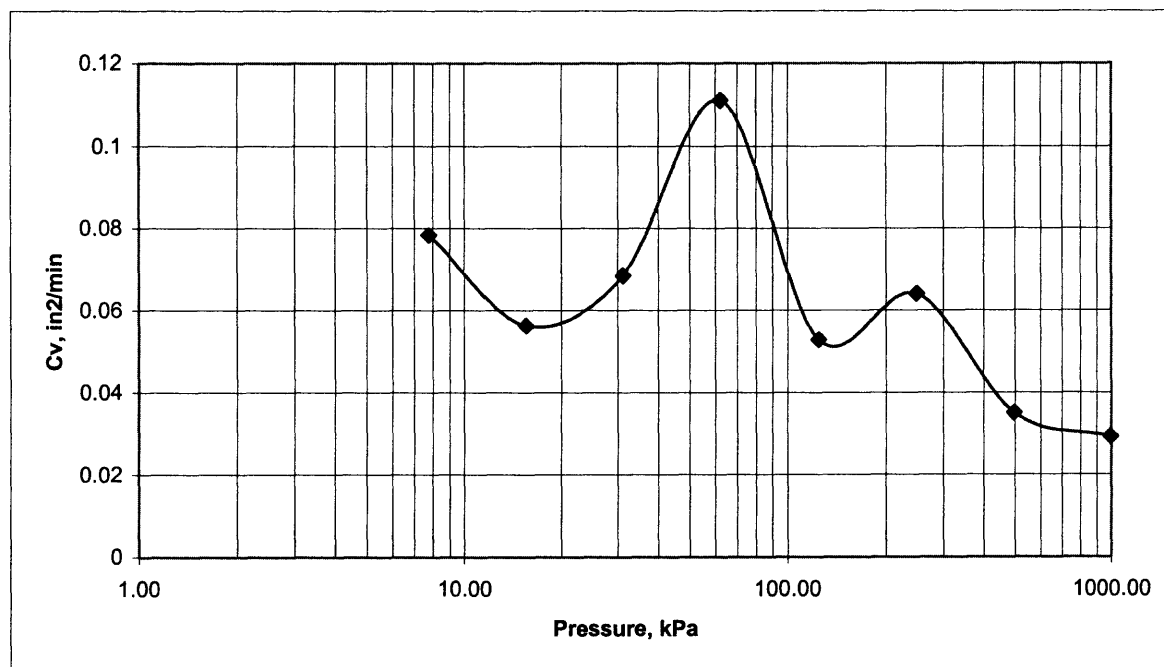


Figure A.31 Cv vs. Pressure (S-2).

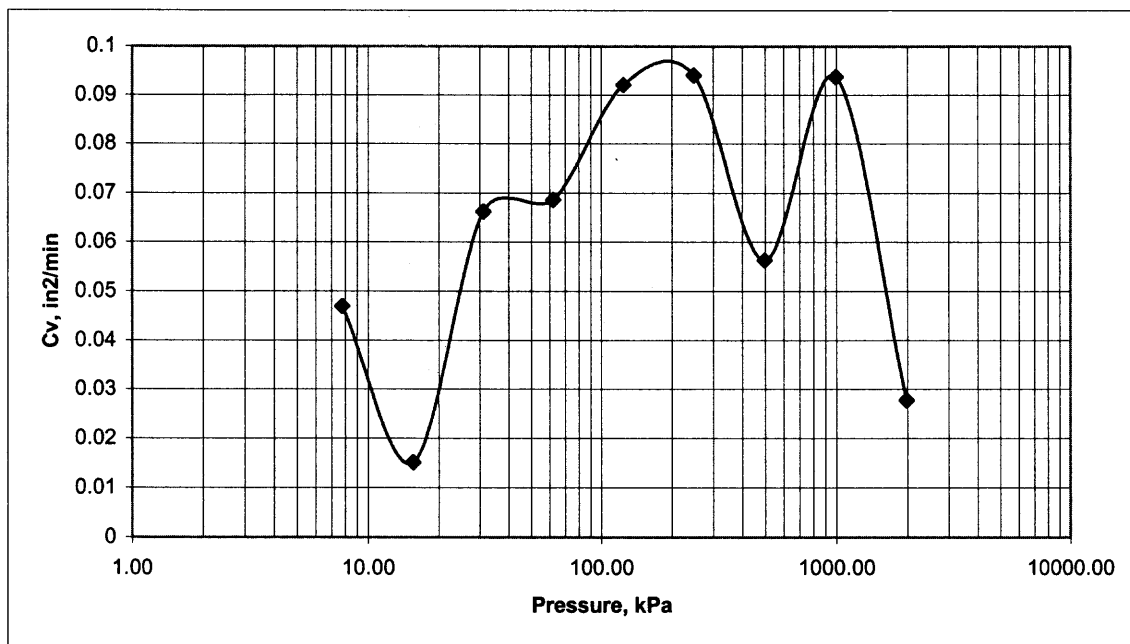


Figure A.32 Cv vs. Pressure (S-3).

APPENDIX B
TRIAXIAL TEST
GRAPHS

The following graphs represent all the data that was plotted for the triaxial test.

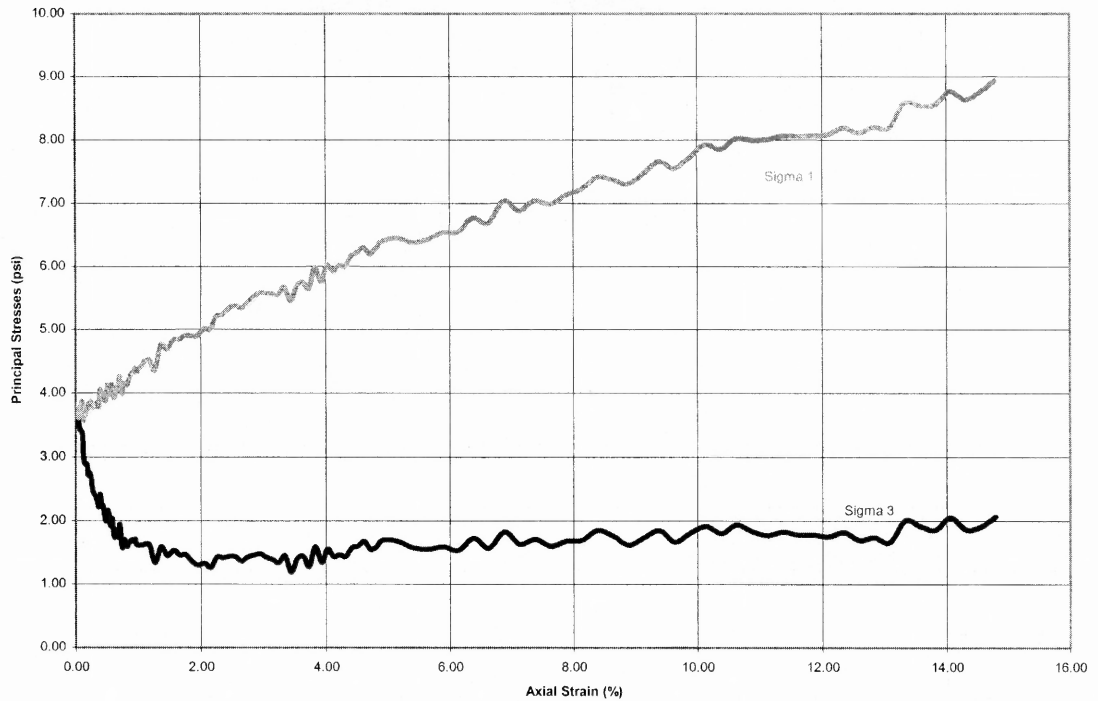


Figure B.1 Effective principal stress vs. strain (S-1).

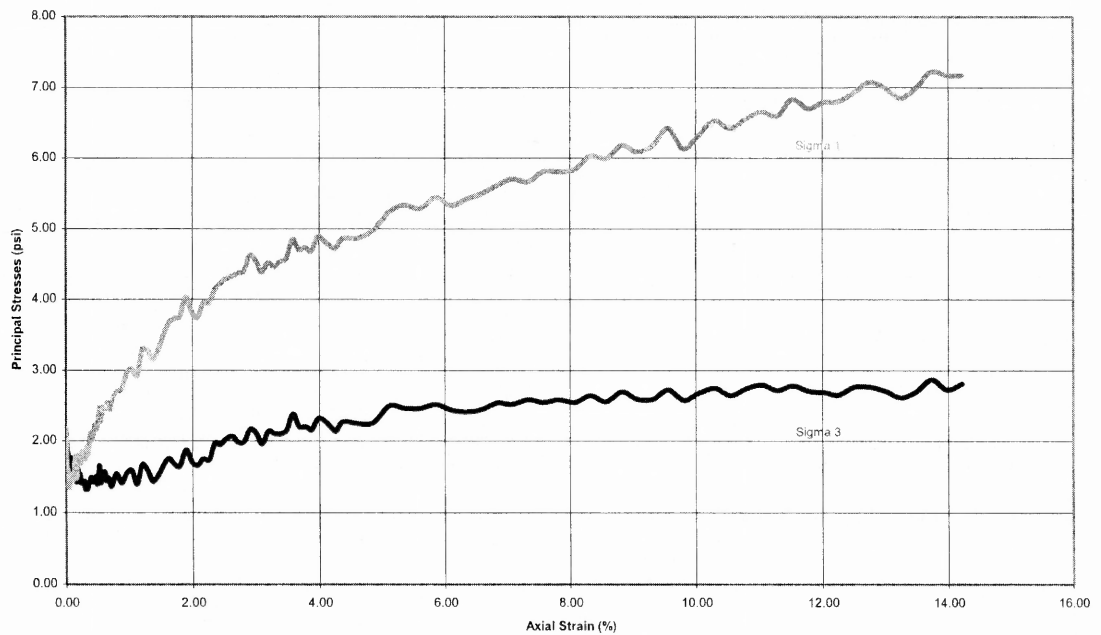


Figure B.2 Effective principal stress vs. strain (S-2).

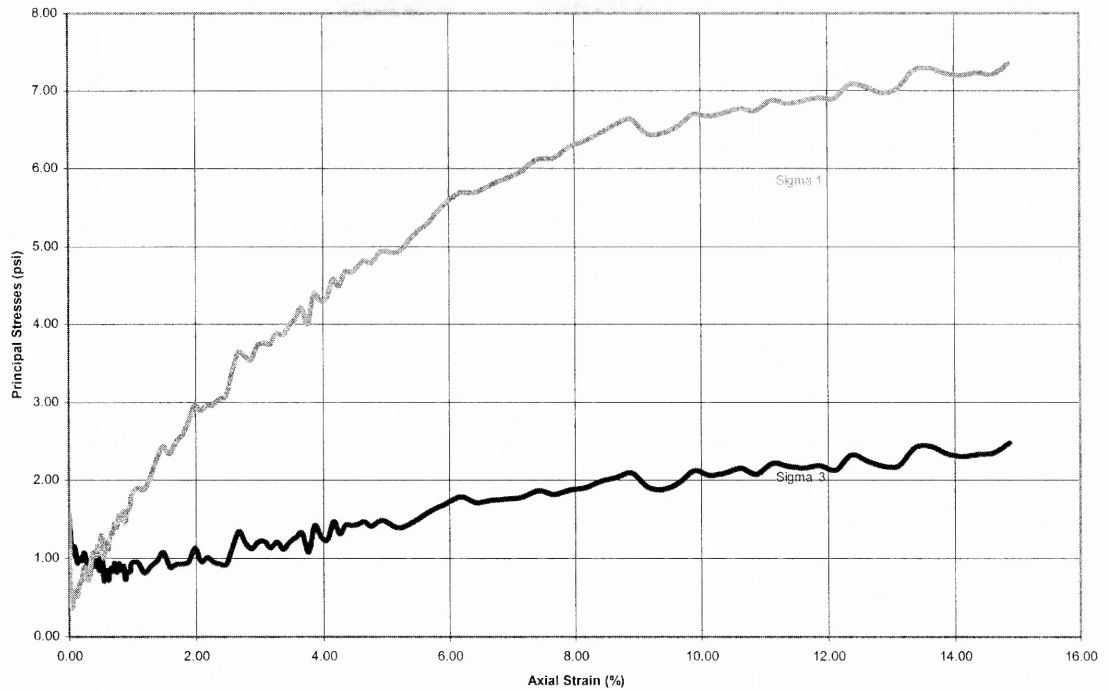


Figure B.3 Effective principal stress vs. strain (S-3).

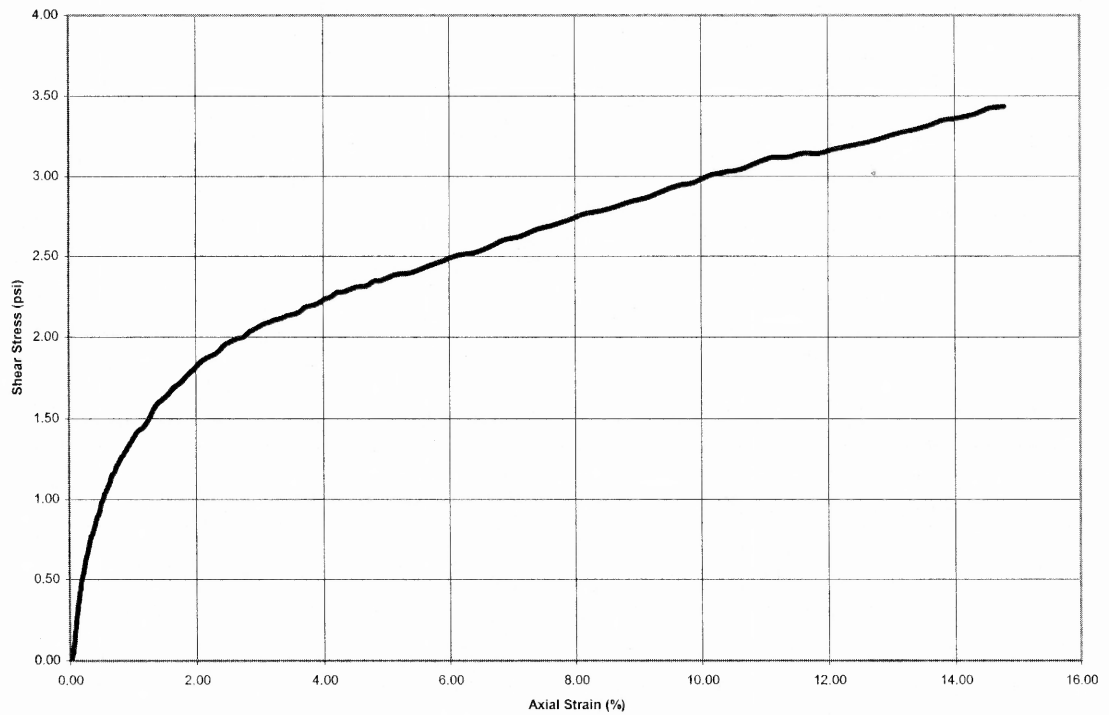


Figure B.4 Effective shear stress vs. strain (S-1).

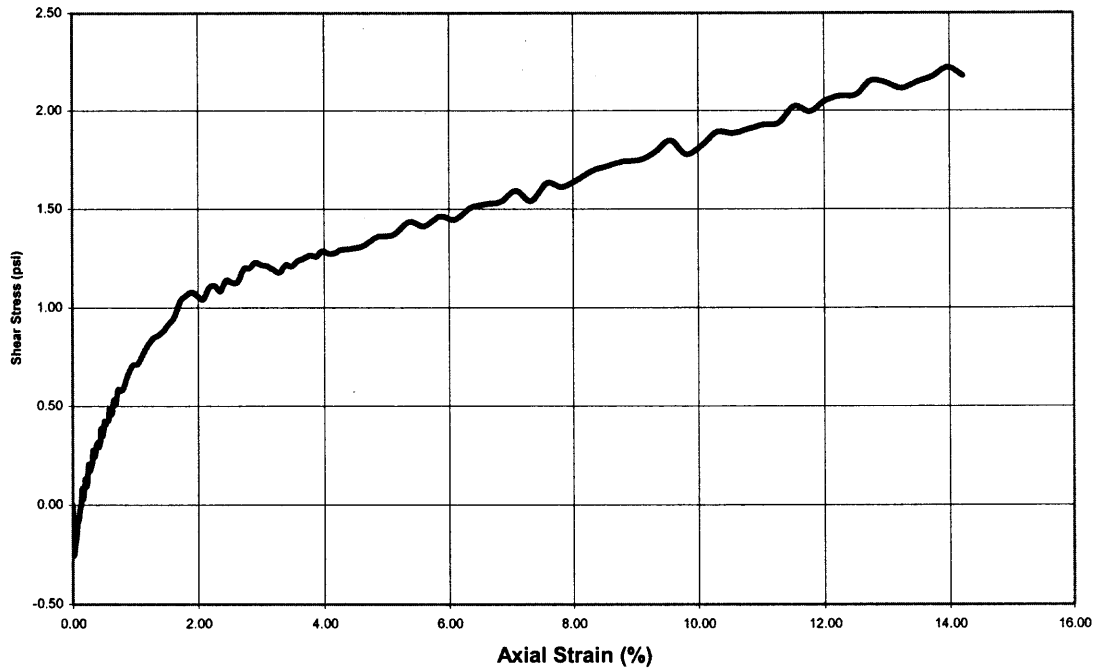


Figure B.5 Effective shear stress vs. strain (S-2).

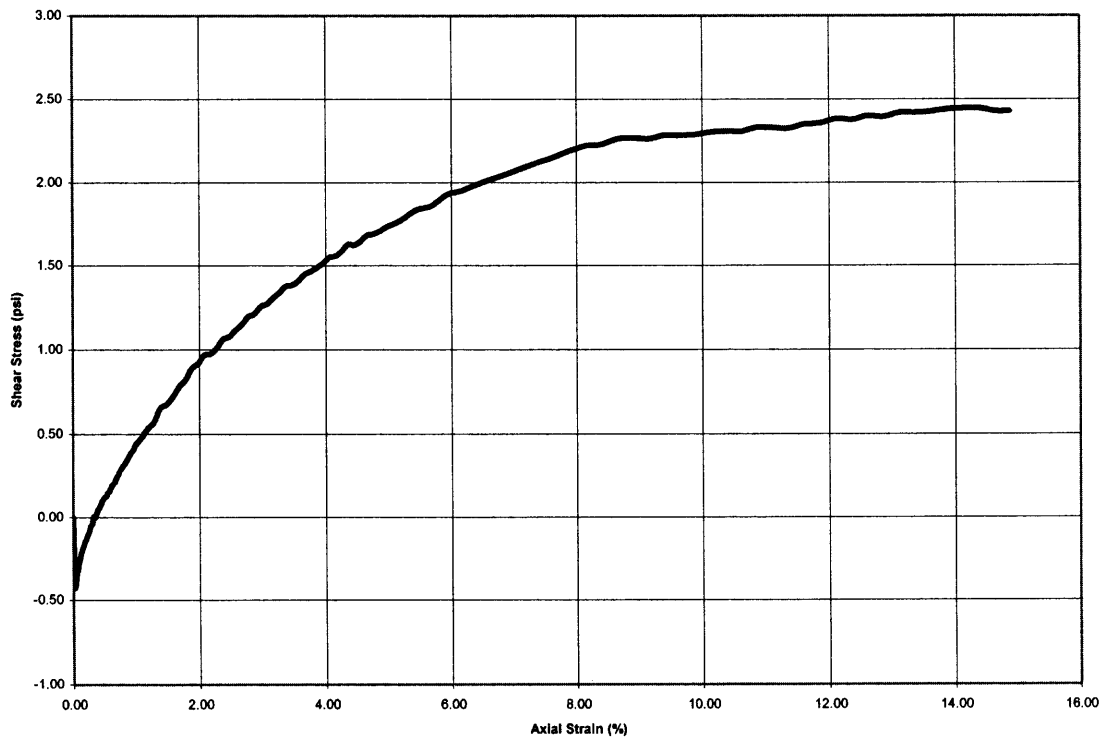


Figure B.6 Effective shear stress vs. strain (S-3).

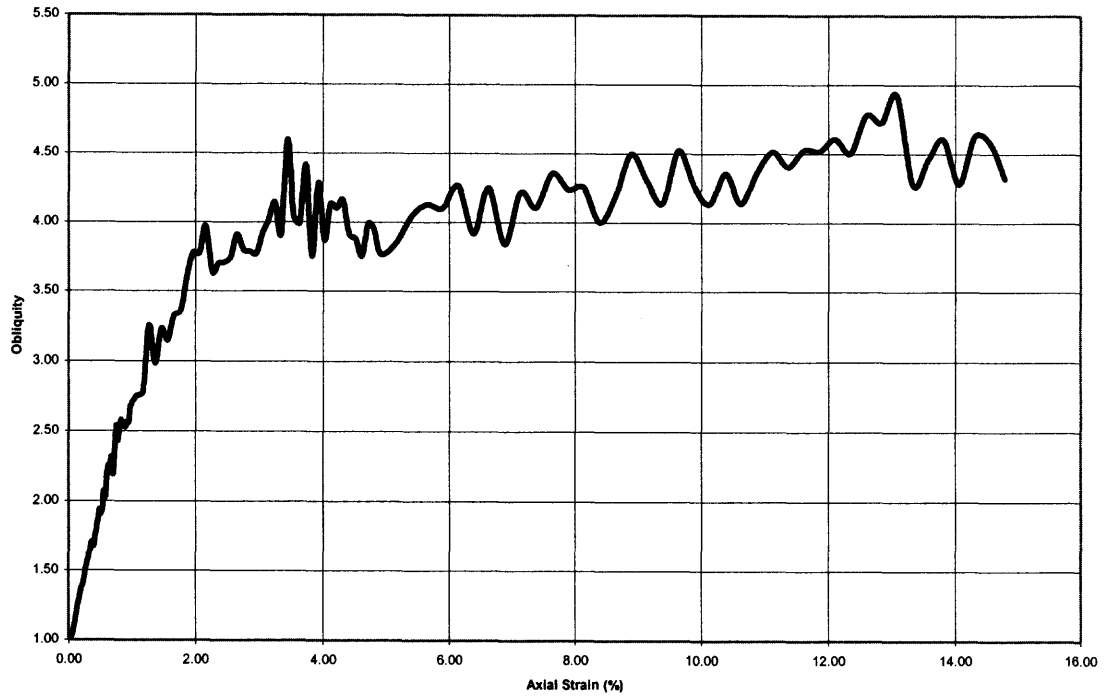


Figure B.7 Obliquity vs. strain (S-1).

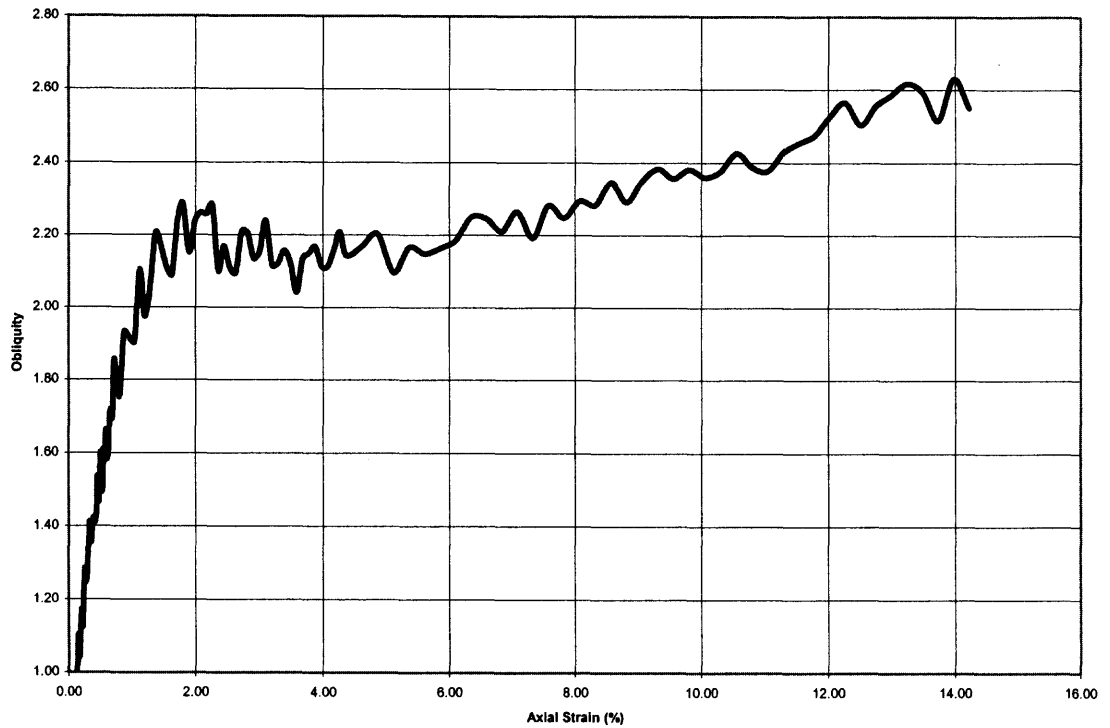


Figure B.8 Obliquity vs. strain (S-2).

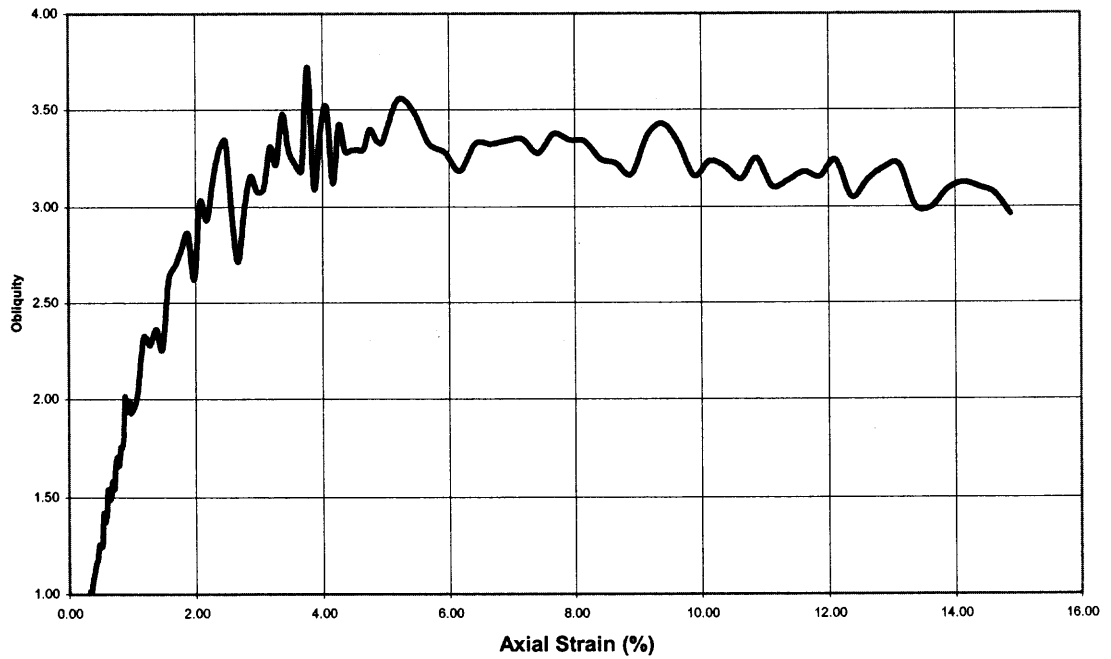


Figure B.9 Obliquity vs. strain (S-3).

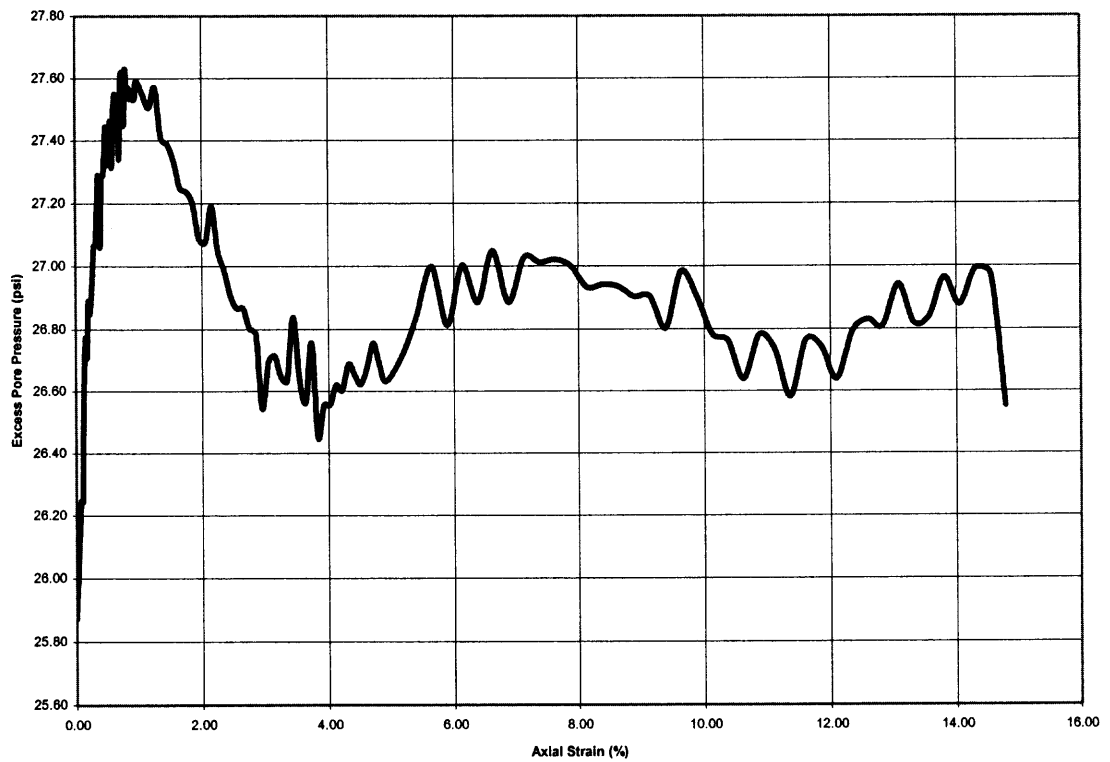


Figure B.10 Excess pore pressure vs. strain (S-1).

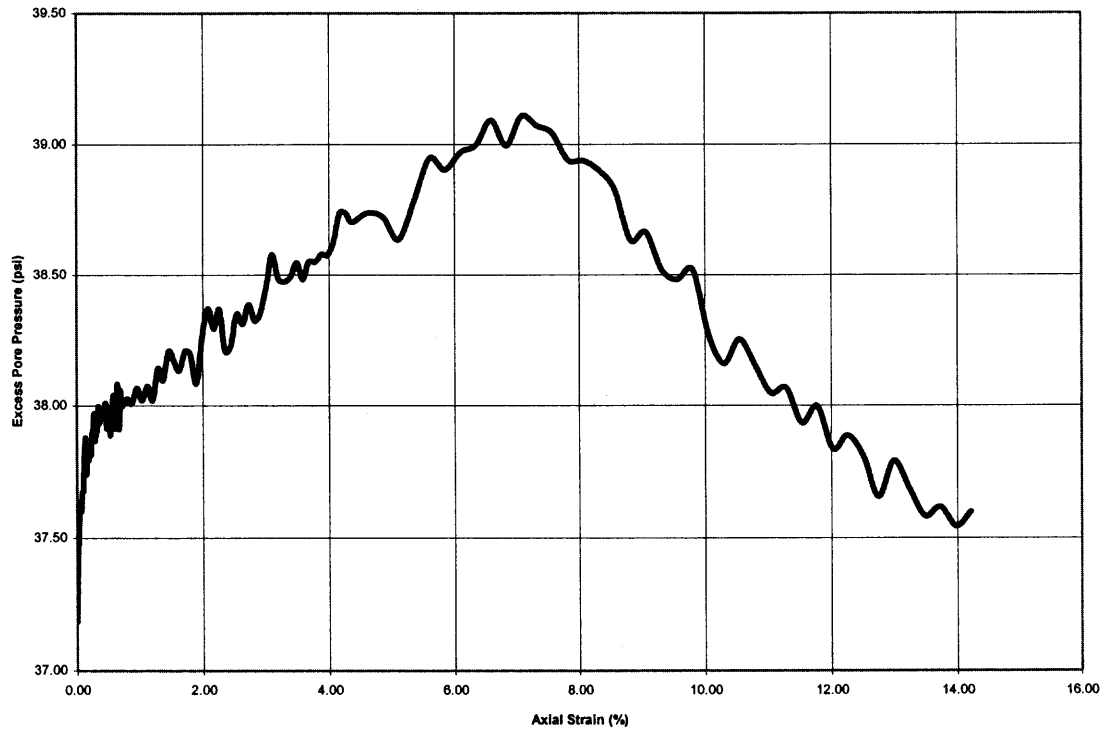


Figure B.11 Excess pore pressure vs. strain (S-2).

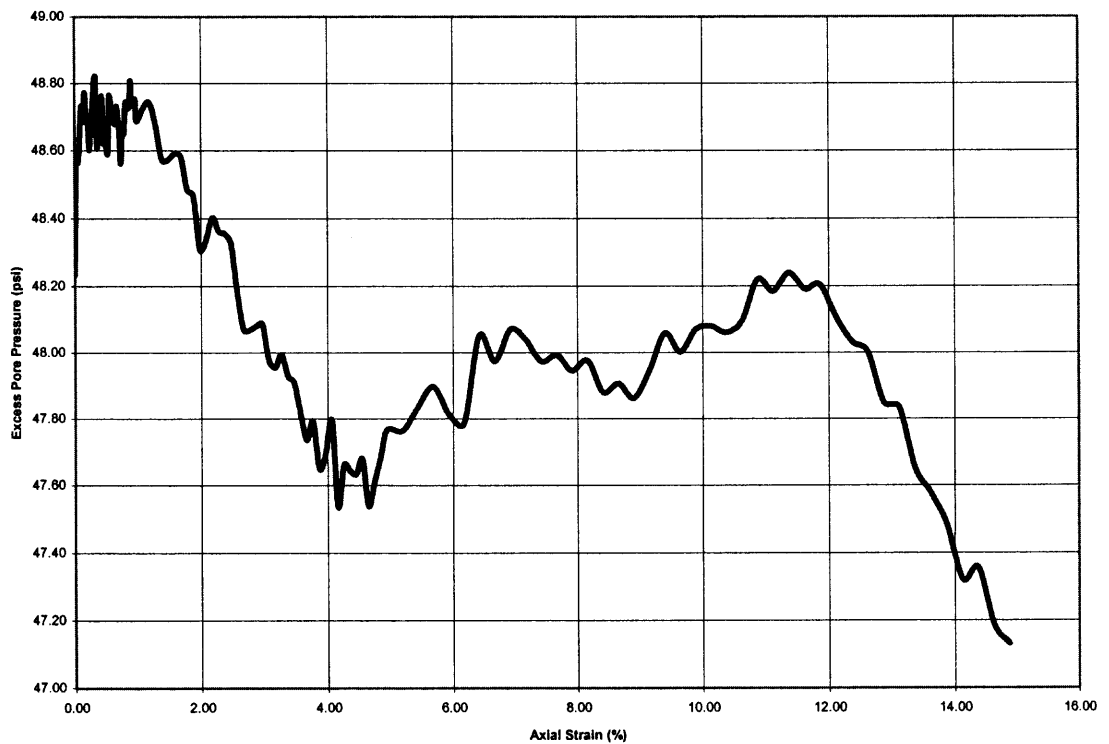


Figure B.12 Excess pore pressure vs. strain (S-3).

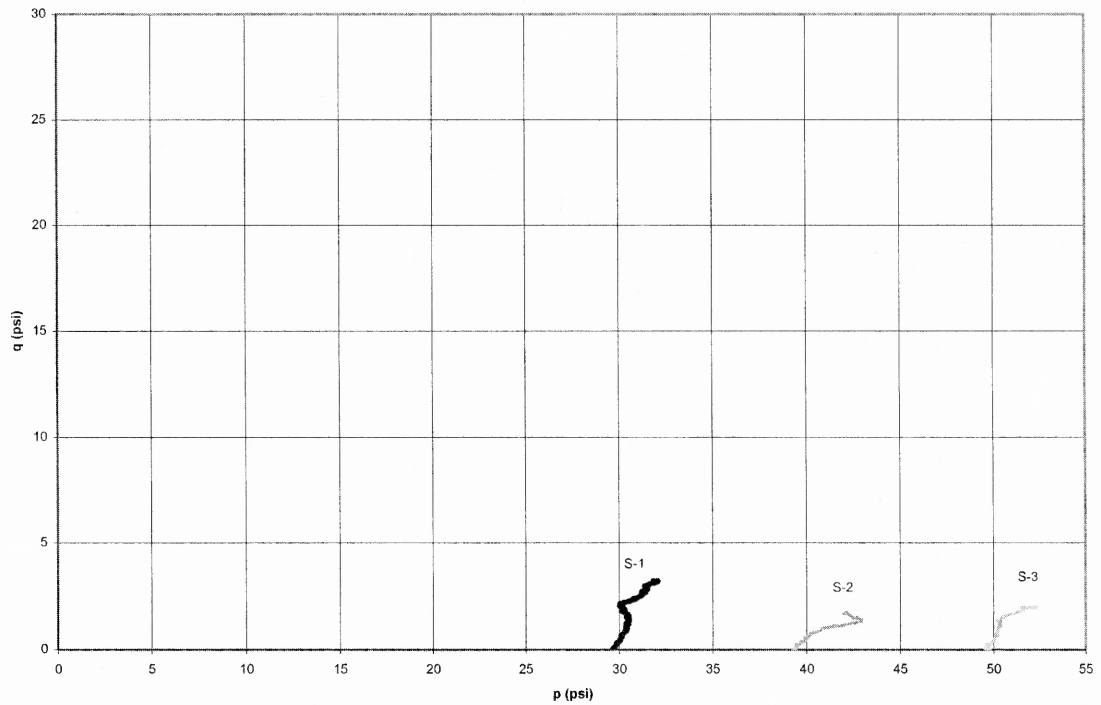


Figure B.13 Total corrected stress paths (S-1, S-2, S-3).

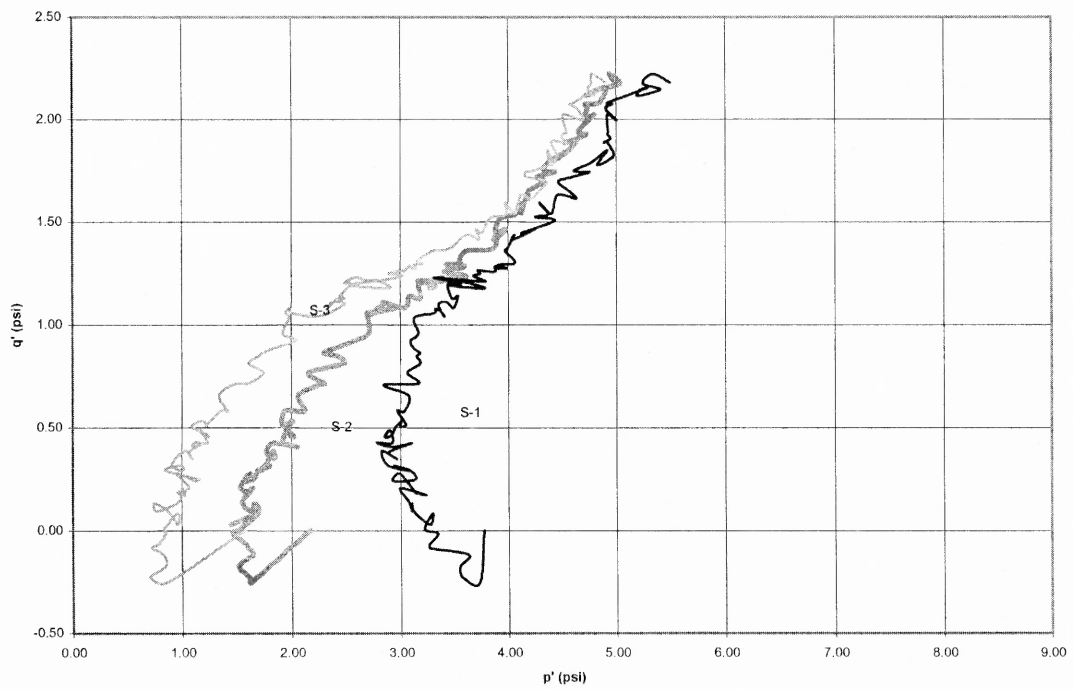


Figure B.14 Effective non-corrected stress paths (S-1, S-2, S-3).

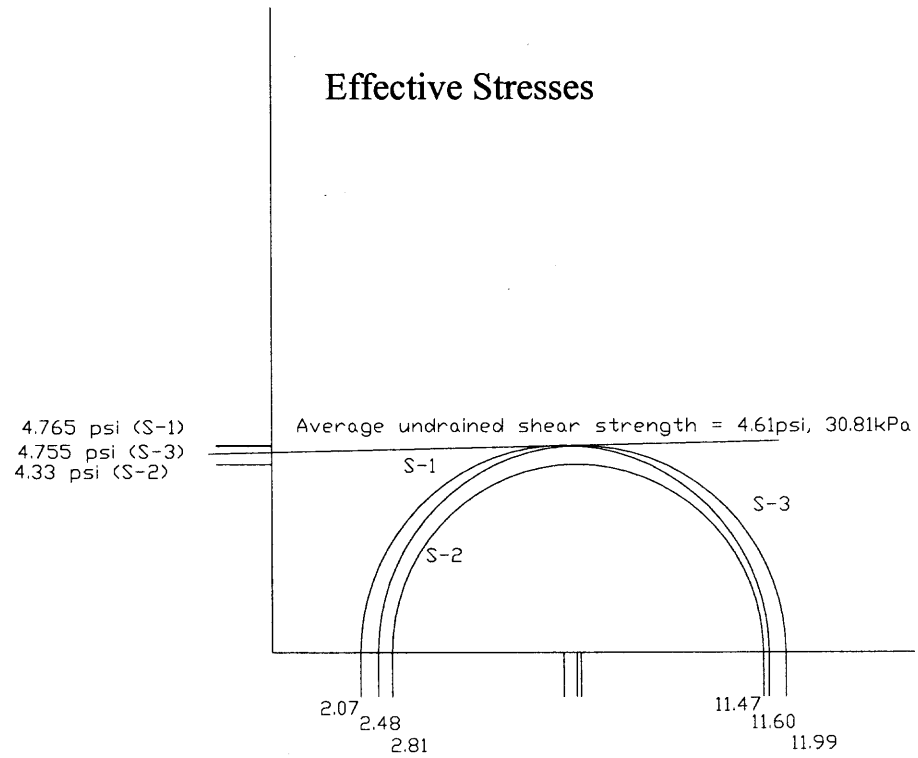


Figure B.15 Mohr's Circle (S-1, S-2, S-3).

REFERENCES

- Alencar Jr., Julio. (1999). Personal Communication.
- Arai, M., Uesugui, N., Rossetti, D. F., Goes, A. M. 1988. "Consideracoes Sobre a Idade do Grupo Barreiras no Nordeste do Estado do Para." Anais do XXXV Congresso Brasileiro de Geologia, Belem, Para, V.2, pp. 738-752.
- Das, Braja M. Principles of Geotechnical Engineering Third Edition. Boston: PWS Publishing Company, 1994.
- Derry, Duncan R. World Atlas of Geology & Mineral Deposits. New York: John Wiley & Sons, 1980.
- Farias, E. S., Nascimento, F. S. & Ferreira, M. A. A. (1992). "Area Belem/Outeiro." Relatorio Final de Estagio de Campo III, Departamento de Geologia, Centro de Geociencias, UFPa, Belem.
- Ferreira, C. S. (1982). "Notas Estratigraphicas sobre o Cenozoico Marinho do Estado do Para." Anais do I Simposio de Geologia da Amazonia, Belem, SBG – Norte, pp. 84-88.
- Goes, A. M. (1981) "Estudos Sedimentologicos dos Sedimentos Barreiras, Ipixuna e Itapecuru, no Nordeste do Para e Nordeste do Maranhao." Tese de Mestrado, Departamento de Geologia, UFPa, Belem.
- Head, K. H. Manual of Soil laboratory testing: New York: Wiley, 1980.
- Holtz & Kovacs. An Introduction to Geotechnical Engineering. Englewood Cliffs: Prentice-Hall Inc., 1981.
- Machado, M. Home page. 1996. Kohan-Saagoyen Ltda.
www.brcactaceae.org/geology.html. Extracted from Brazilian Environmental Mall; www.bem.com.br/bem/index_bem.asp
- Mesri, G. (1973) "Coefficient of Secondary Compression," Journal of the Soil Mechanics and Foundations Division, ASCE, Vol. 99, No. SM1, pp. 123-137.
- Pinheiro, R. V. L. (1987). "Estudo Hidrodinamico e Sedimentologico do Estuario Guajara-Belem (PA)." Tese de Mestrado, Centro de Geociencias, UFPa, Belem.

- Rossetti, D. F. "Sedimentary Evolution of the Late Cenozoic in the Northeast of Para State: Evidences of Sea Level Fluctuations." pp. 1-27. Personal Communication, 1999.
- Rossetti, D. F., Truckenbrodt, W., & Goes, A. M. 1989. "Estudo Paleoambiental e Estratigrafico dos Sedimentos Barreiras e Pos-Barreiras na Regiao Bragatina, Nordeste do Para.." Bol. Mus. Para. Emilio Goeldi, Ser. Cienc. Terra 1(1), pp. 25-74.
- Rossetti, D. F., Goes, A. M. & Truckenbrodt, W. 1990. "A Influencia Marinha nos Sedimentos Barreiras." Mus. Para. Emilio Goeldi, Ser. Cienc. Terra , pp. 17-29.
- Sampaio Jr., J. L. C. (1995). "Estudo da Compressibilidade de um solo Argiloso da Regiao Metropolitana de Belem-Pa." Dissertacao ao Departamento de Engenharia Civil da PUC-RJ.
- Schuring, John R. "Alluvial Fan and Fill Deposits (Piedmont Type)." Class notes CE 644, New Jersey Institute of Technology, 1998.